Assessing Tissue-Specific Female Upper Genital Tract Pathology During *Chlamydia* Infection: Inter-rater Reliability and Virus-Like Particle Vaccine Strategies

by

Grace O'Donnell Wieselquist

A Paper Presented to the

Faculty of Mount Holyoke College in

Partial Fulfillment of the Requirements for

the Degree of Bachelors of Arts with

Honor

Department of Biological Sciences

South Hadley, MA 01075

May 2026

This paper was prepared

under the direction of

Professor Rebeccah Lijek

for eight credits

Dedication

I want to thank my mentor, professor, and PI Becki Lijek for her support and encouragement throughout this thesis process and my time at Mount Holyoke. Your enthusiasm about science itself and creating a positive environment in class and in lab is the reason I was able to grow as a scientist. You teach and lead with care, creating a space that made me feel passionate and heard. Your thoughtfulness about those you teach and lead is inspiring, and I am forever grateful for all that I have learned from you, especially how to bring humanity and teamwork into science.

To my Lijek Labmates, thank you for making research everything I dreamed of. Lucie, if it weren't for meeting you my first year, I never would have taken the leap to apply to be in the lab, and find this passion I never knew I had. You are an incredible friend and brilliant, hardworking teacher. Thank you for training me on all the techniques I know, for the pep talks on the way back from PLUMs, and for being the reason I am where I am today. Akosua and Aria- I miss you both so much. Our late night consensus and graphing meetings always made me laugh, and I felt so lucky to be learning and exploring with you both. You will become excellent doctors. Isabelle, MJ, Ashna, Hattie- you are the most supportive, hilarious, and profound people. I will forever miss our mouse room chats, summer outings, Thirsty Mind trips, and collective cheers when our qPCR or ELISA worked. Ashna and MJ, I am excited to see how you change the world.

Hattie and Isabelle, you are incredible leaders and I hope you enjoy your last year at MHC. Du, Luca, Nipuni, and Sarah- I am so excited to see what you accomplish!

My family is the reason I am here and why I push myself to learn and grow. Mom and Dad, thank you for showing me what it means to work hard, to care deeply, and to push myself to learn and make a difference. You told me I would have a voice at Mount Holyoke, and because of you, I have found it. To my grandparents, thank you for listening to me go on and on about my research and for supporting me in everything I do. Sophie, I am so grateful to have a sister and best friend in one. Thank you for taking care of me when I needed it and being one of my biggest role models. I am so proud of you for becoming a doctor! Henry, thank you for being such a kind, caring brother. I love our long talks, and how we've had them since we were little. I am glad we get to go through life together.

Dan, thank you for sticking by me no matter what. You always believe in me and encourage me, and I love you very much.

To my best friends, I love you all so much and our time together means the world to me. Molly Rose and Phoebe, you are day ones. I couldn't imagine life without you. From finding our first independence in trips to the riverbank to where we are now, I am so grateful to share girlhood with you. Eni, wie dankbar bin ich, um dich kennengelernt zu haben. In nur einer kleinen Zeit habe ich eine

liebe, kluge, beste Freundin gefunden. Francesca, you have no idea how much our dinners and classes together meant to me. I am so excited to see you become a fabulous dentist. Lydia, I can talk to you about anything for hours. Thank you for being a lifelong friend. Natasha, dancing with you at Mount Holyoke has been so special and I am so very grateful to have met you. I cannot wait to see what you do. Sophie, my first college friend! Our friendship means so much to me, and I will cherish our memories forever.

Dominique and Professor McNally, thank you for changing my life and opening your arms to me in German Studies. My worldview has broadened and changed forever because of my classes, travels, and time working in the department. Thank you for being understanding, supportive, and interested in my life. Conversations with you both and our department mean the world to me.

Dr. Summerer, thank you for welcoming me into your family and practice. Because of you, I had the privilege of exploring another culture and healthcare system, and developed a strong passion for obstetrics and gynecology that is so strongly tied to this research. You are an inspiring doctor who advocates for her patients and gives the highest quality care, and you are a kind, dear person.

To my Professors Alan Van Giessen, Barbie Diewald, and Katie McMenimen, thank you for pushing me to accomplish more than I ever thought I could.

ACKNOWLEDGEMENTS

Work in the Lijek lab is often collaborative, especially on days when the experiment requires processing large numbers of mouse samples at once. I am grateful for the contributions of Ashna Mehta ‘26, MJ Pinkes ‘26, Hattie Nichols ‘27, and Isabelle Lian ‘27 for all of their support. This includes helping me collect mouse samples (e.g. serum collection, vaginal lavage) and carry out dissections and downstream tissue processing. All pathology scoring is inherently a team effort, since multiple scores are required to reduce scorer bias. A special thanks to Hattie Nichols ‘27 for taking the gross pathology images, as well as past lab members Everett Webster, Lucie Berclaz, Kyra Seiger, Hannah Knapp-Broas, and Shan Breen for launching these projects and developing methodology.

I would also like to thank our scientific collaborators: the Frietze Lab at the University of New Mexico for creating the QB and QB-CT166 VLPs, and the Fields Lab at the University of Kentucky for sending us *C. muridarum*. Thank you also to the Camp Lab at Mount Holyoke College for plate reader access that was integral to producing ELISA data. Thank you Professor Jared Schwartzer for your enthusiasm and instruction on inter-rater reliability and coding. Thank you Dr. Heather Chenoweth for your expertise in microscopy. The inter-rater reliability and pathology analysis in this work was strengthened by professional

imaging techniques that you provided training and resources on. Without you, none of this work would be possible.

This work was funded by NIH R21 AI178108 and R01 AI66360 grants, as well as Mount Holyoke's Fund the Future Award and Lynk UAF.

TABLE OF CONTENTS

LIST OF FIGURES

LIST OF TABLES & EQUATIONS

ABSTRACT

Chlamydia is the world's most prevalent bacterial sexually transmitted pathogen. *Chlamydia* disproportionately affects people with uteri, inducing severe chronic pathology in the female genital tract if untreated. Because prophylactic screening is limited, it is imperative to develop a safe, accessible, effective *Chlamydia* vaccine. Prior work links the *Chlamydia* putative cytotoxin CT166 to chronic oviduct pathology in mice. This research tests CT166 as an antigen in a Virus-Like Particle (VLP) vaccine, QB-CT166, against *Chlamydia muridarum* infection. Here we show that QB-CT166 induces high titers of IgG in the serum but low levels of IgG in the vagina and uterus. We reveal that the vaccine does not reduce *Chlamydia* bacterial burden nor immunopathology. In parallel with this vaccinology research, we sought to fill a gap in the literature by developing a reliable, teachable *Chlamydia* pathology scoring system. We analyzed the reliability of pilot scales and optimized them to be clear and biologically representative, then tested their teachability with a training intervention for new lab members. This project yielded resources for members during training and pathology scoring and identified an inter-rater reliability analysis method to ensure future scoring robustness. This work moves the *Chlamydia* field forward through insights into vaccinology and inter-rater reliability.

INTRODUCTION

1. Impact and Statement of Purpose

Chlamydia trachomatis is the most common bacterial sexually transmitted pathogen across the globe, with 128.5 million infections documented in 2020 (1–3). In 2024, 1.5 million cases were recorded in the U.S. alone (4). *C. trachomatis* disproportionately affects people with uteri; a 2020 study compiling data from 24 countries found a 3.1% prevalence among females compared with 2.6% in males, though a greater gap was predicted, as the survey excluded pregnant people (4, 5). While acute infections are easily cleared with a course of antibiotics, infected individuals are often asymptomatic and therefore do not seek treatment (1, 6, 7). In these cases, cervicitis, salpingitis, tubal factor infertility from tissue scarring, and pelvic inflammatory disease (PID) may develop (7–10). PID occurs when infection passes the cervix and extends into the uterus, fallopian tubes, and ovaries. This can further progress into perihepatitis, when inflammation continues into the liver and other internal organs. These long term pathologies are painful, dangerous, and difficult to treat: mental and physical wellbeing increasingly deteriorate with increasing levels of chronic pelvic pain (11).

Because of the high global infectivity rate and the dire effects of chronic untreated infection of the female genital tract, prophylactic measures are vital. In the United States, the CDC recommends regular *C. trachomatis* testing for sexually active men having sex with men, sexually active people with uteri under

25, people with uteri over 25 with multiple sexual partners, and pregnant people (12).

However, there are limits to sexually transmitted infection (STI) screening as the only method of disease prevention, including access barriers and social stigma. People with low income may not be able to afford transportation to clinics, and some developing countries lack resources for screening (6, 8). A study by Tilson et al. (2004) used a discussion group style to identify several factors that would discourage adolescents from getting STI tested when asymptomatic, such as lack of awareness that STIs can be asymptomatic, fear of judgment and social stigma, cost of care, transportation, and fear of discrimination due to past negative experiences in a healthcare setting. Because of these barriers, frequency of testing is greatly reduced (6).

This, taken together with historic underrepresentation of gynecological research, emphasizes the imperative to develop an accessible prophylactic vaccine for *C. trachomatis* (13–15). Priming the immune response through vaccination could prevent inflammation and the dire effects of long term infection (10, 16–19). An auspicious direction for a *C. trachomatis vaccine* draws from one of only two STI vaccines on the market, which combats Human Papilloma Virus (HPV). The HPV vaccine utilizes virus-like particle (VLP) technology, which elicits a strong and protective antibody response (20). Recent promising work manipulates this platform by conjugating *Chlamydial* antigens to VLPs (21).

Previous studies have shown that the putative cytotoxin of *C. trachomatis* plays a role in tissue-specific chronic pathology, making it an intriguing target for vaccine antigen selection. Known as CT166 in the human-infecting bacterium, this effector protein is also a strong antigen candidate because of its high sequence conservation across *Chlamydia* serovars and species (21).

A mouse model provides a reliable representation of the human female genital tract and can therefore be used to achieve the goal of developing a *C. trachomatis* VLP vaccine. This model allows quantification of bacteria and antibodies, as well as assessment of tissue-specific pathology, to assess the efficacy of vaccination (22). While bacteria and antibodies can be quantified, pathology assessment requires holistic expertise and is subjective (23, 24). It is vital that a pathology scoring system is reliable between scorers to properly determine whether a vaccine is truly effective. Because it is unclear what causes tissue tropic pathologies, the scoring system should be tissue-specific so phenotypes can be assessed individually. This study will test the reliability of a scoring system for *Chlamydia*-induced tissue-specific pathology, and apply this scoring system in assessment of a novel VLP vaccine against *Chlamydia* infection. This work is valuable because it advances underrepresented research concerning accessible protection from *C. trachomatis*, as well as the tools to assess the efficacy of these protection methods.

2. *Chlamydia* Classification

The *Chlamydia* genus describes a variety of gram negative, obligate, intracellular bacterial pathogens (**Fig. 1)**. These pathogens are dependent on invasion of host cells for nutrients and evade the host immune system to survive and proliferate. The human-infecting *C. trachomatis* has three biovars: trachoma, genital tract, and lymphogranuloma venereum (LGV). Each of these specifically infects a different human tissue. Biovars are subsequently divided into serovars, characterized by different forms of surface proteins. Serovars A-C belong to the trachoma biovar, causing ocular infection (trachoma) and blindness if untreated. Serovars D-K belong to the genital tract biovar, infecting primarily the female genital tract and neonates. The LGV biovar includes serovars L1-L3, which cause genital ulcers, anal cramps, constipation, and discharge (**Fig. 2)** (1, 7, 9, 19).

Chlamydia muridarum is another species of the *Chlamydia* genus **(Fig. 2)**. Also belonging to the Chlamydiaceae family, this separate strain was originally known as the mouse pneumonitis (MoPn) *C. trachomatis* strain, because it can infect mouse lungs. It has since been classified as its own species, and as it infects mouse female genital tracts, it is vital to this discussion (25, 26). This work focuses primarily on *C. trachomatis* serovar D, using *C. muridarum* to model infection.

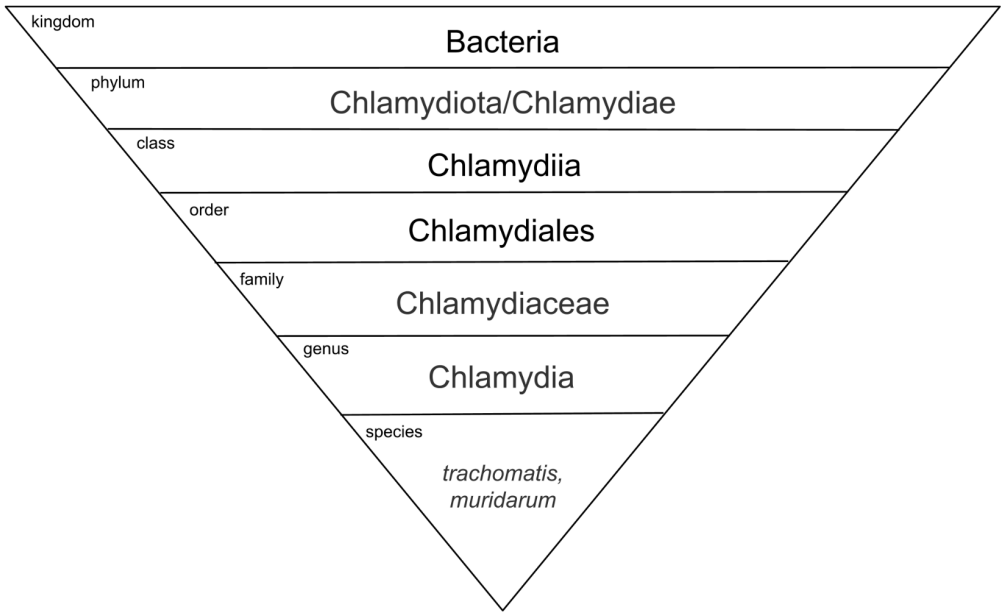

Figure 1. Taxonomy of *Chlamydia trachomatis* and *Chlamydia muridarum*. Adapted from Chen et al. (2019) (26).

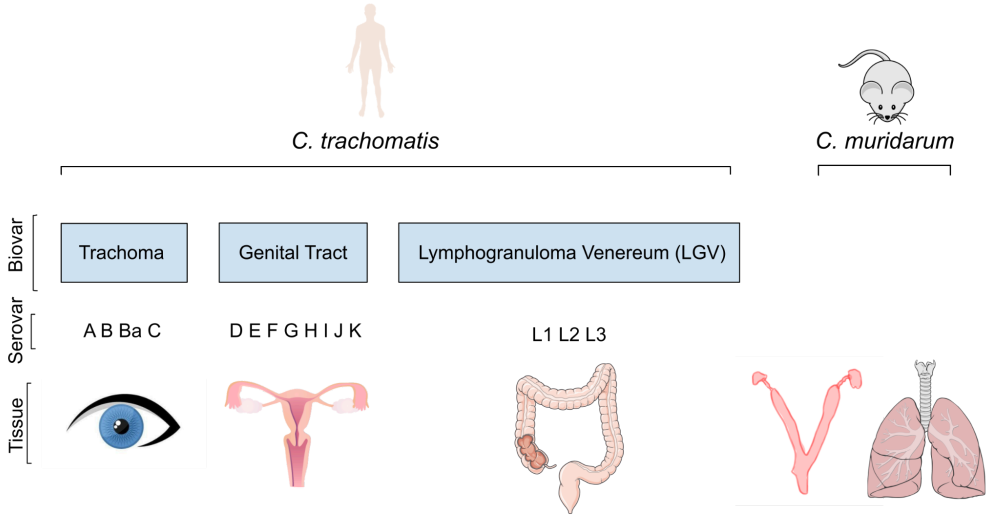

Figure 2. **Comparison of *C. trachomatis* and *C. muridarum* target host species and tissues.** *C trachomatis* is subclassified into biovars and serovars. Adapted from Murray and McKay (2021) (9).

3. *Chlamydial* Developmental Cycle

Chlamydia bacteria proliferate in the host using biphasic development, which involves cycling between two forms: elementary bodies (EBs) and reticulate bodies (RBs). EBs invade host cells and differentiate into RBs. RBs multiply within host cells, then differentiate back to EBs for release. The infectious EBs do not have an active metabolism. EB entrance into host mucosal epithelial cells is made possible by a three component interaction using bacterial adhesin proteins, host receptors, and host coreceptor heparan sulfate proteoglycans (HSPG). *Chlamydial* association with HSPGs is a weak interaction, whereas the association between bacterial adhesins and host receptors, such as growth factor receptors, is very strong (**Fig 3.1**) (1, 7, 9, 27). After adherence, the bacterium forces the host cell to endocytose it using a type three secretion system (T3SS), a protein complex that juts out and pierces host cells like a needle (**Fig. 3.2**). The T3SS releases effector proteins that allow invasion and evasion of the host immune system (9, 27). For example, Tarp protein is released across the host cell membrane after the three step binding process. Once secreted, it is posttranslationally phosphorylated at tyrosine residues. This modification allows it to interact with proteins which in turn activate Rac1, a host protein that recruits actin locally, forcing endocytosis of the bacterium via cytoskeletal rearrangement (28). Once endocytosed, the EB remains encased in a host-derived membrane-enclosed vacuole. This whole unit is known as an inclusion (**Fig. 3.3**).

Once inside the inclusion, the EB turns into an RB, which is larger and metabolically active (7, 29). RBs synthesize proteins that promote proliferation and evasion of the host immune system, with the goal of growing and dividing back into many EBs that can subsequently infect more host cells. Proteins released by EBs early in infection are generated by the RB in advance of differentiation back to EBs. The RB protects itself from destruction by diverting incoming lysosomes (**Fig. 3.4a)** (9, 27). To obtain energy for its new metabolic needs, it intercepts nutrient-packed vesicles on the way to the host cell membrane from the Golgi apparatus (**Fig. 3.4b**). Inclusion membrane proteins (Incs) are an example of effectors that carry out immune evasion and nutrient capture. Embedded into the inclusion membrane, Incs are at the interface between the host cell cytoplasm and inclusion. These proteins can be classified as early, mid, or late cycle Incs, meaning they are expressed at different timepoints in the *Chlamydia* life cycle. Inc *Chlamydia* promoter of survival (CPOS), for example, both captures nutrient vesicles and prevents host lysosome fusion that would otherwise kill the bacteria. It can interact with host RAB GTPase proteins, which regulate vesicle and organelle transport on the cytoskeleton. This allows the inclusion to steal nutrients otherwise meant for the host cell and prevent destructive inclusion-lysosome fusion (28).

Other non-membrane proteins are also important to *Chlamydia* infectivity. These proteins are secreted into the cytosol by the T3SS. For example, the deubiquitinases Cdu1 and Cdu2 use protease activity to remove a protein

degradation tag from the apoptosis-resisting protein MCL1. This prevents MCL1 breakdown, thus reducing the likelihood of apoptosis. Avoiding apoptosis is beneficial to the bacteria because it creates immune system alarm bells known as damage associated molecular patterns (DAMPs) to alert the immune system of a problem. *Chlamydia* protease-like activity factor (CPAF) is a protease that helps *Chlamydia* survive by blocking the movement of host NfkB, a transcription factor made of many proteins, to the nucleus. This prevents inflammation cascades and quells an immune response (28). While these effector protein examples are not exhaustive, they provide a picture of how *Chlamydia* successfully proliferates at the molecular level.

While evading the immune system and stealing host resources, the inclusion moves toward the centrosome, with which it strongly associates (**Fig 3.5**). Here, RBs divide rapidly, transforming back into EBs after several rounds (**Fig. 3.6**) (30). The plethora of EBs, which can infect other epithelial cells, is released by cell lysis (**Fig. 3.7a**) or exocytosis (**Fig 3.7b**), known as "inclusion extrusion" (1, 7, 27). Alternatively, the RBs can enter a state of persistence, where they maintain their size and lie dormant under conditions of stress (27, 31).

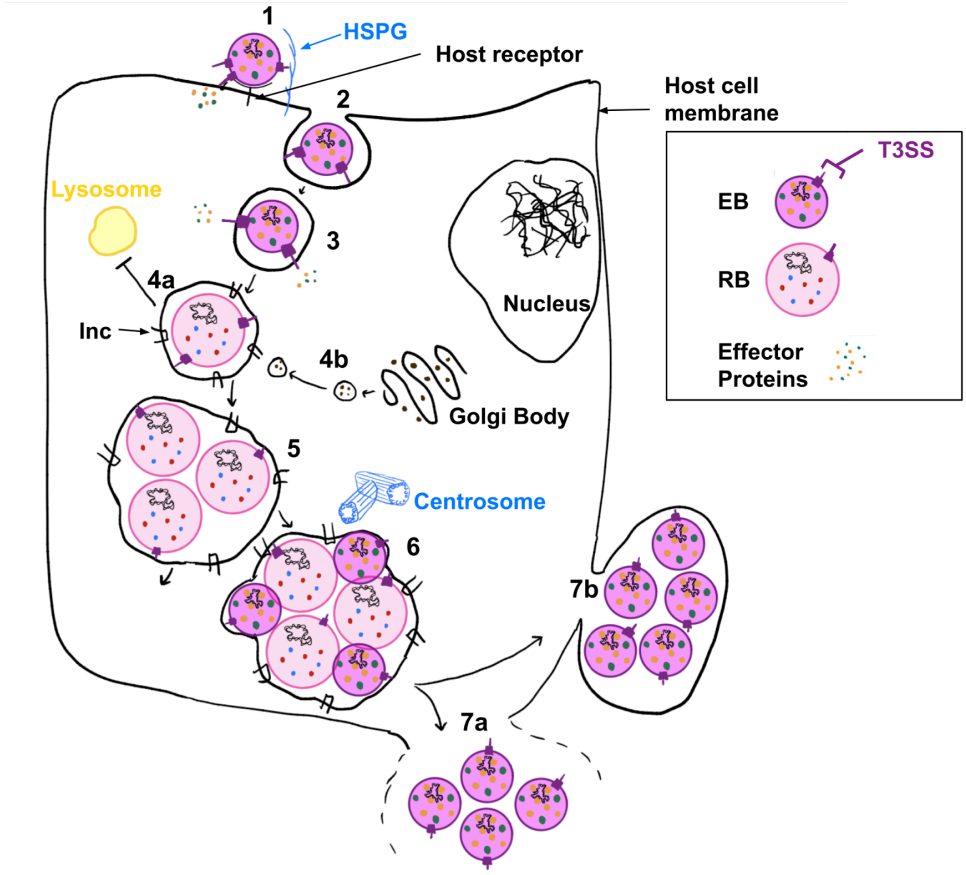

Figure 3. *Chlamydia* biphasic developmental cycle. Step 1: *Chlamydia* binds host cell HSPG with low affinity and host receptor with high affinity. Ejection of preformed effector proteins (orange and green dots) by the T3SS (purple) to remodel host cytoskeleton. **Step 2:** EB is endocytosed by the host. **Step 3:** EB has formed an inclusion. It secretes RB-preformed proteins to manipulate the host. **Step 4:** EB differentiates into an RB. RB effector proteins evade the host immune system. **4a:** Inclusion avoids lysosome (yellow) fusion **4b:** Theft of host nutrient vesicles from the Golgi body (black) for metabolic needs. **Step 5:** Binary fission of RBs and inclusion expansion. **Step 6:** Inclusion migrates to centrosome (blue). RBs begin transition back to EBs after division. During times of low energy supply, persistence occurs. **Step 7:** Exit of bacteria from the host cell by **7a:** apoptosis or **7b:** exocytosis. Drawn by G. Wieselquist with inspiration from Murray and McKay (2021).

4. Tools to Assess *Chlamydia* Infection

Much of what is known about *Chlamydia*, including its developmental cycle, is learned through cell culture and organism models. There are many host options to choose from, as well as strains of *Chlamydia* to infect with. There are also a variety of ways to assess the effects of infection, including tissue pathology assessment, analysis of host immune responses, and bacterial quantification. The following sections will delve into these possibilities and justify the model selected for this work.

4.1 Using a Mouse Model

Studying *Chlamydia* in an organism provides a more representational model of human infection compared with cell or tissue culture. Additionally, the murine female genital tract is highly similar to that of humans, as it contains uterine horns, oviducts, and ovaries that are analogous to the human uterus, fallopian tubes, and ovaries, respectively (**Fig. 4**) (32).

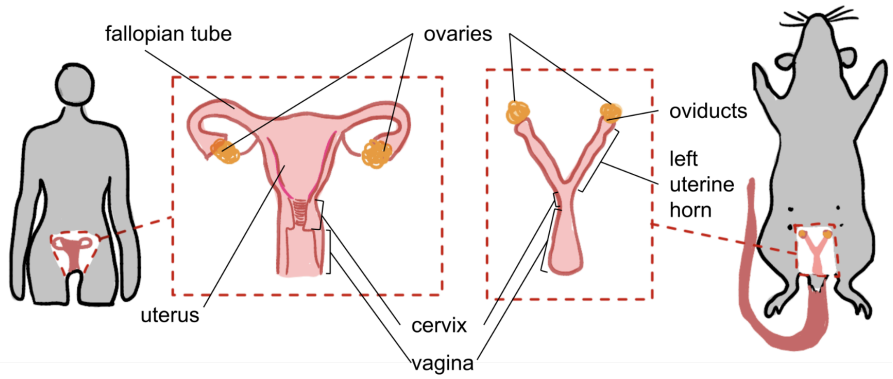

Figure 4. Comparative anatomy of female genital tracts in humans and mice. Tissues are highly similar, including a vagina, cervix, uterus, and two ovaries. Key differences: humans (left) have a wider, non-bifurcated uterus, whereas mice (right) have a bifurcated uterus composed of left and right uterine horns. Human fallopian tubes are proportionally longer in comparison to analogous oviducts in mice. Drawn by G. Wieselquist. Adapted from Chumduri and Turco, 2021.

Additionally, using one inbred strain of mice ensures mice are genetically identical, allowing control over genome-dependent immune responses. To mimic genetic diversity in humans, experiments can be performed on different groups of mouse strains (22).

Like the human menstrual cycle, mice have a hormonal reproductive cycle known as the estrous cycle. During different phases of a four to five day timespan, mouse vaginal epithelium evolves and sheds. Identification of cell types being shed from the vagina and their ratio to each other indicates that the mouse is in one of four stages: proestrus, diestrus, metestrus, or estrus (**Fig. 5**) (33).

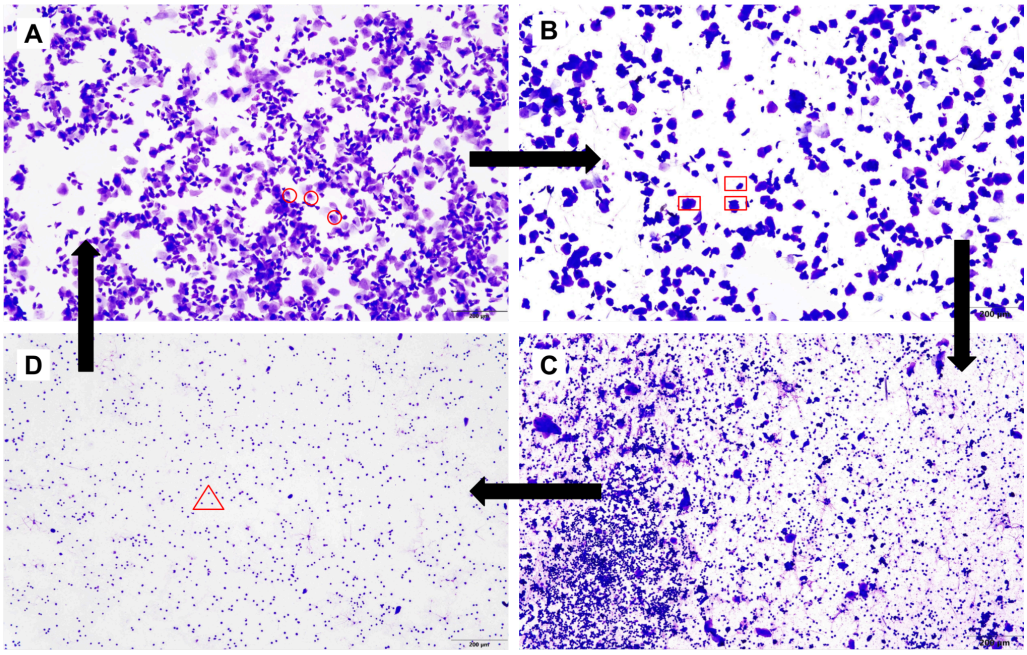

Figure 5. Mouse estrous cycle cellular makeup. Mouse vaginal lavage samples were collected in sterile PBS and dried on glass slides. Slides were stained with crystal violet dye and examined under the microscope to identify cell types for staging. **A:** Proestrus, mostly nucleated epithelial cells (circled) and some cornified epithelial cells. **B:** Estrus, mostly cornified epithelial cells (boxed) and some nucleated epithelial cells. **C:** Metestrus, roughly equal parts cornified epithelial cells, nucleated epithelial cells, and leukocytes. **D:** Diestrus, mostly leukocytes (triangle) with few nucleated epithelial cells and still fewer cornified epithelial cells. Unpublished data from Lijek Lab members: LHB ‘25, AM ‘26, GOW ‘26, MJP ‘26, HN ‘27, & IL’27.

Diestrus is a progesterone-high, estrogen-low phase of the cycle similar to the luteal phase of the human cycle. Depo Medroxy Progesterone Acetate (DMPA) is a synthetic progesterone frequently used by people as a long-lasting injectable contraceptive. It is standard to administer DMPA to mice one week before *Chlamydia* infection to synchronize them in diestrus. This makes mice more susceptible to pathogens, even non mouse-infecting species, which is

valuable when studying the human-infecting *C. trachomatis* (34–40). This standard protocol is helpful because it removes the variable effect of hormones on the immune response, as well (22).

Mice can be infected with *C. trachomatis* or *C. muridarum*, and infection can be via intravaginal or transcervical routes. The former deposits bacterial EBs directly into the vagina, mimicking infection during intercourse. The latter bypasses the cervix to deposit EBs into either uterine horn, assessing questions regarding ascension to the upper genital tract. A so-called intrauterine (or intrabursal) route of infection also exists, a historically more invasive technique where EBs are surgically deposited through the abdomen (41). While no combination of bacterial species and administration route is perfectly representational of human infection, each provides its own helpful nuance and can be selected based on the questions being investigated. *C. trachomatis* is the human-infecting bacterium, therefore any immune responses measured describe responses to the exact pathogen plaguing humans. However, because it has not evolved to a mouse host, it does not reliably induce severe immunopathology seen in some humans. Intravaginal *C. trachomatis* infection rarely causes chronic pathology, and transcervical infection does so only somewhat more frequently (22). In fact, establishing any murine *C. trachomatis* infection requires administration of DMPA (42). Contrarily, infection of mice with *C. muridarum* consistently yields chronic pathology phenotypes such as uterine dilatation, hydrosalpinx, and ovarian edema and deformation (22, 43). This can be achieved

intravaginally, but is more reliable transcervically. While *C. muridarum* is not human-infecting and does not require DMPA pretreatment, it is beneficial to observe the effects of a *Chlamydial* species in its natural host with little hormonal variability (22).

This research will use transcervical infection with *C. muridarum*, because it concentrates on tissue-specific pathology of the upper genital tract. These severe pathologies are expected after *C. muridarum* EB cervical bypass, which is a possible result of natural intravaginal infection.

To ensure that each mouse is cared for and its life is valued, the Institutional Care and Use Committee (IACUC) oversees and approves each experiment for transparency and ethical reasons. An IACUC committee must include a diverse set of opinions, including veterinarian, scientist, non-scientist, and non-institution-affiliated members. The committee reviews rationales for research, protocols, and numbers of mice planned for use. There should be enough mice in a sample size to ensure validity and have control experiments, but not excessive numbers. Additionally, experiments should not duplicate others. Within a mouse lab, researchers are trained in mouse handling to reduce discomfort and recognize distressed mice. Mice are cared for professionally and have regular health checkups (44).

4.2 Immunopathology and Inter-rater Reliability

Because pathology is dependent on *Chlamydia* species and infection route, as well as tissue location and time post infection, a variety of phenotypes can be observed. Pathology scorers should therefore assess tissues using multiple parameters.

During *Chlamydia* ascension in a mouse model, acute inflammatory pathology is exhibited through neutrophil infiltration and edema (**Fig. 6B**). Successful ascension of *Chlamydia* to the upper genital tract can cause chronic immunopathology. Linked to the presence of neutrophils during acute infection, chronic pathology consists of uterine horn dilatation, mucus, oviduct hydrosalpinx, and ovarian edema (**Fig. 6C**) (22, 45–47).

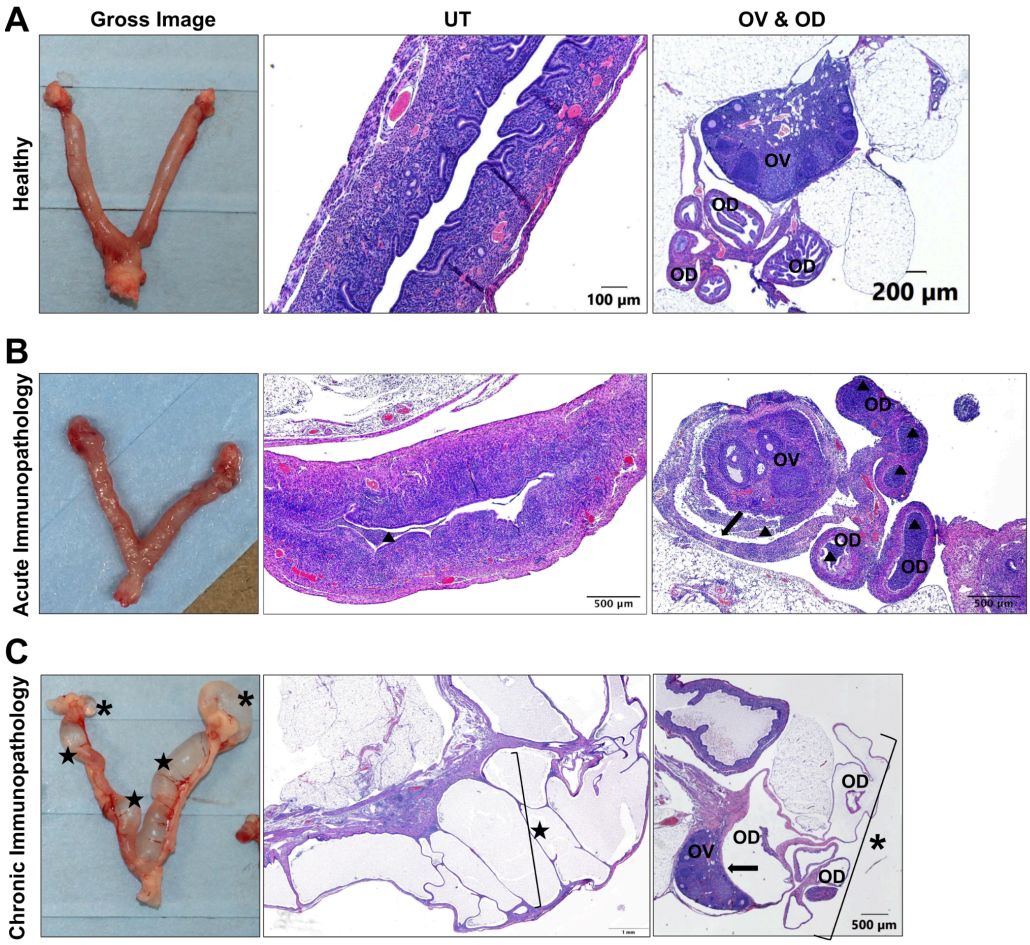

Figure 6. Comparison between healthy mouse upper genital tracts and acute and chronic immunopathology resulting transcervical *C. muridarum* infection. Upper genital tracts were excised and imaged for gross pathology prior to formalin fixation. Fixed tissues were paraffin embedded, H&E stained, sectioned, and mounted onto slides. **A:** Healthy upper genital tract. Uterine horn (UT) lumen is clear of mucus and neutrophils and is not dilated. Ovaries and oviducts (OV & OD) are free of cells and show no edema. **B:** Upper genital tract at 9 days post infection (gross image) and 7 days post infection (UT and OV & OD cross sections). The uterine horn is not dilated but neutrophils are present (triangle). The ovarian bursa is swollen (arrow) and thickened and ovaries and oviducts are infiltrated with neutrophils (triangles). **C:** Upper genital tract at 51 days post infection. Uterine horn is significantly dilated (stars) and visible in gross imaging and under microscope (note the larger scale bar). Light purple shade in lumen indicates mucus. Hydrosalpinx (asterisks) presents as glassy spheres in the gross image and dilated tissue under microscope. Ovary is

deformed (arrow) due to edema. Figure generated from images taken by Lijek Lab members: AF ‘25, AM ‘25, GOW ‘26, HN ‘27.

Previous studies have employed multiple scales for assessing these tissue and time-specific effects, which allows a more nuanced understanding of infection. For example, Chen et al. (2014) assessed uterine horn dilatation separately from oviduct hydrosalpinx. The latter was scored on a scale of 0-4, where 0 represents a healthy oviduct and 4 represents severe hydrosalpinx. Tissues were assigned scores based on the relative size ratio of the oviducts to the ovary, with larger ratios indicating higher severity (48, 49). Scoring these phenotypes separately makes it possible to represent tissue-tropic effects.

These scoring systems are subjective and must be assessed for their robustness (23). Inter-rater reliability is a measure of how consistently individual pathology scorers assess tissues based on their predetermined scale. It can be calculated in a variety of ways and is used to regulate training of pathologists in critical cases such as diagnosis of life-altering medical conditions (24, 50). During experimentation, inter-rater reliability statistically affirms that results are reliable.

The simplest and oldest calculation for inter-rater reliability is known as the percent agreement method, which compares the responses of scorers to each other to assess how often they are perfectly in consensus (**Eq. 1**). For example, if two scorers assessed ten uterine horn sides for dilatation and their answers matched for nine, they would have a ninety percent agreement. While this is a commonly accepted method, it does not take into account when data is on a scale

and is therefore somewhat harsh in that only exact matching scores, not similar scores, contribute to a higher calculated reliability. It is also simplistic in that it does not account for chance agreement (24).

$$\text{Inter-rater reliability} = \frac{\#\ of\ ratings\ matching\ each\ other}{\#\ of\ total\ ratings} \times 100\%$$

or

$$\text{Inter-rater reliability} = 100\% - \frac{\#\ of\ disagreements}{\#\ of\ total\ ratings} \times 100\%$$

Equation 1. Percent agreement method. Numerator represents the number of times scores of two raters exactly match. The denominator is the number of variables scored.

Despite the importance of inter-rater reliability, it is often not reported in the *Chlamydia* pathology field, or in mouse model pathology literature in general. This demonstrates a gap that can be viewed as an opportunity to improve the reliability of immunopathology research. The intraclass correlation coefficient (ICC) is a widely accepted measure of inter-rater reliability during clinical sample evaluation (51–53). It functions by assessing how much the variance, or spread, of scores assigned to each sample is due to the experimental condition of that sample (the experimental goal is to test this) versus how much this variance is attributed to scoring differences between scorers (50). In the context of a mouse model, the sample being scored is a mouse tissue (**Eq. 2**).

$$ICC = \frac{\sigma_b^2}{\sigma_b^2 - \sigma_w^2} = \frac{variance\ between\ mice}{variance\ between\ mice\ - variance\ of\ scores\ within\ one\ mouse}$$

Equation 2. Intra-class correlation coefficient. σ_b^2 , variance between groups (scores of different mice). σ_w^2 , variance within a group (scores for one mouse from different scorers).

As is demonstrated by the formula, the more variance there is between scores assigned to one mouse (σ_w^2), the larger the denominator becomes, and the lower the resulting ICC (**Eq. 2**). The following table describes the quality of inter-rater reliability for given ICC values (**Table 1**).

ICC < 0.5	0.5 < ICC < 0.75	0.75 < ICC < 0.90	ICC > 0.90
poor reliability	moderate reliability	good reliability	excellent reliability

Table 1. Range of Intra-class correlation coefficient and reliability ranges.

No matter the magnitude of variance between different mice, the ICC remains excellent as long as there is little to no variance between scorers. An ICC=1 means that all variance between mice comes from differences in the mice themselves, not the variance between scores. Contrarily, increasing variance between scores is associated with decreasing ICC and inter-rater reliability values (**Fig. 7**) (50).

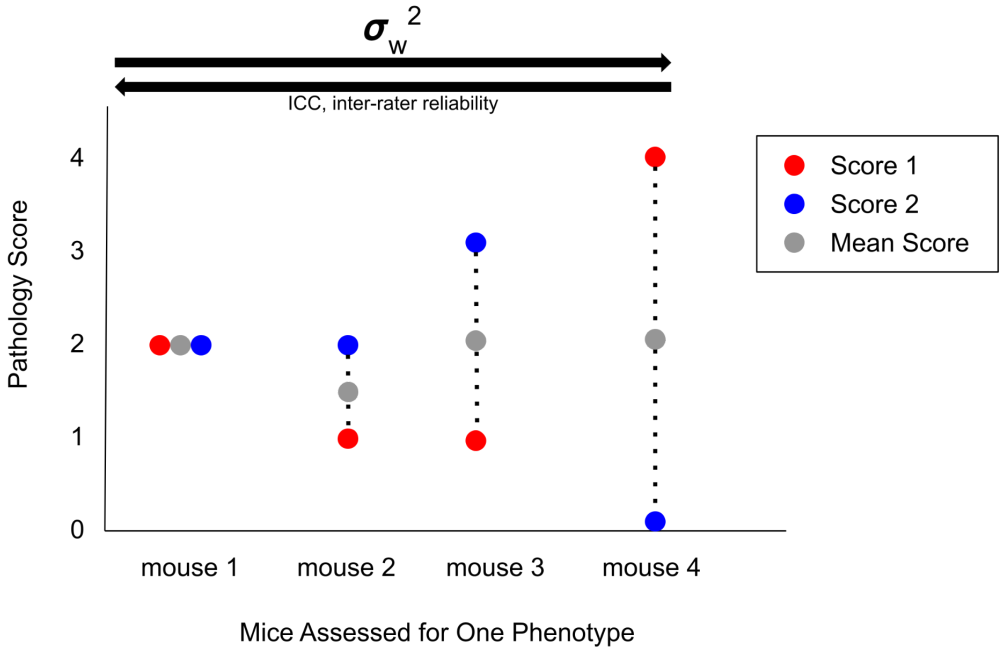

Figure 7. Example dataset of pathology scores to describe the intra-class coefficient (ICC). Pathology score (y-axis) can theoretically depend on two variables: mouse (x-axis) or pathology scorer (red and blue circles). The former dependence is desirable and is the goal of experimental testing. The variance of two pathology scores from their mean (grey circle) demonstrates increased effects of the pathology scorer variable on the pathology score dependent variable. Moving from mouse 1 to mouse 4, variance between scores increases, therefore decreasing the ICC and inter-rater reliability. Note that the mean value between scores is not used in practice to determine overall pathology score, but is rather used as a tool of calculation for inter-rater reliability.

The ICC can be applied to a whole dataset of all tissues assessed for all phenotypes during an experiment. This provides a quick and general inter-rater reliability and can be done with ease using a coding program, which drastically improves efficiency and removes human calculation error. Furthermore, it can also be individually applied to each phenotype assessed during an experiment whether specific scales need improvement. Improvements can be made by having

involved, hands-on, discussions that encourage questions, opinions, and two-way conversation.

The best practice for pathology assessment uses anonymized scoring: scorers are not allowed to see the experimental condition of the tissue they are assessing, such as whether a tissue was infected or not, nor are they allowed to see other scorer's assessments until they have finalized their own scores. This eliminates potential scorer bias (23).

The Lijek Lab previously relied on external professional scoring and recently transitioned to scoring by lab members internally. This research explores various methods of inter-rater reliability assessment to generate a system for the lab, ensuring pathology scoring results are reliable. It employs these assessments on new experiments involving immunopathology and training new lab members on pathology scoring. Training requires a reliable process so scoring is standardized across generations of members, which further emphasizes the value of developing a way to assess reliability.

4.3 Quantification of Bacteria

There are multiple ways to quantify *Chlamydia* infecting the genital tract. One such way is bacterial burden analysis, which uses quantitative polymerase chain reaction (qPCR) to amplify the bacterial 16S ribosomal gene and compare it to the constitutively expressed host glyceraldehyde 3 phosphate dehydrogenase (GAPDH) gene. This analysis is highly useful and shows how many *Chlamydial*

genome copies are present (48). This research will employ both bacterial burden to quantify the bacterial load during transcervical *C. muridarum* infection.

5. *Chlamydial* Putative Cytotoxins Play a Role in Infection and Pathogenesis

Despite extensive research on immunopathology during *Chlamydia* infection, its exact cause remains unclear. One effector protein of interest in the pathogenesis of *C. trachomatis* is CT166, which is encoded in the genetic region known as the plasticity zone (PZ), so named for its variation across serovars and species of *Chlamydia*. CT166 has homology to well-characterized large cytotoxins (LCTs) of *Clostridioides difficile*, a bacterium which infects the gastrointestinal tract (54). *Clostridial* LCTs contain a glucosyltransferase domain responsible for cytotoxicity, which induces apoptosis or cytoskeletal rearrangement in the host cell. The latter disrupts cellular structure, causing rounding and loss of viability. LCTs achieve both cytotoxic effects by transferring a glucose molecule to essential host enzymes. The targeted host proteins belong to the Rho-GTPase family, which regulates the cytoskeleton, and Ras-GTPase family, which regulates the cell cycle. They are active when bound to GTP and modified by LCTs in their inactive GDP-bound form. The glucosyltransferase domain of the cytotoxin cleaves glucose from UDP-glucose or N-acetylglucosamine using a conserved DXD motif (**Fig. 8**), then transfers the sugar to host GTPases at two threonine residues (55, 56). Whereas GDP-bound Rho proteins cycle between the cytosol and membrane, LCT-modified Rho

proteins remain localized to the membrane. Additionally, glucose prevents GTP switching and subsequent activation, as well as binding to downstream effector proteins (57). This immobilization and stabilization of the inactive state renders the GTPases unable to activate downstream pathways of either actin polymerization or cell cycle progression. This causes actin depolymerization and subsequent rounding, or apoptosis, respectively (55).

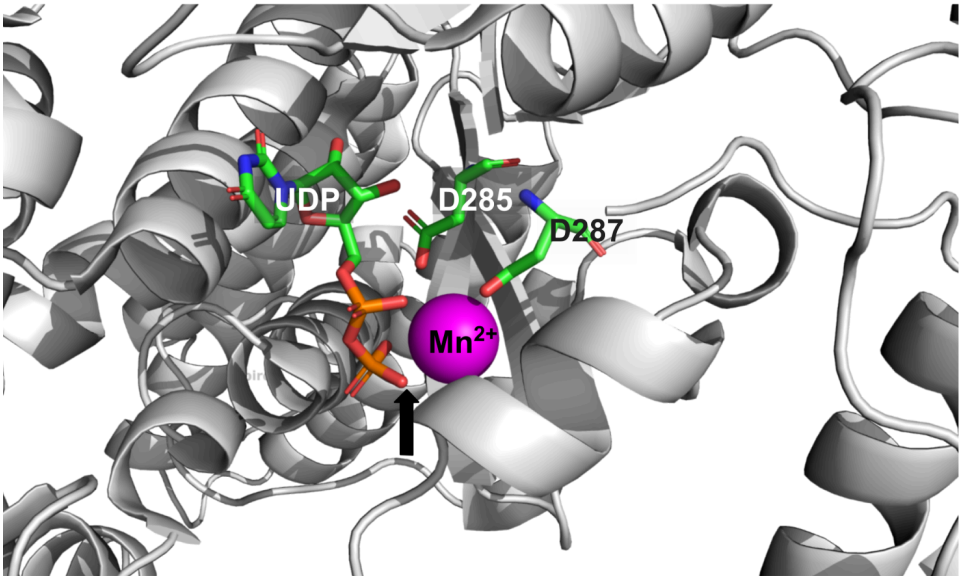

Figure 8. Active site of TcdA. The DXD motif includes aspartate residues 285 and 287 (labelled). Active site and substrate uridine diphosphate (UDP) coordinate with a manganese ion (pink). Black arrow indicates the attachment point where glucose would bond the diphosphate backbone (orange and red) of UDP to create UDP-glucose. Figure generated in PyMol using structure solved by Malito et al. (2012) (56).

Chlamydia putative cytotoxins exhibit sequence conservation with *Clostridioides* LCTs, though the protein is conserved to different extents depending on the serovar or species of *Chlamydia*, and truncations of key UDP-glucose-binding and DXD-containing glucosyltransferase domains render it

nonfunctional in the L2 serovar. However, in both *C. trachomatis* and *C. muridarum,* these domains are present. *C. trachomatis* serovar D contains four homologous ORFs: CT165, CT166, CT167, and CT168, but CT166 is the only sequence with cytotoxic domains (54). In *C. muridarum*, there are three conserved ORFs: Tc0437, Tc0438, and Tc0439, each of which is homologous to *C. difficile* cytotoxins (**Fig. 9**).

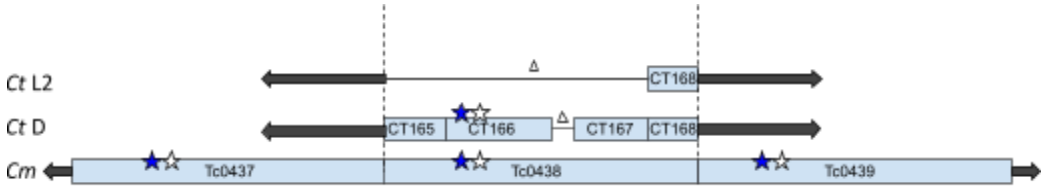

Figure 9. Conservation of potential cytotoxic domains within the plasticity zone across *Chlamydial* serovars and species. Open reading frames (ORFs) with homology to *C. difficile* cytotoxins are boxed and labelled in blue. Black arrows show continuation of the plasticity zone beyond cytotoxin-homologous regions. Dashed lines mark the borders of cytotoxin homology. Delta symbols indicate absence of nucleotides where the cytotoxin has been truncated. Blue star represents UDP glucose domain and white star represents glucosyl transferase domain, only present in *C. trachomatis* serovar (*Ct* D) CT166 and *C. muridarum* (*Cm*) Tc0437-Tc0439, in contrast to *C. trachomatis* serovar L2 (*Ct* L2). Adapted from Belland et al. (2001) (54) and Berclaz et al. (2025) (48).

The cytotoxic domains are phenotypically important for both *Clostridioides* cytotoxins and *Chlamydia* putative cytotoxins. Thalmann et al. (2010) demonstrated that uninfected and *C. trachomatis* serovar L2-infected cells exhibited no cell rounding compared with *C. trachomatis* serovar D and *C. difficile* cytotoxin TcdB treated cells (**Fig. 10**), emphasizing the importance of the UDP-glucose binding domain and glucosyltransferase domains in cytotoxicity and a similar mechanism of action between CT166 and TcdB.

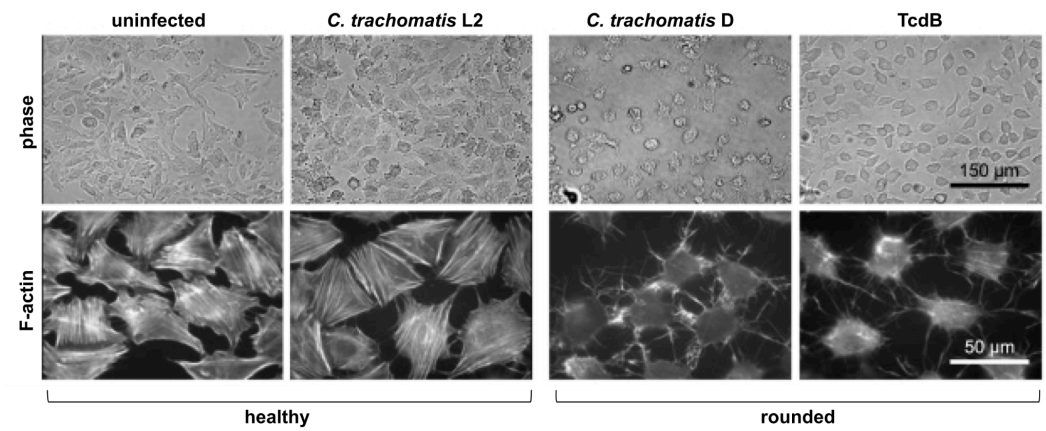

Figure 10. Cytotoxic rounding occurs in *Ct* D- and TcdB-infected cells, but not *Ct* L2 infected cells. Cells were mock infected or infected with *Ct* L2, *Ct* D, or TcdB. Top row images use phase contrast microscopy, bottom row depicts the actin cytoskeleton. Cells remain healthy (left two columns) when mock infected or infected with *Ct* L2. Cells round and lose their shape when infected with *Ct* D or TcdB cytotoxin. Adapted from Thalmann et al. (2010) (58).

Additionally, Thalmann et al. (2010) showed that cells expressing CT166 with a DXD → AXA double point mutation showcased less actin reorganization and less cell rounding than those expressing wild type CT166. Furthermore, cells expressing CT166 mutant were temporarily protected during *C. difficile* TcdB and *C. trachomatis* serovar D infection, because they did not exhibit rounding (**Fig. 11**) (58). Taken together, this demonstrates that loss of the DXD motif prevents chemical glucosylation of host GTPases and therefore prevents their inactivation and resulting cytotoxic cell rounding. However, the mutation does not prevent CT166 mutant binding of the GTPases, which acts protectively against wild type cytotoxin encountered during serovar D infection or TcdB treatment.

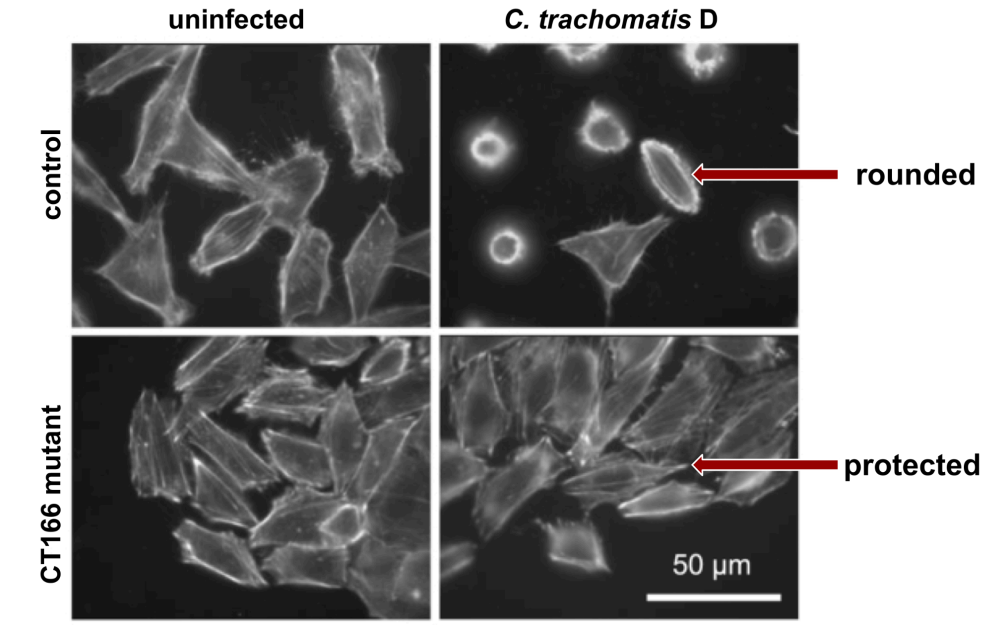

Figure 11. CT166 mutant expression protects from cytotoxic cell rounding. Overexpression of CT166 mutant was induced in HeLa cells. Control cells rounded during infection by *C. trachomatis* serovar D, whereas CT166 mutant-expressing cells remained comparable to healthy uninfected cells. Adapted from Thalmann et al. (2010) (58).

It follows that glucosylation targets of CT166 are similar to those of *C. difficile* LCTs: cytoskeleton regulators Rac1 GTPase, RhoA GTPase, and Cdc42 GTPase, and the cell cycle regulator Ras GTPase. Cells pretreated with functional Rac1 mutant followed by CT166 exhibited reduced rounding compared to wild type Rac1, demonstrating that Rac1 is a CT166 target (58). Another study from Bothe et al. (2015) confirmed this, demonstrating that levels of unglucosylated Rac1, as well as RhoA, Cdc42, and Ras, were reduced in wild type CT166-expressing cells compared to control and mutant CT166-expressing cells (**Fig. 12**). Further evidence supporting Ras glucosylation is that cells infected with

CT166 mutant were more likely to be in S or G2 phase of the cell cycle, indicating division, compared to wild type CT166 treatment (59).

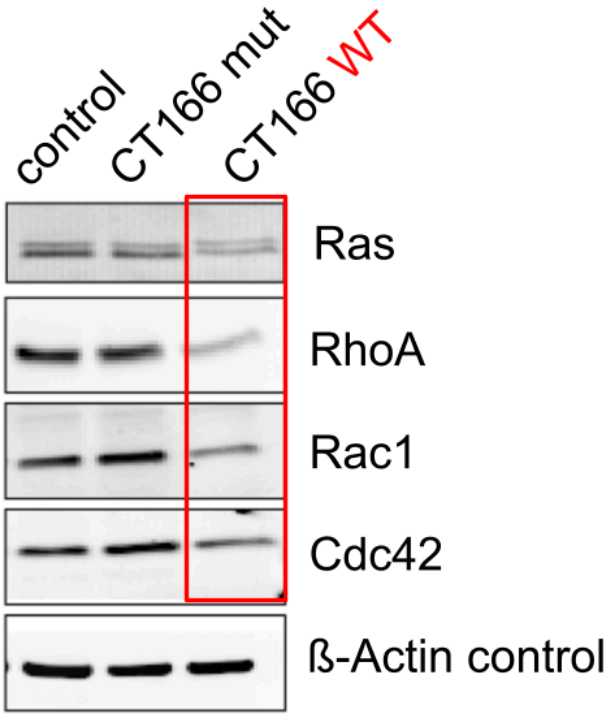

Figure 12. CT166-expressing cells have lower levels of unglucosylated Ras, RhoA, Rac1, and Cdc42 GTPases. Overexpression of CT166 mutant (CT166 mut) and wild type (WT) CT166 was induced in HeLa cells. Non-glucosylated proteins were quantified via Western blot. Red box highlights reduced levels of non-glucosylated GTPases in CT166-expressing cells. Bottom row shows consistent ß-Actin control expression. Adapted from Bothe et al. (2015) (59).

Another study from our lab by Berclaz et al. (2025) completely deleted the three cytotoxin-homologous ORFs from the *C. muridarum* strain, replacing them with a reporter gene for detection and antibiotic resistance gene for selection. The new strain was named Δtox (**Fig. 13**). This study removed the possibility of mutation-caused conformational changes that would be confounding variables in

attenuation of cell rounding. Unlike previous studies, the removal of the three ORFs did not prevent cell rounding of HeLa cells (48).

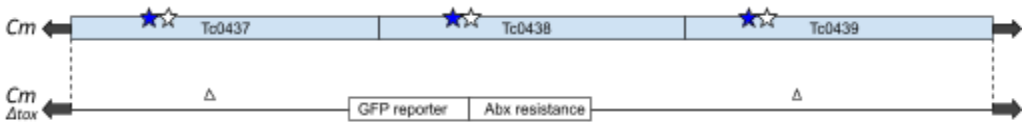

Figure 13. Genome of wild type *C. muridarum* compared with that of modified Δtox *C. muridarum*. Black arrows show continuation of the plasticity zone beyond the cytotoxic region. Blue regions represent ORFs with homology to *C. difficile* cytotoxins. White Green Fluorescent Protein (GFP) Reporter and antibiotic resistance regions allow for detection and selection of altered strain, respectively. Blue star represents UDP glucose domain and white star represents glucosyl transferase domain. Delta symbols indicate absence of nucleotides.

Despite the information mutation and deletion of genes can provide in cell culture, they are not representative of what occurs in an organism, especially because the cell lines used are cancerous. Cancerous cells inherently have dysregulated immune function. Therefore, testing the presence of cytotoxin in an organism model will provide more representative information about what would occur in human *C. trachomatis* infection.

The study by Berclaz et al. (2025) mentioned above used a mouse model to address this. Mice were infected transcervically with WT *Cm*, Δtox *Cm*, and tox^{rep}, a positive control of Δtox with the complemented strand of the deleted Tc0437-Tc0439 ORFs added back. Seven days post infection, an acute time point, there were no differences in pathology or bacterial burden in the upper genital tracts. At the chronic timepoint of 51 days post infection there were also no bacterial burden differences between strains, but there were significant differences

in chronic pathology. Mice infected with Δtox *C. muridarum* had greatly reduced incidence and severity of hydrosalpinx compared with wild type and tox^{rep} *C. muridarum* (**Fig. 14**), indicating that Tc0437-Tc0439 and likely the homologous CT166 play a role in the chronic immunopathology that is so dangerous in humans.

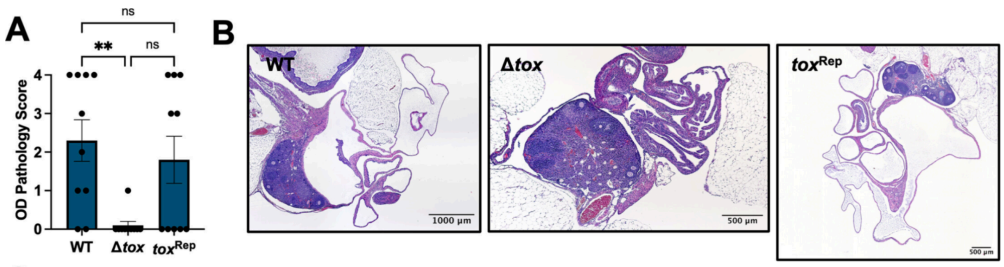

Figure 14. Hydrosalpinx is attenuated when the cytotoxic-homologous region of *C. muridarum* is deleted. Mice were infected transcervically with wild type (WT), Δtox, and tox^{rep} *C. muridarum*. Upper genital tracts were excised and fixed in formalin. Fixed tissues were paraffin embedded, H&E stained, sectioned, and mounted onto slides prior to pathology assessment under the microscope. **A:** Numerical pathology score for oviduct hydrosalpinx for each strain. **B:** Representative images of oviducts for each strain. Oviducts in Δtox infected mice are healthy, whereas oviducts infected with strains containing Tc0437-Tc0439 exhibit severe hydrosalpinx. Taken from Berclaz et al. (2025) (48).

6. Host Immune Response

It is helpful to understand the immunology of the host response in general before delving into the *Chlamydia*-specific host immune response and how *Chlamydia* evades this response. The host immune response to any pathogen is broken into two categories: innate and adaptive. The innate response is the immediate and unspecific response to pathogens, whereas the adaptive response is a delayed, specific reaction after the immune system has learned to recognize

antigens unique to that pathogen. The adaptive immune system is controlled by lymphocytes known as B and T cells. Both innate and adaptive responses have components of cell-mediated and humoral immunity. The former is the response driven by cells, namely innate immune cells and T cells. The latter is the fluid-based response driven by the innate complement system, mucous barrier components, and antibodies produced by B cells.

6.1 Innate immunity

The innate first line of defense uses barriers to defend the body. Barriers are interface surfaces between the host, or "self," and the outside world, which contains "non-self" potential pathogens. Barriers include the skin; mucosa of the respiratory, gastrointestinal, and urogenital tracts; and secretory gland ducts such as the salivary, lacrimal, and mammary glands. Mucus-lined barriers are coated with a viscous mucus that has both physical and chemical protective functions. The vagina is a mucus-lined barrier (**Fig. 15**). Mucus keeps tissues moist and provides a home for commensal bacteria, such as the *Lactobacilli* that make up the majority of bacterial species in the vagina. During invasion, mucus can trap pathogens with its thick, gel-like properties. This characteristic is made possible by mucins, which are highly glycosylated proteins; this carbohydrate saturation makes mucins sticky. Mucus also contains antimicrobial proteins and peptides that kill pathogens. Antimicrobial peptides are cysteine-rich and either cationic or amphipathic, allowing them to bore holes into the phospholipid bilayer of

pathogens. They then enter pathogens and disrupt fundamental processes such as transcription of DNA and translation of mRNA into protein within the pathogen. This disturbance of the central dogma results in pathogen death. Mucus also contains IgA antibodies which are proteins that recognize specific pathogens and help the immune system destroy them (60). At the base of the mucus is a layer of host epithelial cells. These cells are sealed together with tight junction proteins such as claudin and occludin (61, 62).

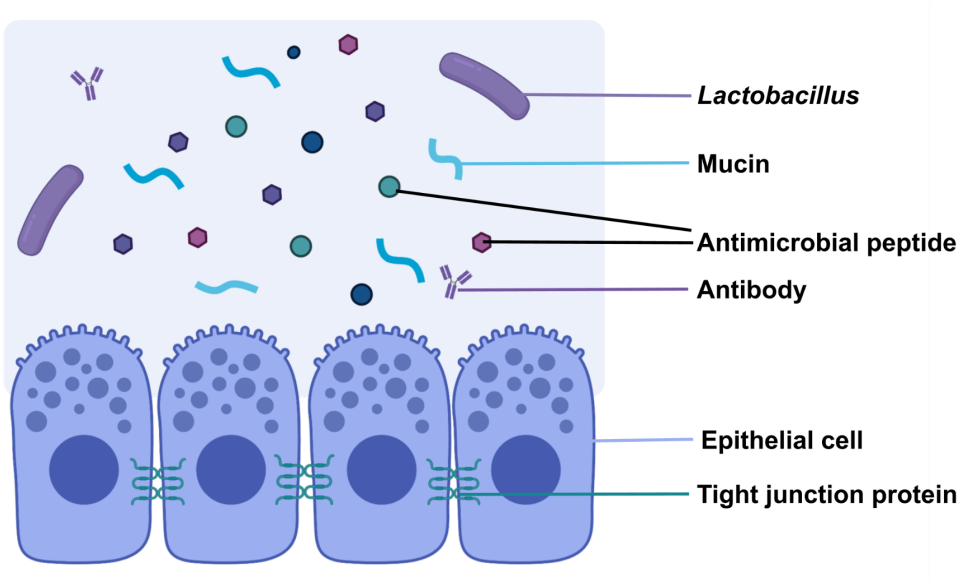

Figure 15. Mucus-lined epithelium of the vagina. Mucus, rich with a variety of proteins and commensal bacteria, lines vaginal epithelial cells. Epithelial cells are sealed with tight junction proteins. Created with BioRender.

In order for pathogens to infect the host, barriers must first be broken. The inflammatory response is the host's reaction to a breached barrier, wherein capillaries and epithelial cell junctions become more permeable to increase local access to cellular and humoral components of immunity. Presenting with

symptoms such as heat, erythema, edema, pain, and loss of function is indicative of the inflammatory response (62).

With the arrival of innate immune cells (cellular component of immunity), the host can interact with the pathogen and recognize invasion. Innate immune cells include monocytes, macrophages, granulocytes (an umbrella term for neutrophils, basophils, mast cells, and eosinophils), dendritic cells, and natural killer cells. These cells have a variety of functions. One function is phagocytosis, meaning the cells engulf and digest pathogens. Phagocytes include macrophages (which differentiate from monocytes), neutrophils, mast cells, eosinophils, and dendritic cells. A second function is carried out by granulocytes, which contain cytoplasmic granules composed of proteins responsible for attacking pathogens, remodelling infected tissue, and regulating other immune cells. Attached to innate immune cells are pattern recognition receptors (PRRs). PRRs have specificity to pathogen associated molecular patterns (PAMPs), molecules that act as unique pathogen signatures. Depending on the PRR that binds a PAMP, a specific signal transduction cascade in the host will result. Upon PAMP-PRR binding, the intracellular signalling domain of the PRR binds an adaptor molecule. This activates transcription factors that induce expression of genes that are helpful in responding to infection, such as signalling molecules, antimicrobial peptides, and apoptosis-inducing genes.

Complement is part of the innate humoral immune response. Complement is a system of proteins in the blood sera. Complement proteins can opsonize

proteins for phagocytosis, upregulate inflammatory signal cascades within cells, and punch holes into pathogen membranes using the membrane attack complex (MAC), which is formed through multimerization.

The immune system is a complex network that spans the entire body. To coordinate a targeted, efficient response to local infections, communication is imperative. Cytokines are signalling molecules that tailor responses by altering many properties in a target host cell. These include: immune cell differentiation, membrane adhesion, enzyme expression, and apoptosis induction. Chemokines are a subclass of cytokines that drive cell movement in a certain direction. Cytokines are mostly produced by helper T cells, dendritic cells, and macrophages. Responses driven by cytokines are incredibly complex. Some cytokines will amplify the effects of others, while some antagonize each other. Additionally, the same cytokine may exhibit pleiotropic action, where it induces different effects binding two different targets. While inflammatory cytokines are beneficial in recruiting immune cells to the site of infection, an overactive immune response can induce immunopathology, or tissue damage resulting from the immune response.

6.2 Antigen Presentation & Adaptive Immunity

The bridge between the innate and adaptive immune responses is antigen presentation. Antigen presenting cells (APCs) such as dendritic cells and macrophages “teach” T cells by presenting a piece of pathogenic antigen to them.

B cells can also present antigen specifically to one class of T cells. All nucleated cells present endogenous antigens on exposed cell membrane glycoproteins called major histocompatibility complex class I (MHC I), which are composed of alpha glycoprotein and beta protein chains. Exogenous pathogen antigens are only presented by APCs on MHC class II molecules, which are made of two glycoprotein chains.

Before presentation, antigen processing occurs (**Fig. 16**). Within the cell, variations of MHC molecules associate with antigen based on affinity of the antigen to the MHC binding groove anchor residues. Variation in residues provides variation in antigens being presented. During MHC Class I presentation (**Fig. 16A**), endogenous antigen is degraded by host proteasomes and associated with MHC I molecules at the rough endoplasmic reticulum with the assistance of host chaperones. The complex of proteins is sent to the Golgi apparatus followed by the cell membrane via vesicular transport along the cytoskeleton.

During MHC Class II presentation (**Fig. 16B**), an exogenous antigen is phagocytosed and degraded when the phagosome associates with a host lysosome. After the MHC II molecule has been sent to the membrane from the Golgi, the antigen and MHC II associate and are displayed on the host cell membrane.

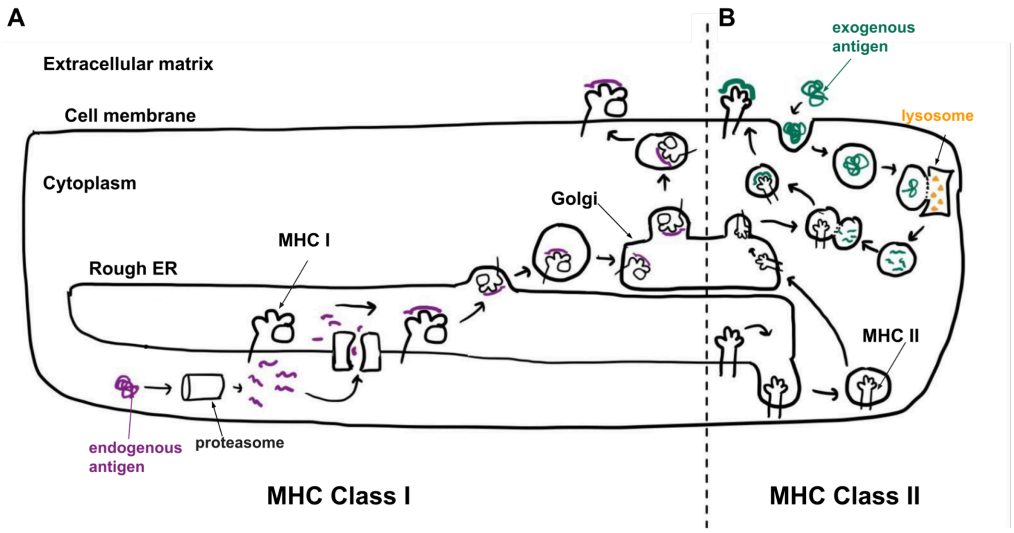

Figure 16. Antigen processing of endogenous antigen (MHC Class I, A) and exogenous antigen (MHC Class II, B). A: The MHC Class I pathway begins with endogenous antigen (purple) breakdown by proteasomes. Antigen associates with MHC I at the rough ER, then buds off, travels to the Golgi body, and buds off once more to remain at the cell membrane. **B:** The MHC Class II pathway begins with endogenous antigen breakdown by lysosome fusion, followed by MHC II association, which has travelled from the ER and Golgi body. The associated complex travels to the cell membrane. Drawn by G. Wieselquist.

T cells can recognize antigen displayed on MHC I and MHC II molecules (**Fig. 17**). T cell receptors (TCRs) are randomly generated and will have affinity for various antigens. If recognition occurs between the TCR and antigen, the T cell will become active and proliferate to form many other T cells that are specific to the antigen that triggered proliferation in the first place. There are two classes of T cells. The first are known as cytotoxic T cells, or CD8+ T cells, because they have a CD8 coreceptor protein. The second class is helper T cells, or CD4+ T cells.

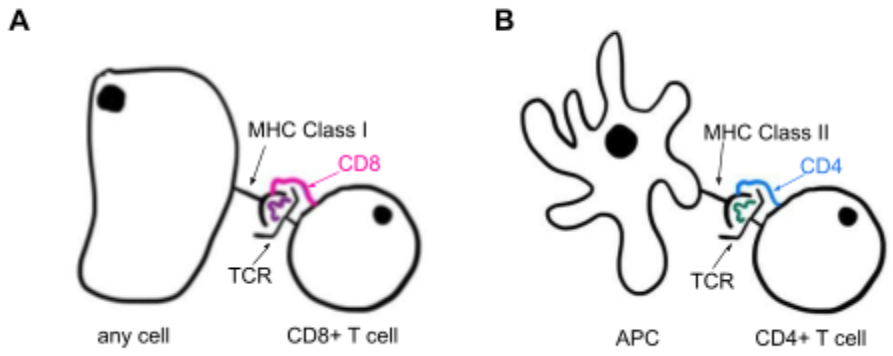

Figure 17. Antigen presentation. A: Presentation of endogenous antigen (purple) to a CD8+ T cell. **B:** Presentation of exogenous antigen (green) to a CD4+ T cell. Drawn by G. Wieselquist.

Recognition requires not only antigen-TCR interaction, but rather three signals: avidity, costimulatory receptor/ligand interaction, and cytokine signalling (**Fig. 18**). The first signal, avidity, is a the sum of two cell-cell interactions: (1) The TCR binds antigen presented on MHC, and (2) CD4 or CD8 coreceptor proteins bind the MHC glycoprotein itself. The CD8 coreceptor binds MHC Class I, so CD8+ T cells can be activated by professional APCs or any other cell (**Fig. 17A**). The CD4 coreceptor binds MHC Class II, so CD4+ T cells can be activated only by professional APCs (**Fig. 17B**). The second signal required for recognition comes from costimulatory receptor-ligand binding. The final signal is that of cytokines. These can be secreted by the T cell itself (autocrine cytokines) or the antigen presenting cell (paracrine cytokines) after signal cascade induction from the first two signals. These cytokines stimulate the T cell to divide. Polarizing

cytokines also determine the fate of the T cell as it differentiates and divides. Throughout this process, anchor proteins stabilize cell interactions further.

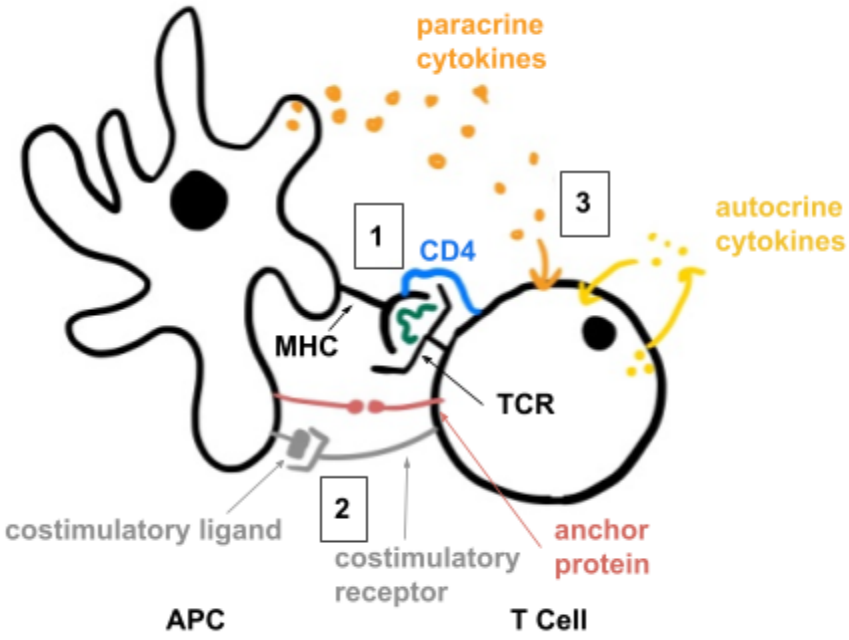

Figure 18. T cell activation. 1: Avidity. MHC presenting antigen (green) binds TCR. Coreceptor (blue) stabilizes interaction. **2:** Costimulatory receptor-ligand binding (grey). **3:** Cytokine signalling (orange and yellow). Drawn by G. Wieselquist.

Activated T cells can recognize pathogens. CD4+ T cells coordinate responses of innate immune cells, CD8+ cells, and B cells by secreting cytokines to direct their movement. CD8+ T cells fight pathogens directly by secreting cytotoxic granules to kill them (62).

B cells have a different function than T cells. The role of B cells is to release B cell receptors (BCRs) from the cell membrane to target pathogens. B cell receptors (BCRs), also known as antibodies when secreted, are

immunoglobulin (Ig) proteins of varying classes (**Fig. 19**). Antibodies are made of two peptide chains, one larger (heavy chain) and one smaller (light chain). These chains are linked by disulfide bridges between cysteine residues to form a "Y" shape. In its folded quaternary structure, the base of the "Y" is the constant region and the tips of the opening of the "Y" are the variable region. The constant region interacts with immune components such as cells and complement. The variable region can take on many forms which increases the number of possible antigens that it can detect. Variability in both regions is determined by genetic recombination, where the DNA encoding portions of the light and heavy chains is rearranged before expression. Antibodies can also be divided into Fab (top half) and Fc (bottom half) regions (62).

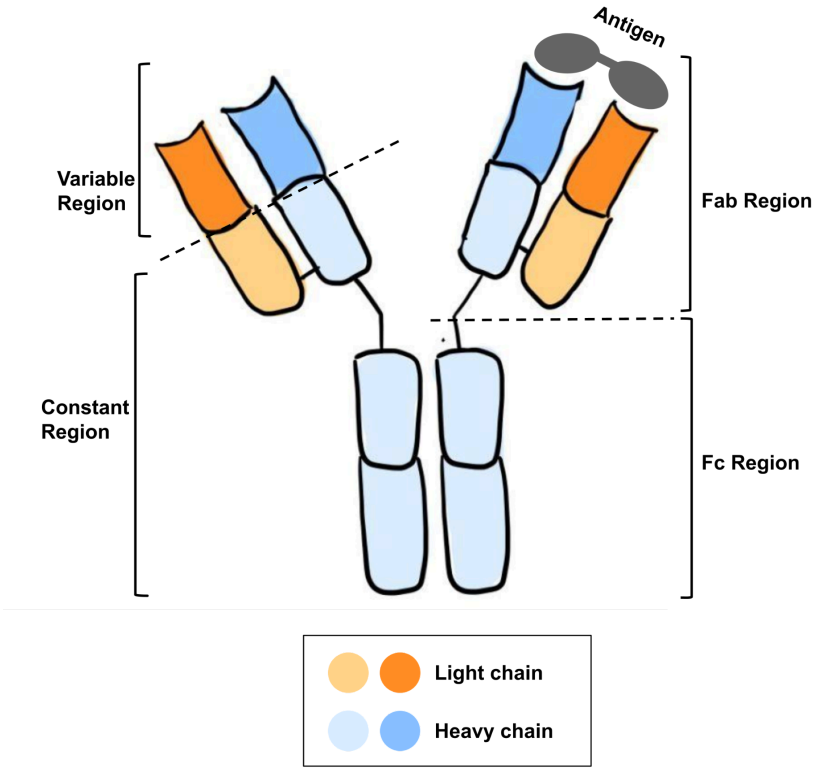

Figure 19. Schematic of an antibody. The heavy chain is shown in blue, the light chain in orange. Dashed lines mark boundaries between variable and constant regions, as well as Fab and Fc regions. Drawn by G. Wieselquist.

There are five isotypes of antibodies, determined by the constant region of the heavy chain. This work will focus on IgG, predominantly found in the blood, and IgA, the most abundant isotype in secretions and mucosal barriers (63). Both IgG and IgA can be found in the mucosa, making them important for clearing genital tract infection. IgA can gain access to the mucosa through transcytosis, which uses a polyIg receptor to cross through epithelial cells (21, 62). IgG can localize to the mucosa via exudation, where it leaks from permeable blood vessels

during an inflammatory response (62).

Once released, antibodies can perform four functions: neutralization, opsonization, complement fixation, and antibody-dependent cell-mediated cytotoxicity (ADCC) (**Fig. 20**). In all cases, antibodies bind pathogens via their Fab region and immune cells or proteins via their Fc region. Opsonization is when antibodies bind pathogens and phagocytes, localizing the phagocyte to the "appetizing" pathogen nearby, thereby encouraging phagocytosis. During neutralization, antibodies bind a PAMP of a pathogen. This prevents the pathogen from invading host cells via receptor-mediated endocytosis after PAMP-PRR binding. During complement fixation, antibodies bind pathogenic antigen and complement proteins simultaneously, allowing the complement system to bore holes into the pathogen. ADCC is when antibodies tag pathogens for recognition by natural killer cells, which secrete cytotoxic materials to destroy the pathogen.

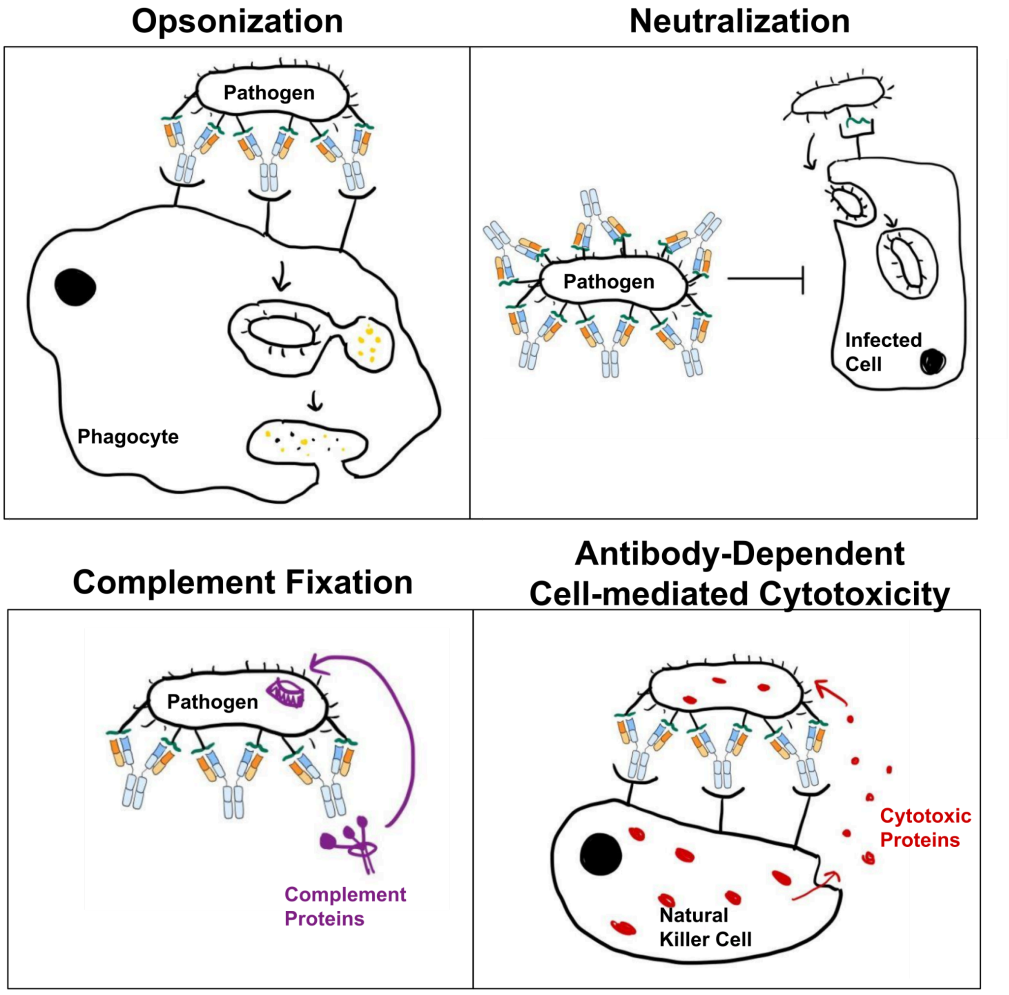

Figure 20. Functions of antibodies. Opsonization: Antibodies encourage phagocytosis by binding a pathogen. **Neutralization:** Antibodies prevent pathogen from infecting cell by blocking PAMPs. **Complement fixation:** Antigen encourages complement proteins to attack pathogen. **ADCC:** Antibodies encourage secretion of cytotoxic proteins by NK cells. Drawn by G. Wieselquist with inspiration from Kuby Immunology (2009) (62).

B cells can become activated in two ways. The first requires help of CD4+ T cells, known as the T-dependent (TD) response. First, the B cell binds exogenous antigen via its randomly generated Ig receptors, then endocytoses it. As an APC, B cells present this exogenous antigen via the MHC Class II pathway

to CD4+ T cells (**Fig. 17A**). As previously described, the TCR of the T cell binds the MHC II of the B cell. Along with costimulatory receptor-ligand binding and cytokine signalling, B cells are activated and can either become plasma effector cells which secrete antibodies, or memory B cells. B cell Ig receptors can undergo class switch recombination (CSR) to become any of the five isotypes of antibody for different locations in the body. This process involves DNA editing of the genes that encode the heavy chain, and is dependent on the cytokines secreted by activating T cells. Activation occurs throughout the body at lymph follicles (62). Cytokine signalling, which is determined by the route through which antigen is introduced into the body, determines whether class switching to IgA occurs. Intramuscular immunization used in this research induces a strong systemic IgG response but not always a strong mucosal IgA response. A strong IgA response often requires a mucosal barrier breach (63).

The second method of B cell activation is the T-independent (TI) response. B cells recognize specific types of antigen called TI-1 and TI-2 antigens along with their own PRRs or coreceptors before activation.

After the initial encounter with a pathogen, the immune system can retain its memory of it for a lifetime. This is made possible through T and B memory cells, which are dormant adaptive cells with specificity for pathogens. They can become activated by innate immune cells and cytokines during a secondary immune response. This response is faster than the primary response because the immune system has already learned about the pathogen.

6.3 *Chlamydia*-Specific Immune Response

The innate immune response to *Chlamydia* is characterized by a unique set of cellular and humoral responses. Important PAMPs on the surface of *Chlamydia* are heat shock protein 60 (Hsp60) and major outer membrane protein (MOMP). Recognition by host PRRs such as toll-like receptor 2 (TLR2) causes the production of inflammatory cytokines TNFα, IL-6, and IL-8. These cytokines recruit phagocytes such as neutrophils, primarily, as well as macrophages and natural killer cells (9).

A prominent inflammatory cytokine produced during *Chlamydia* infection is IFNγ, secreted primarily by CD4+ T cells. Signalling by IFNγ allows the host to starve *C. trachomatis* of tryptophan (Trp) amino acids, which are necessary for survival and unable to be produced by the bacteria. The mechanism of starvation is as follows: the cytoplasmic enzyme Indoleamine 2,3-dioxygenase (IDO) becomes activated within infected cells and metabolizes Trp by opening its five membered indole ring (**Fig. 21**) (7, 64, 65). IDO can also generate reactive oxygen species (ROS) such as nitric oxide (NO), which kill bacteria by destroying important proteins or genetic material (22). In humans, *C. trachomatis* evades Trp starvation by expressing its own evolved Trp synthase gene (9, 10, 27).

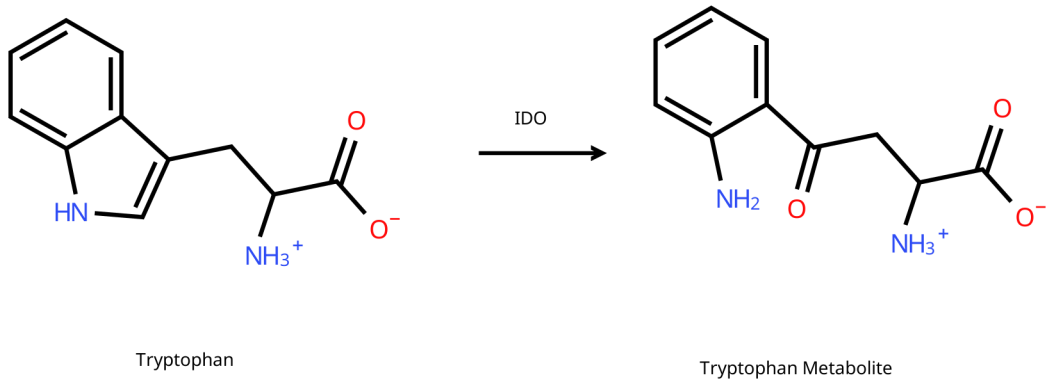

Figure 21. Metabolism of Trp by host IDO to starve *Chlamydia* of essential nutrients. Created in Moldraw.

IFNγ does not cause downstream IDO production and Trp starvation in mice, but a protective response still results from IFNγ signalling. IFNγ upregulates host GTPase expression, which starves *C. muridarum* of GTP. Like *C. trachomatis* employing Trp synthase, *C. muridarum* potentially evades this response using putative cytotoxins Tc0437-Tc0439, described previously, to glucosylate host GTPases, rendering them nonfunctional. This emphasizes the importance of these proteins to *C. muridarum* survival and the value of investigating this protein further, including its potential role as an antigen (22, 66).

IFNγ also has a polarizing role, encouraging CD4+ and CD8+ T cell activation. Additionally, it increases expression of MHC proteins and activates macrophages (67). Each of these functions encourages antigen presentation and destruction of intracellular pathogens.

Other proinflammatory cytokines seen in the host response to *Chlamydia* are IL-1α, IL-17, and IL-6, IL-12 as well as the chemokine IL-8. While these

cytokines recruit helpful leukocytes that can clear pathogens, they also can be linked to immunopathology and *Chlamydia* persistence (64).

Of the adaptive immune cells, CD4+ T cells have been emphasized in adaptive immune response research. Mice lacking MHC Class II complexes, which are involved in antigen presentation to CD4+ T cells, are not able to clear *Chlamydia*. Contrarily, mice lacking MHC Class I complexes, which are used in antigen presentation to CD8+ T cells, are able to clear infection (9). Both T cell subtypes are important, however, as both can secrete IFNγ and contribute to clearance of bacteria from the genital tract (67).

B cells are highly important in clearing *Chlamydia* infection. A study found that treating mice with anti-CD4 and anti-CD8 antibodies prior to *C. muridarum* secondary infection showed no significant differences in bacterial clearance compared with control mice. This demonstrates that the B cell antibody response can clear infection in spite of depleted T cell levels (68). Additionally, B cells work in conjunction with CD4+ T cells via antigen presentation and activation (T-dependent response). In one study, B cells were treated with EBs to process and present antigens, then washed thoroughly. These B cells were combined with naïve CD4+ T cells to activate them, which caused differentiation into IFNγ-secreting T cells. Passive transfer of these cells to mice prior to *C. muridarum* infection was protective against chronic oviduct pathology (69). This emphasizes the role of B cell antigen presentation in protection against immunopathology.

Out of the five major classes of antibodies, important antibodies specific to *Chlamydia* are of the IgA and IgG subtype (1, 16, 70). IgA antibodies target pathogens of the mucous membranes, such as those found in the female genital tract, neutralizing them or encouraging ADCC. IgG, found in the serum, is responsible for encouraging phagocytosis by macrophages via opsonization, and additionally promotes ADCC by natural killer cells and neutrophils (62). To determine antigen targets of these antibodies, one study used ELISA to assess detection of recombinant *Chlamydia* proteins by sera of *C. trachomatis*-positive patients. The result was that antibodies against *C. trachomatis* target antigens on the outside of the bacterium, which is a logical finding because these components are accessible (71). This is useful for vaccine antigen selection. The vaccine platform tested in this work will focus on generating a robust B cell antibody response.

7. Immunology of Vaccines

The goal of a vaccine is to safely provide long-lasting active immunity against a pathogen. Should a vaccinated organism encounter the pathogen, their immune system reacts quickly to clear it, without having to undergo the dangers of natural infection as the first exposure. This is distinct from passive immunity, which is temporary protection against a pathogen in an emergency or preparatory situation. In this case, the host is given antibodies from another organism. While this is helpful, vaccination allows the immune system to learn about a pathogen

and fight it years later. Vaccines expose the adaptive immune system to a safely altered form of the pathogen, inducing antigen presentation and activation of B and T cells, therefore priming for subsequent exposures (62).

Developing a vaccine requires a balance between safety, efficacy, and accessibility. There are a variety of vaccine platforms, each with their own risks and benefits. The closer a vaccine is to a pathogen's original form, the more potent the resulting immune response is. However, these forms come closer to eliciting dangerous symptoms of the actual disease. Some platforms are more costly to produce, distribute, and store, making them less accessible (62).

There are five main types of vaccines: live attenuated, inactivated, recombinant vector, nucleic acid, and subunit. Live attenuated vaccines are made of weakened pathogens which have mutated after infecting a series of different species, becoming non-specific to the original host. The result is a highly immunogenic replicating pathogen that does not harm the host. However, the pathogen could potentially mutate back into a harmful form. Inactivated vaccines use heat or chemical treatment to "kill" the pathogen. This form cannot multiply within the host but remains highly similar to its "live" counterpart which allows the immune system to easily recognize it. Unfortunately, if the vaccine is not properly treated during production, live versions of the pathogen could accidentally be injected into hosts, causing great harm. Recombinant vector vaccines use a harmless virus or bacterium as a vessel that carries genetic information encoding a specific antigen. The vector infects host cells as a

pathogen would, and the antigen gets expressed and displayed, but the host reaction is not as strong as that from a harmful pathogen, and there is no possibility of mutation or insufficient inactivation during production. However, side effects can still develop. Nucleic acid vaccines are similar in that they contain genetic information, either DNA or RNA. These biomolecules encode an antigen that cells can display for the immune system to recognize, and they lack the viral or bacterial vectors which could potentially cause side effects. Subunit vaccines use isolated biomolecules such as whole proteins, peptides, or carbohydrates from pathogens. These alone are employed as antigens to educate the immune system. These vaccines are incredibly safe because they do not contain live or viral pathogens that could be infectious. However, because they are more removed in similarity from the pathogen compared to other vaccine types, they require other components to boost an immune response, such as adjuvants (62).

An adjuvant is a vaccine additive that enhances the host immune response to vaccine antigen. Adjuvants typically function by holding the antigen in place, keeping it localized, so it has a more potent response, as opposed to allowing vaccine contents to spread throughout the body. They also promote antigen presentation and increase expression of inflammatory cytokines (72). Subunit vaccines can also be made more immunogenic by being multivalent. This means that they contain multiple variations of subunits, especially if there are multiple forms of a pathogen, such as different strains or serovars (62).

8. *Chlamydia* Vaccine Research

C. trachomatis vaccine research has been ongoing since 1911. A wide range of vaccine platforms have been trialed in this time span. Much research has focused on inducing a CD4+ T cell response and the production of IFNγ based on the natural protective response to *Chlamydia* (16). However, T cell responses localized to the genital mucosa are hard to induce in a vaccine administered outside of the mucosa, which is the case for intramuscular or subcutaneous vaccination. This is because memory T cells will localize to the original site of antigen presentation, which is logical as the body prepares for reinfection at the same site, but challenging in vaccination. Solutions to this issue include genital tract vaccination, which is invasive, or "prime and pull" technologies, which use the application of cytokines to the genital tract to pull activated T cells to the area after vaccination elsewhere. This can be challenging because the hormonal cycle can impact immunity and mucosal barrier makeup, therefore altering vaccine efficacy (16).

These work-arounds are clever, but perhaps not necessary. The Gardasil® and Cervarix® Human Papilloma Virus (HPV) vaccines, aside from Hepatitis B vaccines, are the only approved STI vaccines on the market, and they do not rely on a T cell response. Approved in 2006, their technology relies on B cell responses. HPV, like *Chlamydia*, is an intracellular pathogen that naturally exhibits a CD4+ T cell response. The previous consensus on producing a protective response against HPV was that this response was required. However,

the current virus-like particle (VLP) technology employed by the vaccine relies more heavily on high titre antibody production (21). The vaccine produces highly concentrated serum IgG, as well as localized mucosal IgG and IgA at the cervix (73).

VLP vaccines belong to the subunit platform classification. They utilize the L1 capsid protein of HPV, which self-assembles after induced overexpression in yeast or viral vector-infected cells (74). Because antibodies formed to recognize protein can cross from the blood into the mucosa through active transcytosis or exudation, the vaccine has been highly successful in preventing genital tract infection. In the genital tract, these antibodies neutralize viruses to prevent entry into host cells (21). Clinical trial data have shown that this vaccine is both safe and 90.4% effective against HPV-induced precancerous cells in the cervix (20).

HPV vaccines are being developed to focus on epitopes of antigens not typically targeted in natural infection. The reason for this is because naturally immunogenic epitopes do not always provide the host with lifelong immunity, because they can mutate to evade the immune system (75). These studies use the external L2 protein of the virus, and have been successful in inducing a robust immune response. This demonstrates the value of cryptic epitopes, which are transiently expressed portions of pathogen proteins that are (1) highly conserved across strains of the pathogen, (2) not naturally immunogenic, and (3) vital to the pathogen in host infection (21). In terms of *C. trachomatis* vaccine development,

search for such an antigen is useful because the commonly used major outer membrane protein (MOMP) has presented challenges with inducing long-lasting immunity and is very difficult to produce recombinantly in a properly folded and glucosylated form (16, 76).

Recent work by Webster et al. (2022) applies VLP technology to *C. trachomatis* vaccine development. One such vaccine used *C. trachomatis* peptides conjugated to the Qβ bacteriophage capsid protein. This VLP vaccine is "self-adjuvanting," meaning there is no additional adjuvant required because the VLP itself will promote a strong immune response. Because the Qβ capsid, which the host recognizes as non-self, is chemically conjugated to the peptide antigen, a strong response can be produced from capsid recognition alone. Qβ capsids are expressed in *E. coli* and multimerize independently into icosahedral shaped capsids made of 90 protein dimers. Lysine residues on their surface are used as an attachment point for Succinimidyl 6-[(β-maleimidopropionamido) hexanoate] (SMPH) cross linker protein and three glycine spacers (77). The function of SMPH is to stick out of the VLP, making the peptide attached on its end accessible to B cells (**Fig. 21**).

Another common problem with selecting antigens for vaccines is selecting those known as immunological decoys, which can be targeted by the immune system but are not essential to the function of the pathogen. It is also vital to select a portion of the antigen that is accessible to antibodies. Selecting from a database of antibodies such as the Immune Epitope Database (IEDB) helps with

both of these issues. The IEDB stores sequences and structures of B cell epitopes with parameters such as hydrophilicity, flexibility, accessibility, turns, exposed surface residues, polarity, and antigenicity, allowing scientists to be selective about which portion of the target protein to display. The antigen selected for the aforementioned *C. trachomatis* Qβ VLP vaccine was CT584. In parallel with the HPV VLP administration route, Qβ-CT584 vaccination was performed intramuscularly in mice. Challenge was performed transcervically with *C. trachomatis* serovar D. The Qβ-CT584 vaccine induced high titer serum antibody production against CT584, indicating the vaccine was highly effective at creating a B cell response (77).

CT166 is a *C. trachomatis* antigen that does not induce a natural antibody response, and it therefore qualifies as a cryptic antigen. Preliminary data show that it may localize to the surface of the EB for immune recognition, as well. It is an especially motivating candidate because of the novel gene technology mentioned previously that completely deleted homologous putative cytotoxins from the *C. muridarum* genome, which showed their prominent role in chronic pathology. The potential role of *C. muridarum* cytotoxins in evading host IFNγ-induced GTP starvation via GTPase glucosylation, as well as their role in cytoskeletal rearrangement for host cell entry, emphasizes their vitality in bacterial invasion and survival (22, 58, 66).

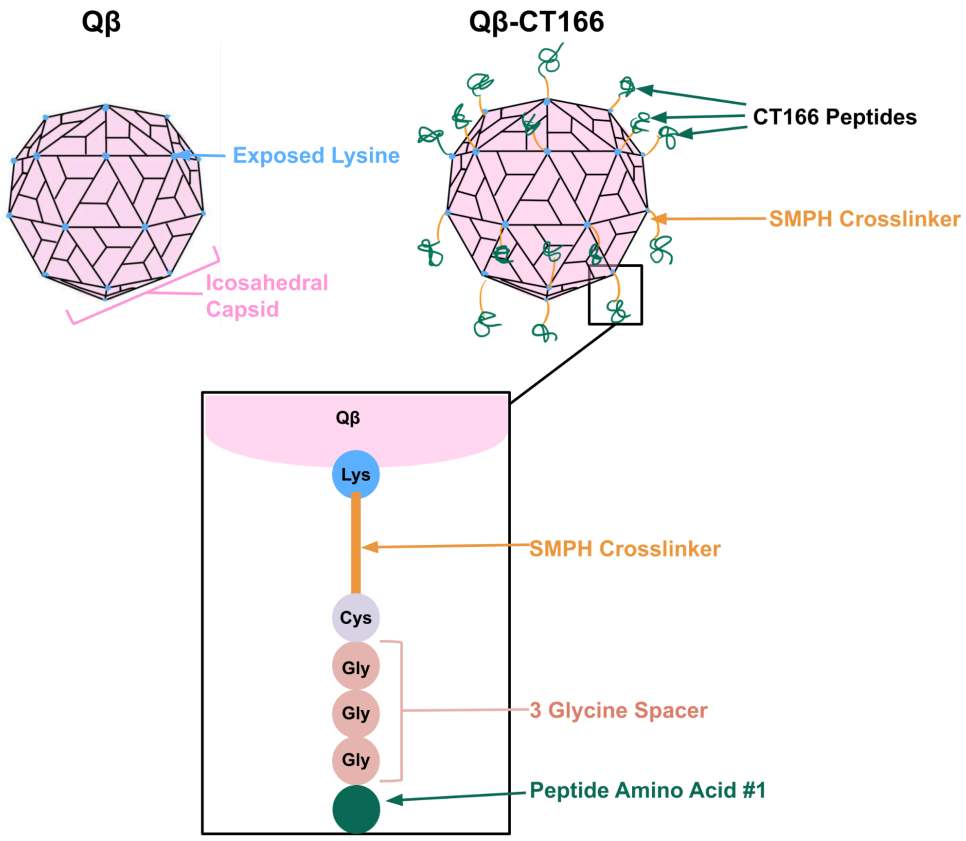

Figure 22. Qß-CT166 VLP Technology. Qß icosahedral capsid (pink) contains exposed lysine residues (blue) that can be conjugated to SMPH crosslinkers (orange). Box shows a magnified schematic of the lysine-SMPH-peptide chain, which includes an extra cysteine (light purple) and three glycines (mauve) before the peptide sequence (green) begins. Drawn by G. Wieselquist.

In unpublished research, Lijek Lab members tested the protectiveness of Qβ VLPs conjugated to five CT166 peptides (**Fig. 22**) in an equal ratio mixture. The peptides chosen were predicted to generate a B cell response using the aforementioned IEDB. This study went further than the CT584 VLP to examine immunopathology. The Qβ-CT166 VLP produced high titer antibodies (**Fig. 23A**) and ameliorated acute immunopathology (**Fig. 23C, Fig. 23D**) after transcervical *C. trachomatis* challenge (78).

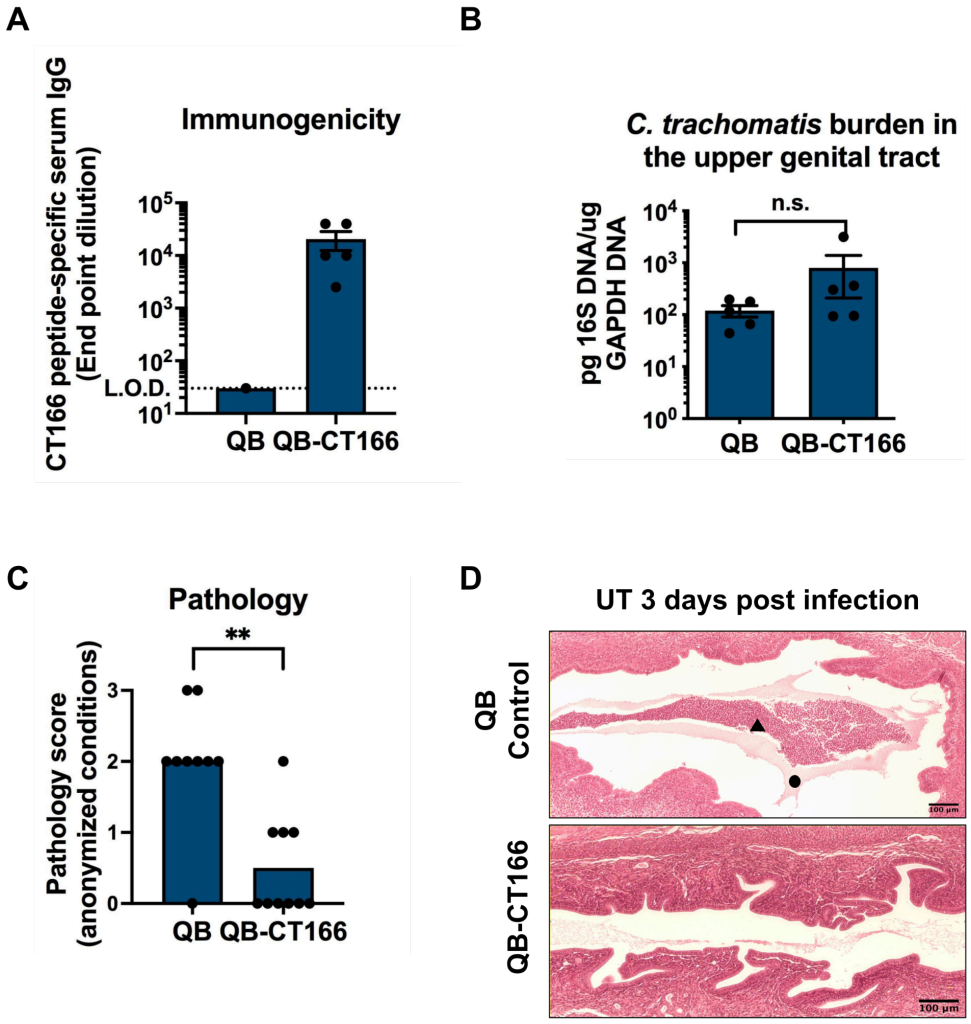

Figure 23. QB-CT166 VLP induces high titer IgG and protects against immunopathology, but does not affect bacterial burden. A: Compared with control QB immunization, QB-CT166 generates significantly higher IgG levels in sera of mice. **B:** There is no statistically significant difference in bacterial burden between control and QB-CT166 mice. **C:** Quantified pathology assessment is significantly worse in QB control mice compared with QB-CT166 mice. **D:** Representative images of uterine pathology for QB and QB-CT166 administered mice. Neutrophils (triangle) and mucus (circle) are more abundant in the control compared with the experimental group. Adapted from Berclaz et al. (2023) (79).

It has yet to be discovered whether this vaccine is also protective against chronic and tissue-specific pathology, which can be tested using *C. muridarum*

infection. The CT166 peptides on the QB-CT166 vaccine have high sequence homology to *C. muridarum* Tc0437-0439, justifying the use of the *C. trachomatis*-based vaccine during *C. muridarum* infection (**Fig. 24**).

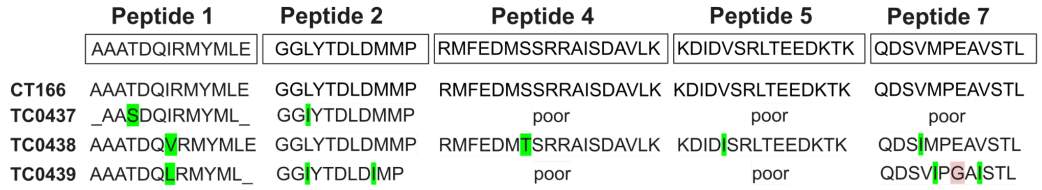

Figure 24. Sequence homology between QB-CT166 VLP vaccine peptides and *Chlamydia* putative cytotoxins. BlastP was run comparing amino acid sequences of Qβ-CT166 VLP peptides to *C. trachomatis* serovar D CT166 and *C. muridarum* TC0437-TC0439. Peptides conjugated to Qβ capsids are boxed. CT166 amino acid sequence is the first unboxed line, followed by amino acid sequences of TC0437-TC0439 in subsequent rows. No highlight demonstrates homology. Green highlight indicates similar properties and structure between putative cytotoxin residue and VLP peptide residue. Red highlight represents dissimilar residues in the middle of the putative cytotoxin. Underscores represent dissimilar residues on the ends of homologous putative cytotoxin regions. Sequences do not include 3-glycine spacers and cysteine residues used for SMPH conjugation to Qβ. NCBI GenBank accession numbers: CT166 ABA42639.1, TC0437 AAF39291, TC0438 AAF39292, TC0439 AAF39293. Created by G. Wieselquist.

There is value in infecting with *C. muridarum* because, as previously explained, transcervical infection reliably produces chronic immunopathology representative of the dangerous long term symptoms in humans. Additionally, *C. muridarum* infecting its natural host is analogous to *C. trachomatis* infecting its natural host, humans (22). This research will employ transcervical *C. muridarum* infection to assess the efficacy of a CT166 VLP vaccine. It will simultaneously investigate the reliability of immunopathology assessment during experimentation.

9. Specific Aims and Hypotheses

9.1 Specific Aim 1a: To test and maximize the reliability of a scoring system for *Chlamydia*-induced tissue-specific pathology.

9.1.1 Hypothesis for Specific Aim 1a: If double anonymized scoring does not yield perfect agreement among scorers, clearly defining multiple scales for tissue-specific phenotypes and their severities will generate a nuanced and reliable scoring system.

9.2 Specific Aim 1b: To assess immunogenicity and protectiveness of a novel CT166-conjugated VLP vaccine against *Chlamydia* infection.

9.2.1 Hypothesis for Specific Aim 1b: QB-CT166 will generate a robust B cell response because peptide conjugated VLPs are highly immunogenic. QB-CT166 vaccination will protect against chronic oviduct pathology because high titer antibodies produced by the vaccine will neutralize *Chlamydia* by binding putative cytotoxins localized to EB surfaces. This is an immunological approach that theoretically accomplishes the same goal as genetic removal of these putative cytotoxins from *C. muridarum,* which attenuated chronic oviduct pathology in previous work.

METHODOLOGY

1. Experimental Outline

The preliminary inter-rater reliability analysis in this work assesses immunopathology scoring in past experiments as the Lijek Lab transitioned from external professional pathology scoring to tissue assessment by lab members. During this time, the lab ran its first long term pathology experiments, necessitating new scales for chronic pathological phenotypes. Independent scoring followed by consensus meetings led to a variety of trial scales depending on route and timepoint of *C. muridarum* infection.

The inter-rater reliability investigation in this research is productive in two ways. First, it determines the most applicable pathology scoring system for a variety of specific phenotypes. Second, it determines a sound statistical method to assess pathology scoring in the future of the lab.

To do so, a variety of inter-rater reliability assessment methods were explored. These were applied to the finalized scores of two past pathology scoring datasets, one acute and one chronic, to see what improvements must be made. The results of this analysis were used to improve and more clearly define scoring parameters, which were applied to the vaccinology section of this research, wherein vaccine protectiveness against pathology was assessed. Pathology scores from this section were once more assessed for reliability. This workflow creates a feedback loop (**Fig. 25**) between pathology scoring in practice and inter-rater reliability assessment that develops a robust and dependable system.

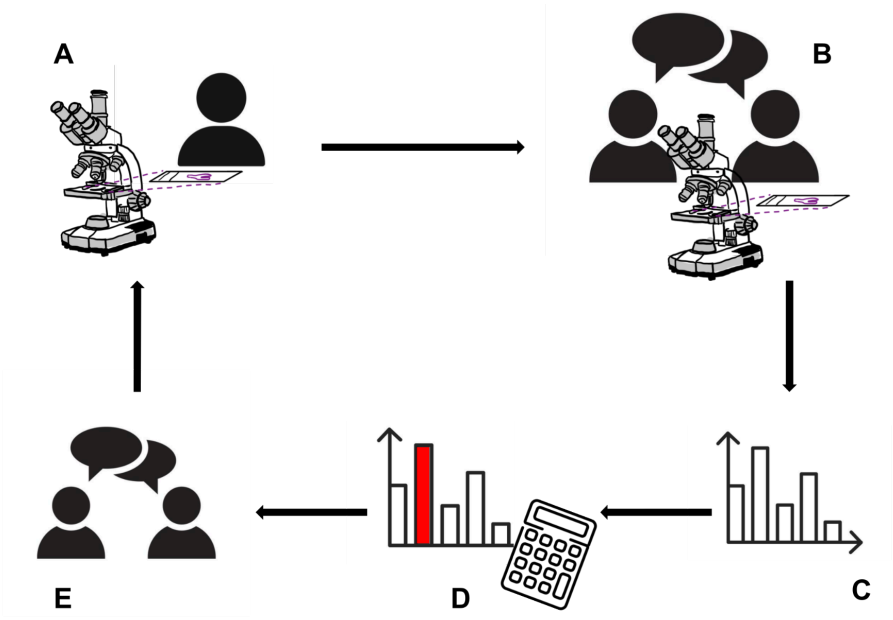

Figure 25. Workflow of developing a reliable pathology scoring system. A: Individual assessment of tissues. **B:** Consensus meeting between scorers to discuss and agree upon scoring. **C:** Final scoring dataset is generated by group. **D:** Inter-rater reliability calculations are performed to compare original score agreement and identify unreliable scoring categories. **E:** Conversation on how to clarify and adjust scoring parameters.

The vaccinology portion of this study links prior mouse experiments in the Lijek Lab that emphasized the promise of CT166 VLP vaccines and the role of CT166 homologous proteins in chronic immunopathology. Mice were vaccinated with either QB control VLPs or QB conjugated to CT166 peptide antigens (QB-CT166). Blood was collected to quantify anti-CT166 peptide antibodies in serum prior to and post vaccination. Additionally, vaginal lavage samples were collected post vaccination for mucosal anti-CT166 antibody quantification. While no mucosal antibody was collected prior to vaccination, genetically identical mice of the same age from another experiment were used as control samples. Mice

were vaccinated three times at three week intervals starting nine and a half weeks pre-infection. Seven days pre-infection, they were given DMPA subcutaneously to synchronize them in diestrus. All mice were infected transcervically with 10^6 inclusion forming units (IFU) of *C. muridarum*. Three days post infection, the female genital tracts of twenty mice were excised. Ten genital tracts were homogenized and were assessed using qPCR for bacterial burden and ELISA for antibody quantification. The other ten were assessed for immunopathology. Seven days post infection, bacterial burden and antibody analysis was repeated for ten mice**.** Fifty one days post infection, ten mice were assessed for immunopathology (**Fig. 26**).

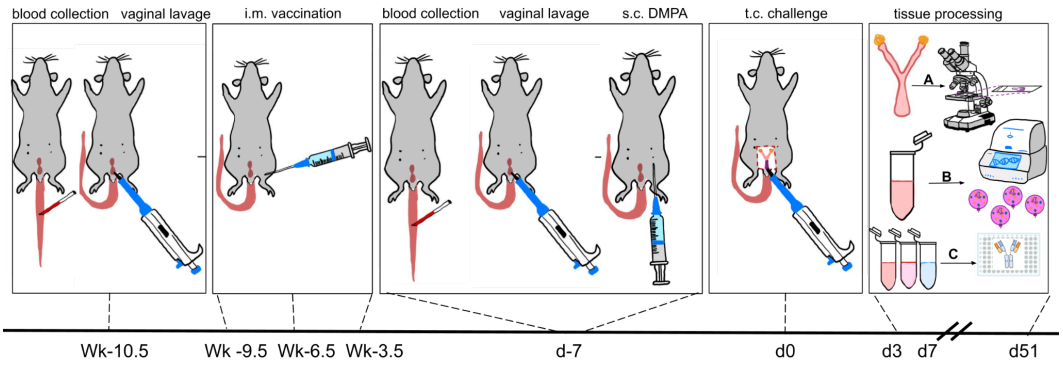

Figure 26. Experimental timeline for VLP vaccination. Mouse or experimental procedure is pictured in boxes. 10.5 weeks prior to infection, mice were given blood draw and vaginal lavage for antibody collection. At 9.5, 6.5, and 3.5 weeks pre-infection, mice were vaccinated intramuscularly with either QB or QB-CT166 mixed peptide VLPs. Within a week pre-infection, mice were given post vaccination blood draw and vaginal lavage. Seven days pre-infection, mice were injected with DMPA subcutaneously to synchronize them in the diestrus phase of their hormonal cycle. Mice were challenged transcervically with 10^6 IFU *C. muridarum* on day 0. Post-infection tissue processing (rightmost box) included

the following: **A:** genital tracts were fixed and sent for paraffin embedding, H&E staining, slicing, and slide fixation. **B:** genital tract homogenates were analyzed for bacterial burden via qPCR. **C:** Pre- and post-vaccination sera and vaginal lavages, as well as genital tract homogenates, were analyzed for antibodies via ELISA. Three days post infection, n=20 mice were analyzed via **A** (n=10) and **B** (n=10). Seven days post infection, n=10 mice were analyzed via **B.** Fifty one days post infection, n=10 mice were analyzed via **A.** Post vaccination analysis via **C** was performed on vaginal lavages and sera prior to infection, and at 3 and 7 days post infection on homogenates. Wk, week. i.m., intramuscular. s.c., subcutaneous. t.c., transcervical. Drawn by G. Wieselquist.

2. Procedural Methodology

2.1 Mice

All mouse procedures were performed in accordance with protocols approved by the Institutional Animal Care and Use Committee (IACUC) of Mount Holyoke College (Protocol BR-66-0624). Female C57Bl/6 mice were purchased from The Jackson Laboratory, housed at Mount Holyoke College, and provided with food and water *ad libitum*. The mice were given regular health checkups and housing cleanings. Blood collection and vaginal lavage were performed when the mice were 3 and 12 weeks old, vaccination was performed at 4, 7, and 10 weeks old, DMPA administration was performed at 12 weeks old, and transcervical infection was performed at 13 weeks old.

2.2 Vaccination

The QB and QB-CT166 VLP vaccines were synthesized as previously described (77) by the Frietze Lab at the University of New Mexico. Female C57Bl/6 mice were given a dose of 5ug per peptide (for a total dose of 25ug

peptide) in 50uL intramuscularly through the thigh. Mice were vaccinated at three week intervals 9.5, 6.5, and 3.5 weeks prior to infection (**Fig. 26**).

2.3 Sera Antibody Collection

To measure the serum antibody response to the vaccine, blood was collected from a small incision in the tail vein using glass capillary tubes (Thermo Fisher Scientific). Samples were collected before the first immunization ("pre-immune sera") and after the final immunization ("post-immune sera") before bacterial challenge. Blood samples were allowed to clot at room temperature and then centrifuged at 10,000g for 10 minutes at room temperature to pellet the clot and blood cells. The supernatant, serum, was removed and stored at -20℃ until further use.

2.4 Vaginal Lavage for Mucosal Antibody Collection

To measure the local antibody response to the vaccine, vaginal mucus was collected prior to and post vaccination in 200uL sterile 1x PBS from the vagina of C57Bl/6 mice using vaginal lavage technique. The sample was frozen at -20˚C for later use.

2.5 ELISA

ELISA was used to detect and quantify antibodies in sera, vaginal lavage, and uterine homogenate samples prior to and post vaccination. Immulon 2 HB

plates (Thermo Fisher Scientific) were coated with 50uL of 0.01ug/uL streptavidin (Thermo Fisher Scientific) in 1x PBS and incubated at 37℃ for two hours. The plates were washed 3 times with 1x PBS. Wells were then coated with 50uL of 0.02 ug/uL SMPH (Thermo Fisher Scientific) in DMSO and incubated at room temperature with rocking for 1 hour. The plates were washed three times with 1x PBS. The plate wells were then coated with 50uL of 0.02ug/uL CT166 peptide (GenScript) and incubated at 4℃ overnight. After peptide coating was complete, plates were washed 3 times with 1x PBS and blocked with 150uL of 0.5% milk in 1x PBS buffer with rocking for an hour at room temperature. The plate was washed twice with 1x PBS. Samples were then added in serial dilution in blocking buffer. For sera and upper genital tract homogenates, sample dilution began at 1:40 and was followed by 1:4 serial dilutions. For vaginal lavages, sample dilution began at 1:2 and was followed by 1:4 serial dilutions. The plate was rocked for two hours at room temperature to allow antibody binding to the peptide coat, then washed five times with 1x PBS. To detect antibody binding, 50uL of HRP-conjugated goat anti-rabbit IgG (Bio Rad) were added to positive controls, or goat anti-mouse IgG or IgA (Thermo Fisher Scientific) for experimental samples. Goat anti-rabbit IgG was diluted to a 1:5000 ratio in blocking buffer, and goat anti-mouse IgG and IgA was diluted to a 1:1000 ratio in blocking buffer. The plate was rocked at room temperature for 45 minutes, then washed five times with 1x PBS. HRP substrate TMB (Sigma-Aldrich) was equilibrated to room temperature, then added in volumes of 50uL per well to the

plate, which was rocked for 15 minutes before stopping the reaction with 0.1% HCl (Thermo Fisher Scientific). The plate was read at 450nm.

2.6 Transcervical *Chlamydia* Challenge Infection

Mice were infected with *C. muridarum* as previously described by our lab (48). One week prior to challenge, mice were treated subcutaneously with 2.5mg of depomedroxyprogesterone acetate (DMPA, Prasco) as is standard in this model system. On the day of challenge, *C. muridarum* was diluted to a concentration of $1x10^6$ IFU/10uL dose. Transcervical infection was performed using a Non-Surgical Embryo Transfer Device (NSET, ParaTechs) to open the vaginal vault, traverse the cervix, and deposit *Chlamydia* directly into the uterus. All mice were observed for wellbeing and no signs of distress were observed.

2.7 Dissection and Tissue Processing

The upper genital tract was removed by cutting at the cervix. Whole tissues were either placed in 2mL of PBS on ice for homogenization or 2mL 1:10 buffered formalin (Applied Biosystems) for fixation. 24 hours after formalin fixation, tissues were transferred to 2mL 1x PBS. Tissues placed immediately in PBS were mechanically homogenized. Aliquots of homogenate were taken for DNA extraction. Remaining homogenates were stored at -20˚C.

2.8 DNA Extraction

DNA was extracted from upper genital tract homogenates using the DNeasy blood and tissue purification kit (Qiagen). 20µL of Proteinase K and 80µL of Buffer ATL were added to 100uL of genital tract homogenate. Mixtures were vortexed briefly and then incubated at 56˚C overnight. The following day, 200µL of Buffer AL were added to lyse cells at 56˚C for 10 minutes. To allow DNA precipitation, 200µL of 200 proof ethanol (Pharmco) were added prior to incubation at 4˚C for 5 minutes. Samples were added into DNeasy mini spin columns and centrifuged at 6000 x g (8000 rpm) for 1 minute. The column was washed with 500µL Buffer AW1 using centrifugation at 6000 x g (8000 rpm) for 1 minute, then washed with 500µL of Buffer AW2 at 19000 x g (13300 rpm) for 3 minutes. DNA was eluted by adding 100µL of Buffer AE and incubating at room temperature for 15 minutes, then centrifuging at 6000 x g (8000 rpm) for 1 minute. To measure DNA concentration, nanodrop of eluate was conducted at 260 nm. Extracted DNA was stored at -20˚C for future analysis.

2.9 Bacterial Burden Assessment via Quantitative Polymerase Chain Reaction (qPCR)

To quantify *Chlamydia* burden in gential tract homogenates, qPCR was performed as previously described by our lab (48). Recipes for the rodent GAPDH (**Table 2A**) and bacterial 16S (**Table 2B**) master mixes are below, as

well as custom sequences for bacterial 16S forward and reverse primers and probe (**Table 3**).

A: GAPDH Master Mix Reagent	Volume per well (uL)
Taq 2x Buffer	12.5
GAPDH Forward Primer	0.6
GAPDH Reverse Primer	0.6
GAPDH Probe	0.25
MilliQ H_2O	6.05

B: 16S Master Mix Reagent	Volume per well (uL)
Taq 2x Buffer	12.5
16S Forward Primer	0.3
16S Reverse Primer	0.3
16S Probe	0.2
MilliQ H_2O	1.7

Table 2. qPCR master mix components. **A:** GAPDH master mix. 20uL GAPDH master mix and 5uL gDNA were combined in each well. **B:** 16S master mix. 15uL 16S master mix and 10uL gDNA were combined in each well.

16S Forward Primer	5’ - GGA GGC TGC AGT CGA GAA TCT - 3’
16S Reverse Primer	5’ - TTA CAA CCC TAG AGC CTT CAT CAC A - 3’
16S Probe	5’ - / 56-FAM / TCG TCA GAC TTC CGT CCA TTG CGA / 36-TAMSp / - 3’

Table 3. Nucleotide sequence of bacterial 16S forward and reverse primers and probe.

DNA samples were added to a PCR plate in triplicate for both GAPDH and 16S master mixes. The plate was run in the AriaMx PCR machine according to the following plan:

1. 50℃ for 120 seconds

2. 95℃ for 600 seconds
3. 2 step amplification (40 cycles)
    a. 95 deg C for 15 seconds
    b. 60 deg C for 60 seconds

Quantification cycle (Cq) values when probe fluorescence passed a detectable threshold were measured for each sample. The mean of the triplicate Cq values was used in **Equation 4** (**Appendix B**) to determine the concentration of GAPDH gDNA and 16S gDNA based on standard curves generated by Lijek Lab member KS (80). The ratio between [GAPDH gDNA] and [16S gDNA] was calculated, and a student's unpaired T test was performed on values to determine statistical significance.

2.10 Tissue sectioning, Slide fixation, and Staining

Formalin-fixed tissues were sent to the Histopathology Core Facility at Harvard Medical School for paraffin embedding, sectioning to 4–5 μm, and H&E staining.

2.11 Pathology Scoring

Assessment of pathology was performed in a double-anonymized manner (see **APPENDIX A**). Two scorers assessed each tissue individually, after which scorers came to a consensus on scores.

Below are the refined scoring scales used to assess each tissue type and pathology type for the vaccinology portion of the experiment. These scales were adapted from previous scales after inter-rater reliability analysis; the original

scales can be found in the appendix (**Tables 7 and 8**), and their evolution is discussed in the results and discussion sections.

Table 4. Acute immunopathology scoring scale. A: Uterine horns were scored on a 0-3 scale. "Pathology" was considered any immune cell infiltration (i.e. neutrophils), mucus, or dilation. **B:** oviducts were scored on a 0-2 scale. "Pathology" was considered cellular infiltration or mucus. **C:** Ovaries were scored on a 0-2 scale. "Pathology" was considered cellular infiltration, mucus, edema, and bursa thickening.

A: Uterine horn general pathology	
0	No pathology
1	Mild/rare pathology; less than 1/3 of tissue affected
2	Moderate/multifocal pathology; between 1/3 and 2/3 of tissue affected
3	Severe/coalescing pathology; greater than 2/3 of tissue affected
B: Oviduct general pathology	
0	No pathology
1	Mild/moderate pathology, affects some of tissue
2	Severe pathology, significantly affects all tissue
C: Ovary general pathology	
0	No pathology
1	Mild/moderate pathology, affects some of tissue
2	Severe pathology, significantly affects all tissue

Table 5. Chronic immunopathology scoring scale. A: Uterine horns were scored on a 0-4 scale. "Pathology" was considered mucus and dilatation. Dilatation consisted of lumen stretching to an abnormal diameter and epithelial "folds" due to edema. **B:** Oviducts were scored on a 0-4 scale based primarily on edema, which at its severest, is known as hydrosalpinx. The presence of mucus was considered pathological due to its role in inducing edema. The severity of

hydrosalpinx was deduced by size comparison to the ovary. **C:** Ovaries were scored on a 0-2 scale. “Pathology” was considered mucus, edema, and bursa thickening.

A: Uterine horn dilatation	
0	No significant dilatation, no mucus
1	Mild dilation of a single field of view, some mucus
2	One to three dilated fields of view, typically mucus mostly throughout or all throughout
3	More than three dilated fields of view/consistent dilation, typically mucus throughout
4	“Confluent-pronounced” (merging) dilation, extreme diameter swelling, mucus throughout
B: Oviduct hydrosalpinx	
0	No hydrosalpinx
1	Hydrosalpinx detectable visually but requiring microscopic confirmation, mucus likely present.
2	Hydrosalpinx clearly visible with naked eyes but oviduct size is smaller than the ovary on the same side
3	Oviduct size equal to the ovary on the same side
4	Oviduct size larger than the ovary on the same side
C: Ovary general pathology	
0	No pathology
1	Mild/moderate pathology, affects some of tissue
2	Severe pathology, significantly affects all tissue

2.12 Inter-rater Reliability Analysis

To determine the reliability of the pilot and adapted pathology scoring systems, the Intracclass Correlation Coefficient (ICC) and scaled percent agreement were calculated. Using RStudio, ICCs were calculated based on

agreement. For instances where there was no number assigned to a tissue (i.e. “no score,” or “missing,”), the set of two scores for that tissue and phenotype was removed from the analysis. In the rare case that a scorer could not make a decision about a score (i.e. “1/2”), the number chosen was that which matched the other scorer’s designation, because that would be the score agreed upon in consensus. Scaled percent agreement is a new methodology proposed and discussed in the results section.

2.13 Pathology Scoring Training Intervention

To test whether the refined pathology scoring system could be taught to learning scientists, a training module was developed and evaluated. All procedures were verified by the Mount Holyoke Institutional Review Board as Exempt according to 45CFR46.101(b)(1): (1) Educational Research on 02/08/2026. Participants were fully informed about the risks, benefits, and procedures in the study. Participation was considered voluntary and terminable at any time without penalty.

A pathology scoring assessment was created using tissue images from past experiments taken by Lijek Lab members. The assessment was composed of sixty questions, with ten each devoted to the following phenotypes: acute uterine horn, oviduct, and ovary pathology; and chronic uterine horn dilatation, oviduct hydrosalpinx, and ovary pathology (**Fig. 50**). Lijek Lab members with little to no experience with pathology scoring completed the assessment with no outside

resources or collaboration. Their answers were deidentified using anonymous IDs and compared using the intraclass correlation coefficient (ICC) to a trained scorer's answers to assess reliability before intervention.

Participants then received pathology scoring training with a trained scorer (GOW) where they learned about mouse anatomy, immunopathology phenotypes, and the new pathology scoring scales developed in this research. They were given access to the pathology scoring guide (**Fig. 49**) developed as part of this research. They completed individual practice scoring slides and were encouraged to ask questions. Following practice, participants took the same assessment once more, and their answers were once again assessed using the ICC.

2.14 Microscopy and Imaging

Slides were viewed using Köhler illumination on an Olympus BX51 Microscope set to transillumination brightfield. Images on the same microscope were taken with an Olympus DP74 camera and CellSens software. Brightness, contrast, gain, exposure, and white balance image adjustments were linear.

2.15 Other Statistical Analyses

A Student's unpaired T test was performed on qPCR bacterial burden, immunopathology scores, and ELISA data comparing mice in different groups (QB and QB-CT166). A Student's paired T test was performed on ELISA data comparing the same mice (QB-CT166) pre- and post- vaccination.

RESULTS

1. SPECIFIC AIM 1A: To test and maximize the reliability of a scoring system for *Chlamydia*-induced tissue-specific pathology.

1.1 ICC Inter-rater Reliability of Pilot Pathology Scoring Systems Reveals a Need for Scale Adjustment

The first pathology scoring system developed was designed to assess pathology at either an acute (seven days post infection) or chronic (fifty one days post infection) timepoint. At both timepoints, uterine horns, oviducts, and ovaries were assessed. The Intraclass Correlation Coefficient (ICC) was used to assess reliability of scoring (**Fig. 27** and **Fig. 31**). Based on these scores and the comparison of pathologies at different timepoints, scales were adjusted to be more representative of what occurs during infection. A pathology scoring guide using these adjusted scales was created to aid scorers while they scored new tissues. The guide contained bulleted information about expected phenotypes for each tissue, the language associated with each score, and representative images of each score. Multiple examples were provided for different scores, and the images were annotated to emphasize various pathologies in the images (**Fig. 49**).

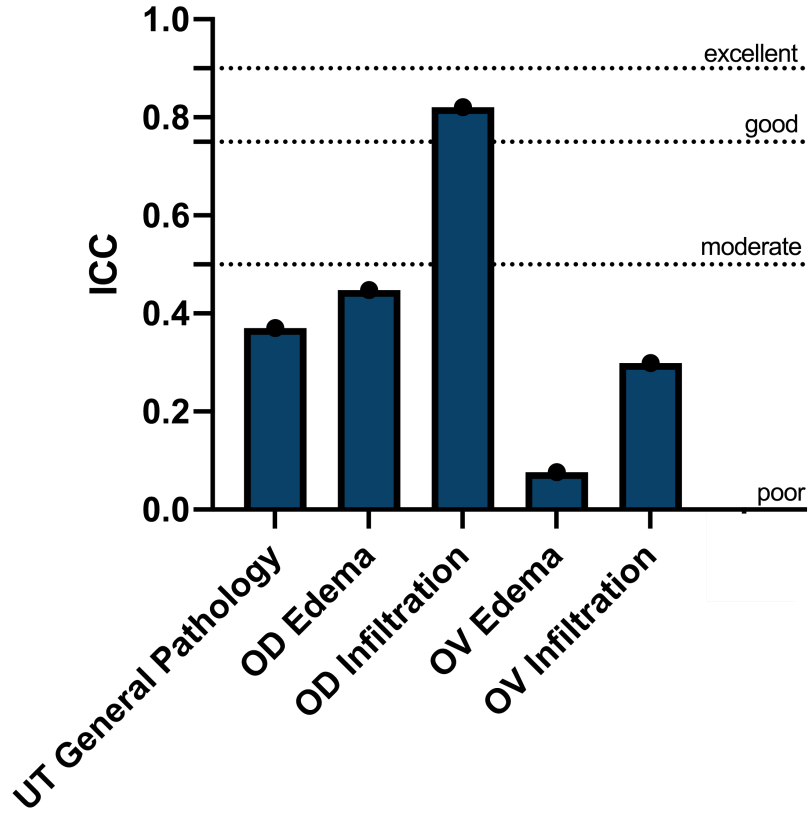

Figure 27. Inter-rater reliability of pilot acute pathology scoring system using the Intraclass Correlation Coefficient (ICC). C57Bl/6 mice were infected transcervically with *C. muridarum.* 7 days post infection, genital tracts were removed and fixed in formalin. Following fixation, tissues were embedded in paraffin, sliced to 4–5 μm, mounted onto slides, and stained with H&E. Tissues were assessed by two pathology scorers in an anonymized manner for the given phenotype on the x-axis. Original acute pathology scores for each phenotype were analyzed with the Intraclass Correlation Coefficient in RStudio to compare variance between groups (between mice) to the variance within groups (between scorers). ICC < 0.5, poor reliability; 0.5 < ICC < 0.75 moderate reliability; 0.75 < ICC < 0.90, good reliability; ICC > 0.90, excellent reliability. ICC, Intraclass Correlation Coefficient. UT, uterine horn. OD, oviduct. OV, ovary.

At the acute timepoint, uterine horns were assessed for “general pathology,” defined as the presence of immune cells, mucus, or edema in the uterine horn lumen. Inter-rater reliability analysis of this scale revealed poor reliability (ICC = 0.37) (**Fig. 27**). This was likely due to confusion about the difference between a “1” and a “2,” which is based on the area of tissue affected. To improve reliability, a pathology scoring guide was created for all tissues and their corresponding scales with annotations, explanations, and representative images corresponding with each score (**Fig. 49**). **Figures 28-30** and **33-35** display the representative images used in the guide, marked with shapes to clarify why each tissue received its score. The guide emphasizes the same features in annotation form.

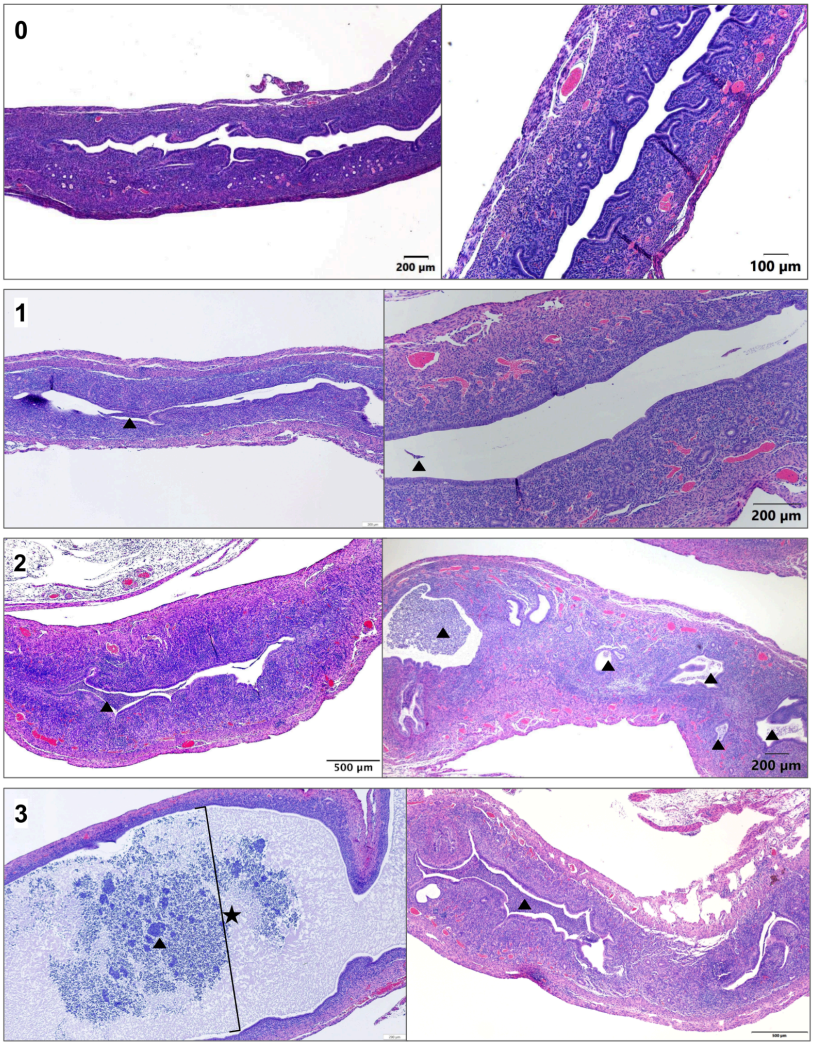

Figure 28. Acute uterine horn general pathology scores with representative images. Score is bolded in the top left of associated grouped images. Triangles indicate immune cells. Stars indicate edema. Images were taken by Lijek Lab members: AF (‘25), AM (‘25), GOW (‘26).

The uterine horn general pathology scale was clarified by explaining each number in words and images. The scores "1" and "2" are differentiated by the fraction of the lumen affected. The former is defined as "Mild/rare pathology; less than 1/3 of tissue affected," and the latter is defined as "Moderate/multifocal pathology; between 1/3 and 2/3 of tissue affected" (**Table 4**). The guide begins by defining what qualifies as pathology. For uterine horns at the acute timepoints, this is either mucus or immune cells in the lumen. The guide then explains how to determine the fraction of tissue affected, which can differ in two ways. Sometimes, there are completely empty lumenal spaces in one portion of the uterine horn, while another portion is saturated with immune cells. In this case, the fraction affected is determined by looking at the fraction of filled sections compared with the total number of sections. However, sometimes lumenal sections are partially filled with immune cells or mucus. In this case, the scorer must look at the area of filled lumen within each section and compare it to the total area of lumen. The guide provides examples such as:

"Sometimes, one section of lumen is packed with cells, and another section is empty. In this case, look at the **whole** tissue. If the packed, sick section makes up only ¼ of the whole lumen, this qualifies as a 1. But, if it makes up ¾, it qualifies as a 3."

Example sentences, annotations, and images are meant to assist pathology scorers as they assess new tissues, providing them with a reference to help them think consistently and clearly.

At the acute timepoint, oviducts and ovaries were assessed for both cellular infiltration and edema separately. The ovary cellular infiltration scale was unreliable (ICC = 0.299) (**Fig. 27**), due to differences in opinion about what constitutes moderate versus severe pathology. The pathology scoring guide was employed to address this discrepancy. The strategy deemed most helpful in this case was providing representative images of what can be classified as severe (**Fig. 29** and **30**). In contrast to the ovary cellular infiltration scale, the oviduct cellular infiltration scale had good reliability (ICC = 0.821) (**Fig. 27**). This result is sensible because oviducts have less lumenal space than ovaries, making it easier to confidently differentiate between a moderate versus severe quantity of immune cells within them. Inter-rater reliability analysis (**Fig. 27**) demonstrates that the edema scales for both oviducts and ovaries were unreliable (ICC = 0.448 and 0.0766, respectively) (**Fig. 27**). This makes sense qualitatively, because it can be unclear what constitutes severity of edema at the acute timepoint when it is most often, but not always, seen in tandem with cellular infiltration.

Deliberation deemed it unnecessary to separate edema and cellular infiltration pathologies at this timepoint, because it is often cellular infiltration itself that causes expansion and therefore edema of tissues. For this reason, the scales were collapsed into a broader “general pathology” scale for both oviducts (**Fig. 29**) and ovaries (**Fig. 30**). While this scale removes the phenotypic specificity of maintaining separate scales, it paints a more accurate picture of what occurs at an acute timepoint: immune cell infiltration from the innate

response, rather than edema alone, which is seen isolated at later timepoints. In the rare cases that edema is seen alone without cellular infiltration, it can still be scored using the same scale, based only on the severity of edema. To clarify what constitutes “moderate” versus “severe” edema in the ovary, the scoring guide was designed to differentiate between the two. Slight but clear pushing of the bursa away from the ovary, some bursa thickening, and some mucus qualifies as “moderate,” while extreme pushing and thickening of the bursa on all sides of the ovary due to mucus was categorized as “severe.” It is worth noting that while severe edema alone has been observed during intravaginal infection, it has not yet been observed in our lab during transcervical infection, which is the infection method around which this research centers.

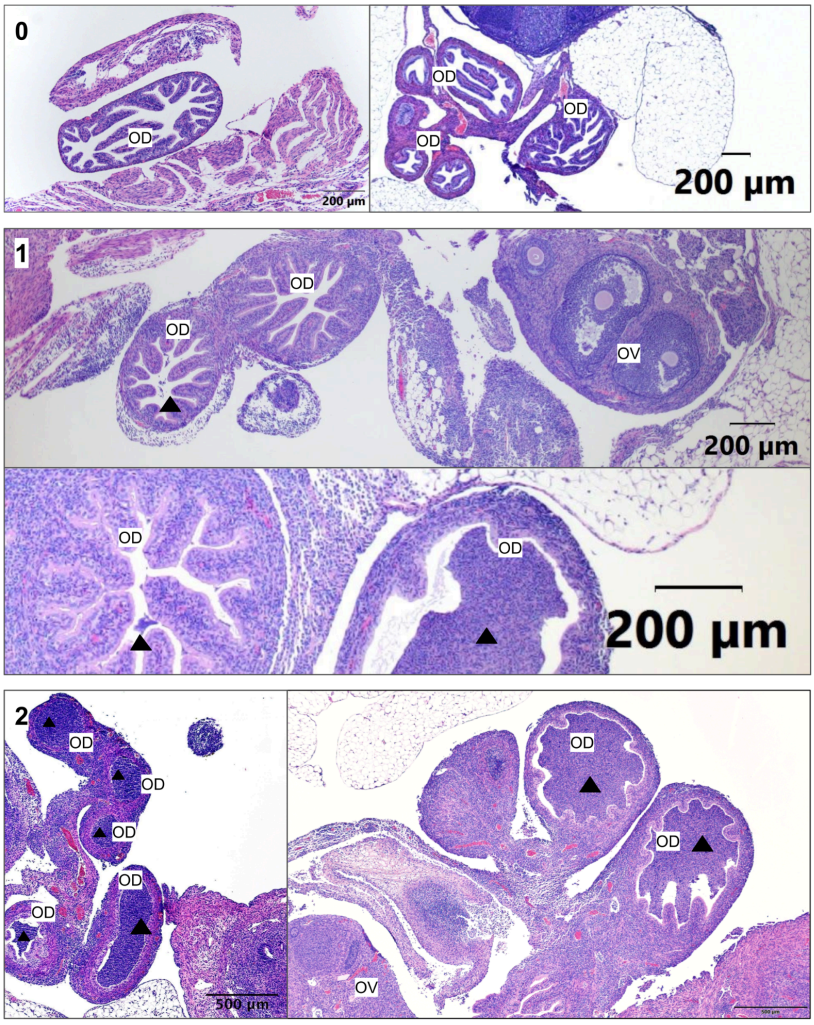

Figure 29. Acute oviduct general pathology scores with representative images. Score is bolded in the top left of associated grouped images. Triangles indicate immune cells. OD, oviduct. OV, ovary. Images were taken by Lijek Lab members: AF (‘25), AM (‘25), GOW (‘26).

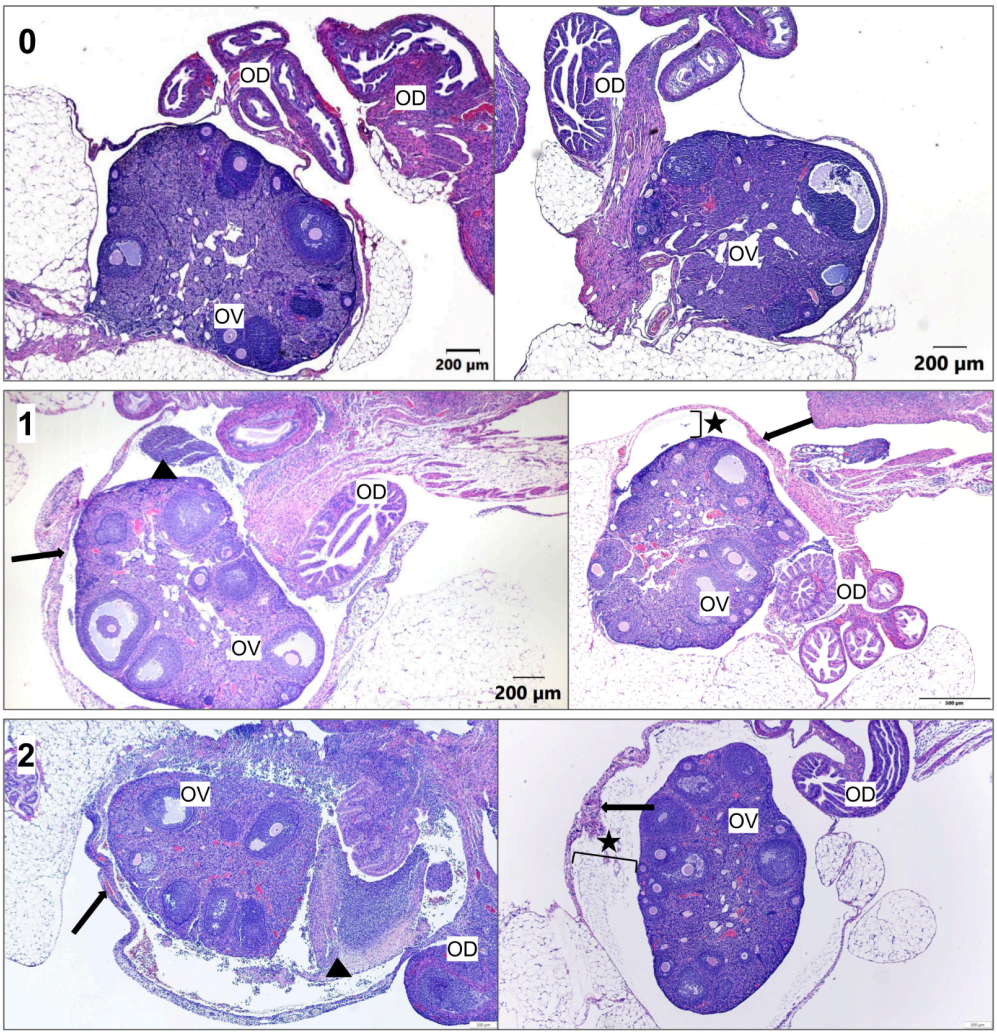

Figure 30. Acute ovary general pathology scores with representative images. Score is bolded in the top left of associated grouped images. Triangles indicate immune cells. Stars indicate edema. Arrows indicate bursa thickening. Images were taken by Lijek Lab members: AF (‘25), AM (‘25), GOW (‘26).

At the chronic timepoint, uterine horns were assessed for both “general pathology” and “dilatation.” The latter scale was adapted from Chen et al. (2014) (49), and was adopted to encapsulate the extremely dilated nature of uterine horns during chronic *Chlamydia* infection. However, adding a second scale mystified the exact parameters of the “general pathology” scale. At the acute timepoint, this scale focuses on the presence of immune cells in the lumen, but during chronic infection, there are rarely immune cells present. Using the original general pathology scale, mucus counts as pathology, but mucus is linked to the “dilatation” scale as well, because fluid and mucus influx is what causes stretching and dilatation of tissues.

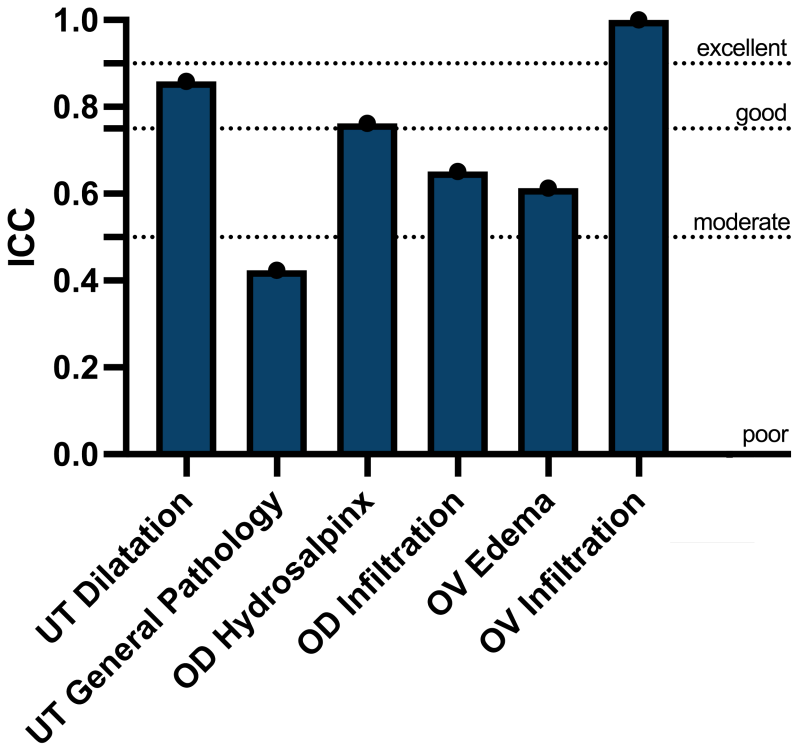

Figure 31. Inter-rater reliability of pilot chronic pathology scoring system using the Intraclass Correlation Coefficient (ICC). C57Bl/6 mice were infected transcervically with *C. muridarum.* 51 days post infection, genital tracts were removed and fixed in formalin. Following fixation, tissues were embedded in paraffin, sliced to 4–5 μm, mounted onto slides, and stained with H&E. Tissues were assessed by two pathology scorers in an anonymized manner for the given phenotype on the x-axis. Original chronic pathology scores for each phenotype were analyzed with the Intraclass Correlation Coefficient in RStudio to compare variance between groups (between mice) to the variance within groups (between scorers). ICC < 0.5, poor reliability; 0.5 < ICC < 0.75 moderate reliability; 0.75 < ICC < 0.90, good reliability; ICC > 0.90, excellent reliability. ICC, Intraclass Correlation Coefficient. UT, uterine horn. OD, oviduct. OV, ovary.

As demonstrated in **Figure 31**, the "general pathology" scale was poorly reliable (ICC = 0.424). Therefore, we decided to collapse the two scales into one "uterine horn dilatation" scale. This scale specified the parameters of the original scale from Chen et. al (2014) to include the presence of mucus as an indicator of pathology. Having one scale that focused on dilation and mucus rather than immune cells was more representative of chronic pathology phenotypes. Additionally, the language describing each score was adjusted to be more understandable. Originally, the scale used the language "cross sections" (**Table 8**) to mean "microscope field of view" (i.e. "dilation of a single cross section"), which was confusing because technically the slide contains one whole genital tract cross section. To amend this, "cross section" was replaced with "field of view" (**Table 5A**). Additionally, the phrase "confluent pronounced dilatation" was deemed confusing and was more clearly defined as "merging dilatation" and "extreme diameter swelling" (**Table 5A**). Finally, because the new scale included mucus in addition to edema as a pathology qualifier, each number was also described in terms of the level of mucus in the lumen.

This scale has a wider range than the uterine horn general pathology scale at the acute timepoint, because there is a wider range of pathology severity from chronic pathology (**Fig. 33**). To help scorers determine the more granular difference between a "2," "3," and "4," a flow chart (**Fig. 32**) was created asking pointed questions about the tissue. Following the flow chart, the pathology scorer

can more easily arrive at a decision. An excerpt from the chart below details the distinction between a "2" (**Fig. 32A**) and a "3" (**Fig 32B**).

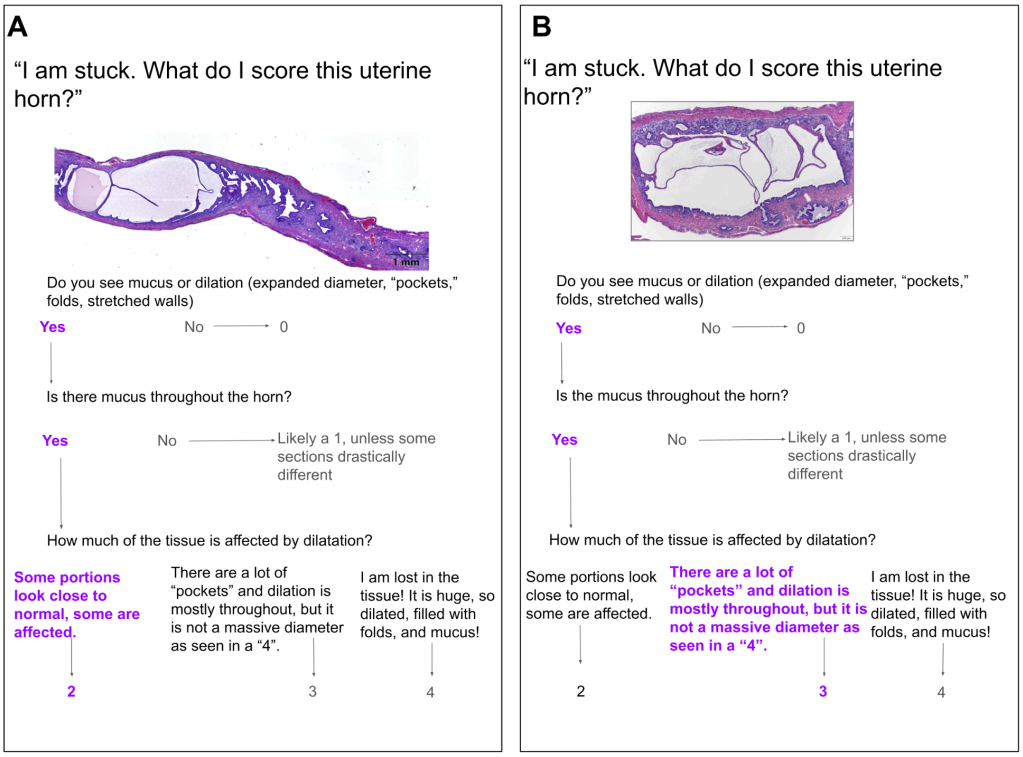

Figure 32. Pathology scoring guide flowchart excerpt. A: Example of thought process for assessing a "2." **B:** Example of thought process for assessing a "3."

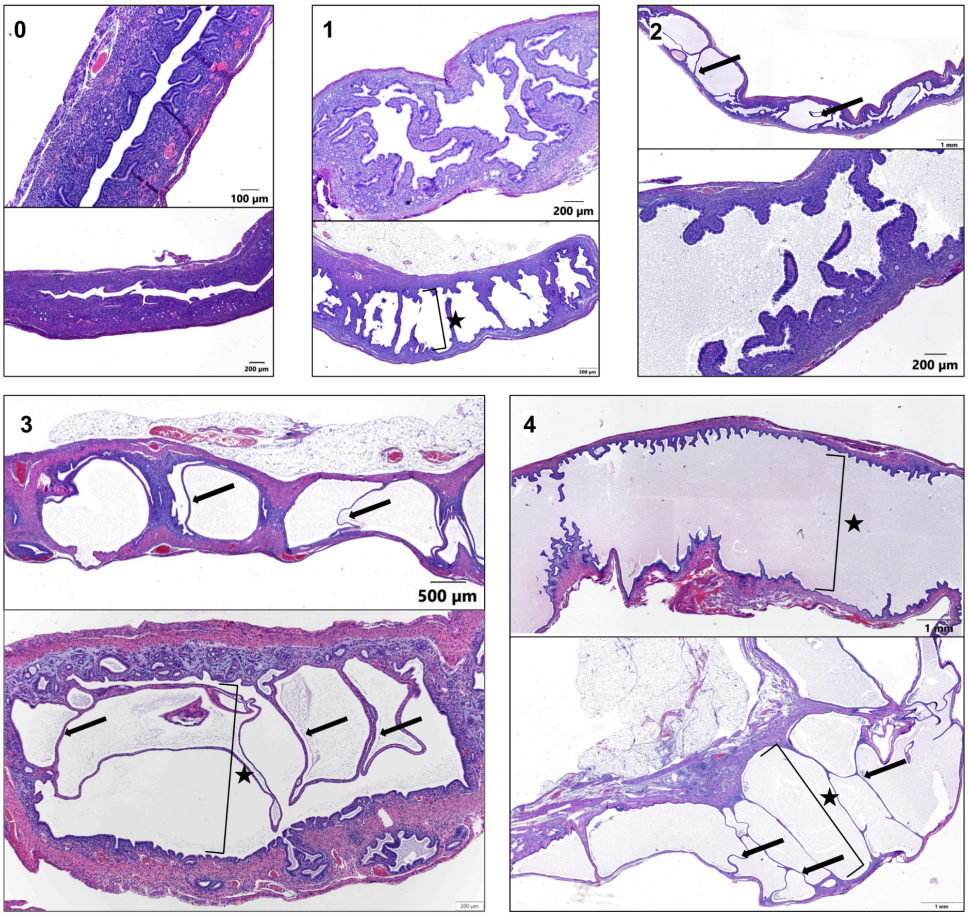

Figure 33. Uterine horn dilatation scores with representative images. Score is bolded in the top left of associated grouped images. Stars indicate dilatation. Arrows indicate folds characteristic of dilatation. Images were taken by Lijek Lab members: AF (‘25), AM (‘25), GOW (‘26).

The pilot scoring system introduced a new scale to assess the extreme swelling, or hydrosalpinx, of oviducts, unique to chronic infection. The scale uses the simple tactic of comparing oviduct size to ovary size. As oviduct size approaches and exceeds the size of the ovaries, hydrosalpinx score increases in severity (**Table 5B, Fig. 34**). This scale had moderate reliability (ICC = 0.72) and was more reliable compared to its counterpart oviduct "cellular infiltration" scale (ICC = 0.651) (**Fig. 31**). Qualitatively, this makes sense, because the latter scale actually becomes irrelevant at chronic timepoints, as there is usually no cellular infiltration in the genital tract. Pathologists looking for both cells and mucus, a characteristic of acute infection, may have been confused with the presence of mucus or other debris alone and therefore disagreed with pathologists attempting to use the same scale and apply it to the level of mucus alone. To more accurately reflect the immune response at this timepoint, the "cellular infiltration" scale was removed entirely.

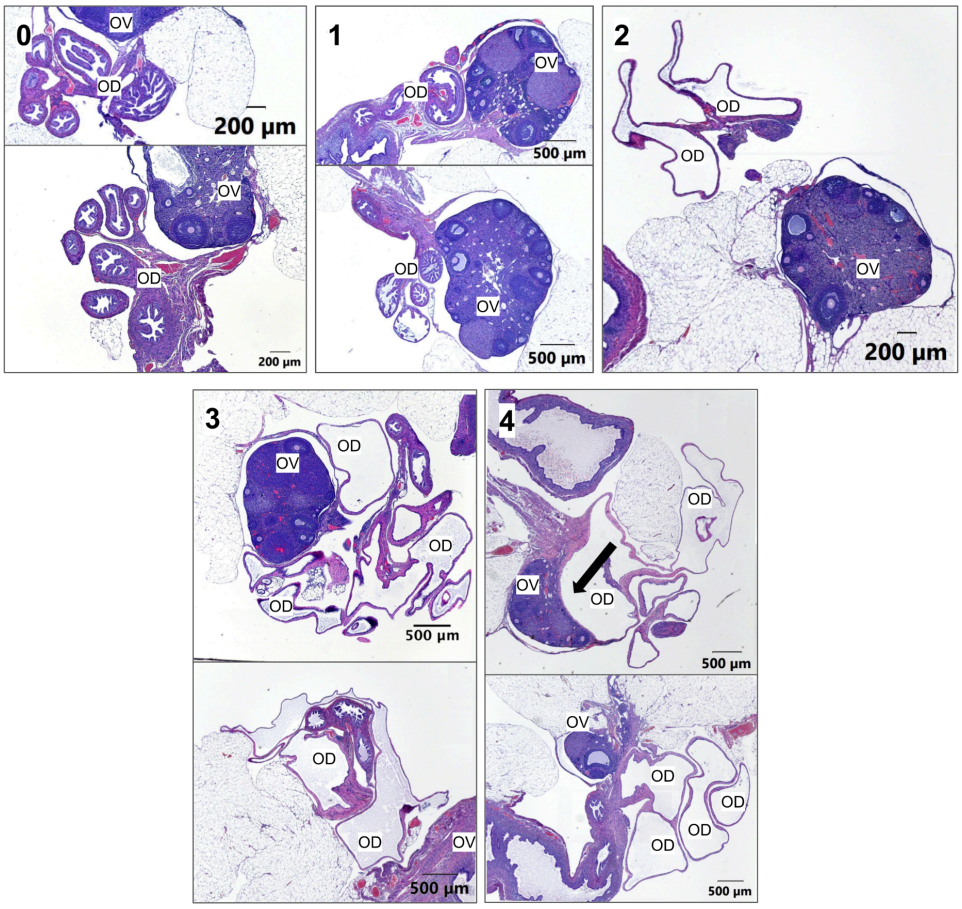

Figure 34. Oviduct hydrosalpinx scores with representative images. Score is bolded in the top left of associated grouped images. Arrow indicates ovary deformation due to hydrosalpinx. Images were taken by Lijek Lab members: AF (‘25), AM (‘25), GOW (‘26). OV, ovary. OD, oviduct.

Due to similar logic, “ovary edema” and “ovary cellular infiltration” for this chronic timepoint were also collapsed into one “ovary general pathology scale,” defined by the presence of mucus, bursa thickening, and bursa separation from the ovary. The lack of immune cells at the chronic timepoint explains the excellent reliability (ICC = 1.0) (**Fig. 31**), because there were no cells to determine the level of. The ovary edema scale had moderate reliability (ICC = 0.613) (**Fig. 31**). This scale has the same range of scores as the acute timepoint, because there is less of a dynamic range of severity when compared to uterine horn dilatation and oviduct hydrosalpinx. It differs from the acute timepoint “ovary general pathology” in that the expected phenotypes are mucus and edema as opposed to cellular infiltration, mucus, and edema. This may have caused confusion, so the optimized scale was adjusted such that the only qualifiers for pathology were mucus and edema. Representative images in **Figure 35** display this and clearly contrast the acute general pathology for ovaries (**Fig. 30**) due to the lack of immune cells present.

An additional characteristic of ovaries at the chronic timepoint is deformation due to pressure from swollen oviducts. This was deemed a parameter for oviduct hydrosalpinx, because it was more dependent on oviduct swelling than swelling of the ovarian bursa (**Fig. 34**).

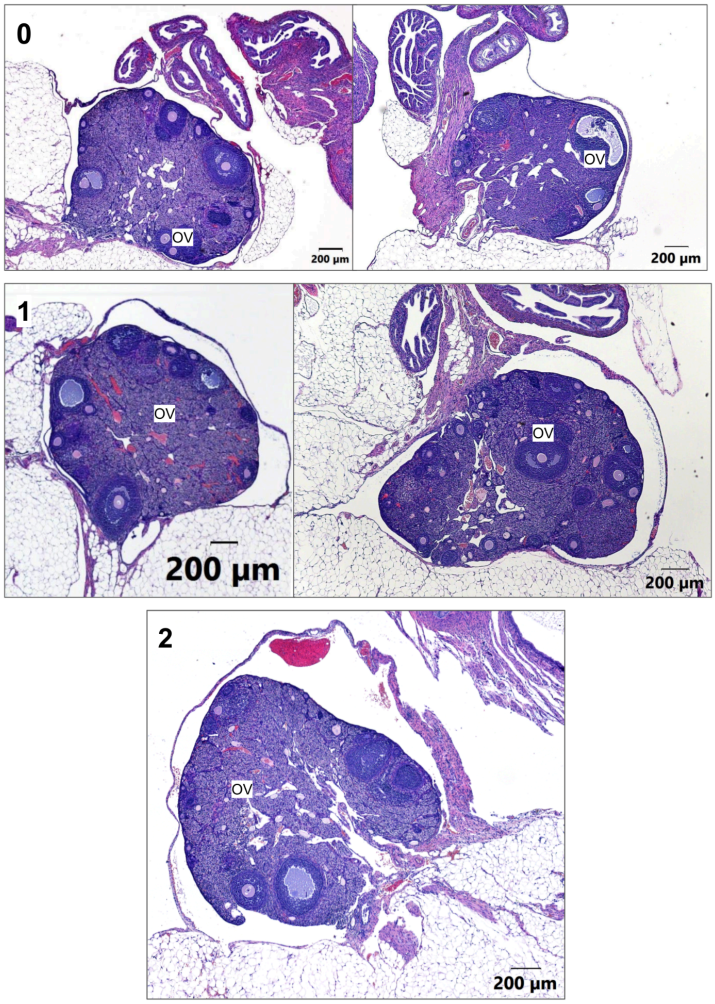

Figure 35. Chronic ovary general pathology scores with representative images. Score is bolded in the top left of associated grouped images. Images were taken by Lijek Lab members: AF (‘25), AM (‘25), GOW (‘26). OV, ovary.

1.2 Biological Ambiguity of ICC Suggests Need for a Secondary Inter-rater Reliability Analysis Method

It is important to note that the ICC, while an accepted inter-rater reliability analysis method in the literature, determines reliability based on agreement between scorers and does not consider the range of possible scores on a given scale. It is a strictly statistical assessment. While it is a trusted analysis method, it does not have a direct biological consideration, because it cannot differentiate between "sick" versus "healthy." For example, disagreement between a "2" and "3" is biologically not as drastic as the difference between a "0" and a "3," but the ICC would still deem the former as not in agreement. The difficulty in pathology scoring comes not from deciding whether there *is* pathology, and not even whether that pathology is severe or not, but rather, what granular degree of severity characterizes a given tissue. Because of the limitations of the ICC, we propose an additional method of inter-rater reliability assessment that scales the discrepancy between scorers to the range of the scale. The following equation (**Eq. 3**) describes this mathematically.

$$\text{Inter-rater reliability} = \text{AVERAGE}\left[\, 100\% - \left(\frac{|score\ 1 - score2|}{highest\ possible\ score - lowest\ possible\ score}\right) \times 100\%.\right]$$

Equation 3. Inter-rater reliability percent agreement using a scaled difference between scores. Equation can be applied to each set of two scores from each scorer, and the average of each value generated can be the overall percent agreement for one category or phenotype.

This equation is an adjustment to the traditional percent agreement method for determining inter-rater reliability (**Eq. 1**), where the denominator does not scale the difference between scorers, and the numerator focuses only on whether scorers agreed or not in binary. Percent agreement determined by this new method can better represent the expertise of scorers, as well as the biological application of each score (**Fig. 37**). Below is a mathematical example using a small data sample of uterine horn general pathology scores **(Fig. 36A**) that compares this proposed method to traditional percent agreement.

A

Rater 1	Rater 2
0	0
3	3
2	3
2	1
1	1

B

$$\textbf{Inter-rater reliability} = 100\% - \frac{\textbf{\# of disagreements}}{\textbf{\# of total ratings}} \times 100\%$$

$$= 100\% - \frac{2}{5} \times 100\%$$

$$= \textbf{60\%}$$

C

$$\textbf{Inter-rater reliability} = \textbf{AVERAGE}\left[100\% - \left[\frac{|\textbf{score1} - \textbf{score2}|}{\textbf{3}}\right] \times \textbf{100\%}\right]$$

$$= \text{AVERAGE}\left[\begin{array}{l} [100\% - [\frac{|0-0|}{3} \times 100\%] \\ + [100\% - [\frac{|3-3|}{3} \times 100\%] \\ + [100\% - [\frac{|2-3|}{3} \times 100\%] \\ + [100\% - [\frac{|2-1|}{3} \times 100\%] \\ + [100\% - [\frac{|1-1|}{3} \times 100\%] \end{array}\right]$$

$$= \text{AVERAGE}\,[100\% + 100\% + 66.7\% + 66.7\% + 100\%]$$

$$= \textbf{86.7\%}$$

Figure 36. Mathematical example comparison of traditional percent agreement to proposed scaled percent agreement. A: Random dataset for uterine horn general pathology, scored on a scale of 0-3. **B:** Inter-rater reliability analysis of **A** using traditional percent agreement method. **C:** Inter-rater reliability analysis of **A** using proposed scaled percent agreement method, where range of 0-3 scale is equal to 3. Red highlight indicates disagreeing scores.

Traditional percent agreement yields a low reliability of 60% agreement (**Fig. 36B**), but the scaled percent agreement method yields a higher reliability of 86.7% agreement (**Fig. 36C**) which highlights that although not all scores agreed, those that did not agree were only dissimilar by 1 point on the scale (**Fig. 36A**). The literature establishes that using the traditional percent agreement method, inter-rater reliability of 75% to 90% is acceptable, and any reliability above this threshold is excellent (81, 82). While these ranges are subjective, a qualitative comparison of inter-rater reliability using these methods reveals that the scaled percent agreement method is more generous and offers a less harsh view of how similarly pathologists were thinking, rather than emphasizing the importance of a singular "correct" answer about how to score a tissue. This perspective is important and was therefore used to analyze the reliability of the pilot pathology scoring system (**Fig. 37**).

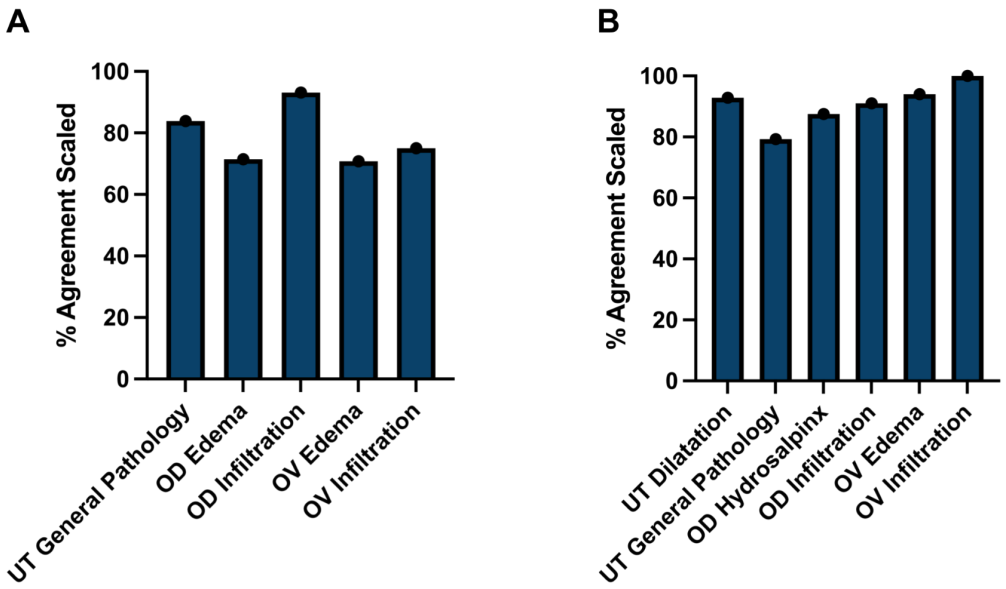

Figure 37. Inter-rater reliability using scaled percent agreement assessment of pilot acute and chronic immunopathology scales. C57Bl/6 mice were infected transcervically with *C. muridarum.* 7 (**A**) or 51 (**B**) days post infection, genital tracts were removed and fixed in formalin. Following fixation, tissues were embedded in paraffin, sliced to 4–5 μm, mounted onto slides, and stained with H&E. Tissues were assessed by two pathology scorers in an anonymized manner. Original pathology scores were analyzed for agreement between scorers using proposed scaled percent agreement method (**Eq. 3**)**.** UT, uterine horn. OD, oviduct. OV, ovary.

Using this method to assess the pilot pathology scoring systems revealed similar trends emphasized by ICC analysis. Notably, for the acute timepoint, oviduct edema (71.4% agreement), ovary edema (70.8% agreement) and ovary infiltration (75%) were low (**Fig. 37A**), which was also found during ICC analysis (ICC = 0.448, 0.0766, and 0.299, respectively) (**Fig. 27**). This further supports the idea of consolidating the edema and infiltration scales into one "general" pathology scale to avoid confusion of differentiating between these phenotypes. Uterine horn general pathology was scored more generously using this method (83.9%) (**Fig. 37A**) compared with the ICC, which yielded low reliability (ICC = 0.37) (**Fig. 27**). This is mathematically sensical, because uterine horns are assessed on a 0-3 scale. Adjusting for similarity using the scaled percent agreement method will be more forgiving than adjusting for the 0-2 scales oviduct and ovary scales, because the fractional difference between a "1" and a "2" is technically smaller with a wider range.

Analyzing chronic timepoint scores for percent agreement also produced values that indicated similar reliability to the ICC analysis. The same trend was identified where uterine horn dilatation (92.9% agreement and ICC = 0.859) was more reliably assessed than uterine horn general pathology (79.3% agreement and ICC = 0.424) (**Fig. 37B** and **Fig. 31**). This further supports the idea that there should be one pathology assessment scale for chronic uterine horn pathology to avoid confusion about which pathologies fall on which scale. The scaled percent

agreement for oviduct hydrosalpinx was relatively high (87.5%) (**Fig. 37B**), which reflected the good reliability (ICC = 0.762) using the ICC (**Fig. 31**). The oviduct infiltration (91.1% agreement and ICC = 0.651) (**Fig. 37B** and **Fig. 31**) (and the ovary edema scale (94% agreement and ICC = 0.613) (**Fig. 37B** and **Fig. 31**) were both higher using this assessment method than the ICC, which yielded moderate reliability values for both scales. The ovary infiltration scale had 100% agreement using this method (**Fig. 37B**), clearly matching the ICC value of 1 (**Fig. 31**).

Overall, the scaled percent agreement method proposed is more generous than the ICC. Although it is not a widely accepted method like the ICC, it may better reflect the experience of pathology scorers in the Lijek Lab, as well as the fact that the severity of immunopathology is a spectrum, not a rigid, one-answer integer, because it takes into account a scale of possible answers. The following inter-rater reliability analysis of the optimized pathology scoring scales will therefore employ both tactics to offer a literature-based and holistic view of inter-rater reliability.

1.3 Testing the Reliability of the Modified Scoring System through a Vaccinology Experiment

Following adjustments and clarifications to the pathology assessment scales, scorers met to discuss them. They were shown the pathology scoring guide and had a conversation while viewing slides wherein they collectively assigned

scores based on the guide. They then scored a set of completely new slides from the vaccinology portion of this research. The tissues assessed were removed at the acute timepoint following transcervical infection. Scorers were encouraged to use the guide while scoring. Intraclass Correlation Coefficient (**Fig. 38**) and scaled percent agreement (**Fig. 40**) analyses were performed on the scoring data.

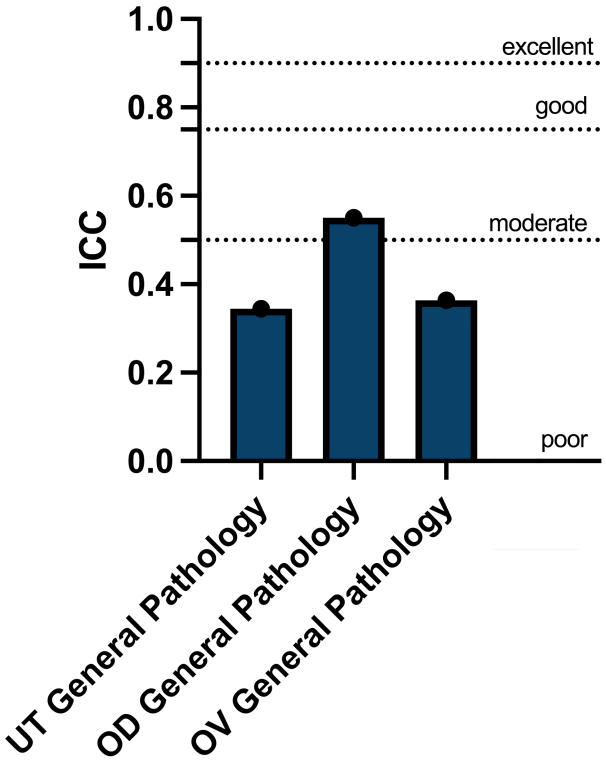

Figure 38. Inter-rater reliability of modified acute pathology scoring system using the Intraclass Correlation Coefficient (ICC). C57Bl/6 mice were infected transcervically with *C. muridarum.* 3 days post infection, genital tracts were removed and fixed in formalin. Following fixation, tissues were embedded in paraffin, sliced to 4–5 μm, mounted onto slides, and stained with H&E. Tissues were assessed by two pathology scorers in an anonymized manner for the given phenotype on the x-axis. Original chronic pathology scores for each phenotype were analyzed with the Intraclass Correlation Coefficient in RStudio to compare variance between groups (between mice) to the variance within groups (between scorers). ICC < 0.5, poor reliability; 0.5 < ICC < 0.75 moderate reliability; 0.75 < ICC < 0.90, good reliability; ICC > 0.90, excellent reliability. ICC, intraclass correlation coefficient. UT, uterine horn. OD, oviduct. OV, ovary.

The ICC reliability of each category was low considering the pathology scoring guide resource and conversation prior to scoring. The uterine horn and

ovary general pathologies had poor reliability (ICC = 0.345 and 0.364, respectively), and the oviduct general pathology scale had moderate reliability (ICC = 0.55) (**Fig. 38**). There are several possible explanations for this. Of significance is that the tissues were embedded, stained, and sliced by a different scientist than on previous experiments. Pathology scorers agreed during the consensus meeting that several tissues were confusing to score (**Fig. 39**), because the lumen was not clearly defined. Epithelial cells that typically demarcate the lumen clearly were unevenly sliced and therefore not always visible (**Fig. 39A**). Additionally, the staining appeared darker. This made it difficult to tell the difference between neutrophils and uterine horn tissue, especially when epithelial cells were not present as a clear border. Darker staining also gave mucus a thicker and less recognizable appearance (**Fig. 39B**). Finally, some of the tissues were folded into themselves during embedding, leaving dark gashes across them (**Fig. 39C**). This confusion made scorers less confident and therefore reduced their ability to definitively assign scores to each tissue.

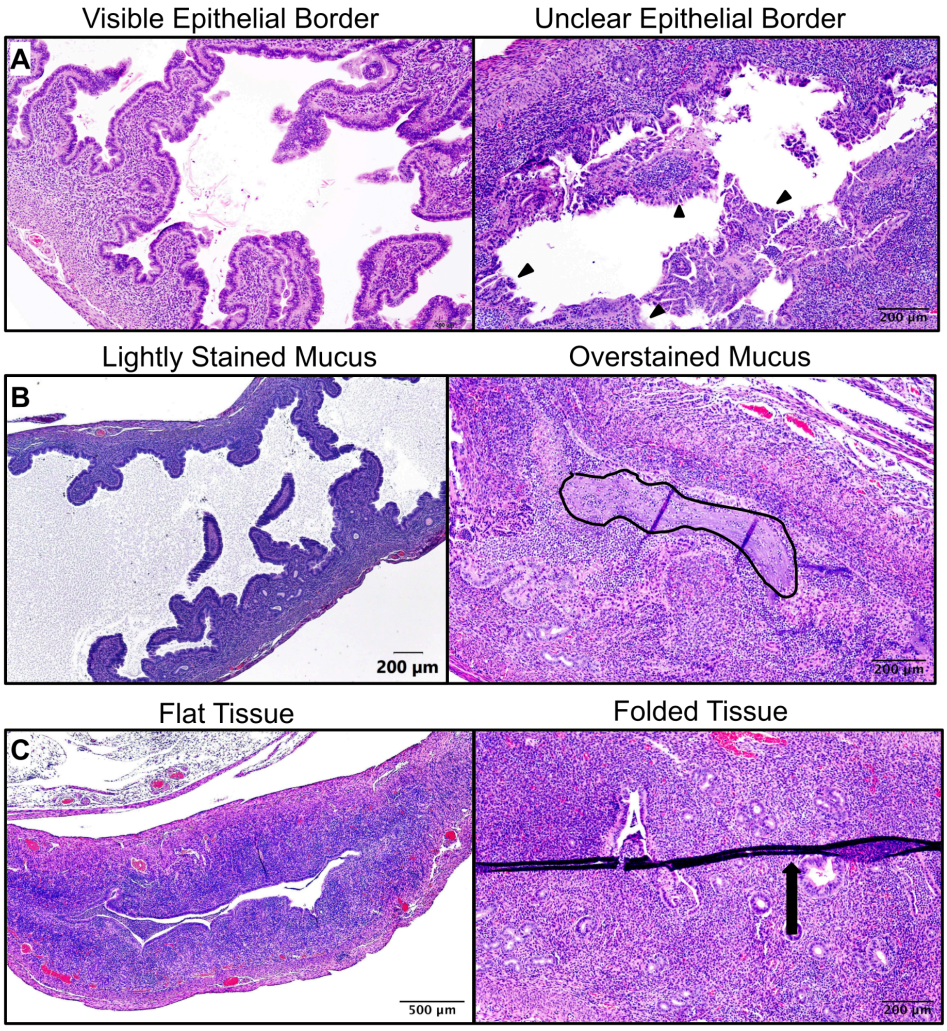

Figure 39. Slide fixation errors interfering with pathology scoring confidence. Left column contains slides from previous experiments that are well fixed and stained. Right column includes slides from the current experiment that were confusing. **A:** Differences in clarity of epithelial cell border due to slicing. Triangles indicate faded and unclear epithelial cell lining. **B:** Differences in mucus staining. Black border outlines overstained mucus. **C:** Differences in tissue levelness. Arrow indicates folded tissue.

Additionally, the group of scorers assessing these tissues was entirely new, besides one scorer. While these scorers had previously undergone extensive pathology scoring training and officially scored other experiments, they were not the same scorers as those who piloted the scoring systems analyzed above. This adds another variable to the analysis. Furthermore, there were fewer slides (n=10 mice) to assess, compared with the previous experiments analyzed (n=15). This caused discrepancies between scorers to have a larger weight statistically and provided fewer opportunities for scorers to agree on their assessment of tissues.

For this particular case where poor slicing impacted confidence in scoring, the scaled percent agreement method is valuable, because it better measures similarity in original scores rather than perfect agreement. Analysis using the scaled percent agreement method was therefore performed on the data (**Fig. 40**) for the reason that the ICC harshly grades disagreement about pathologies that are both sick, but deemed differently severe.

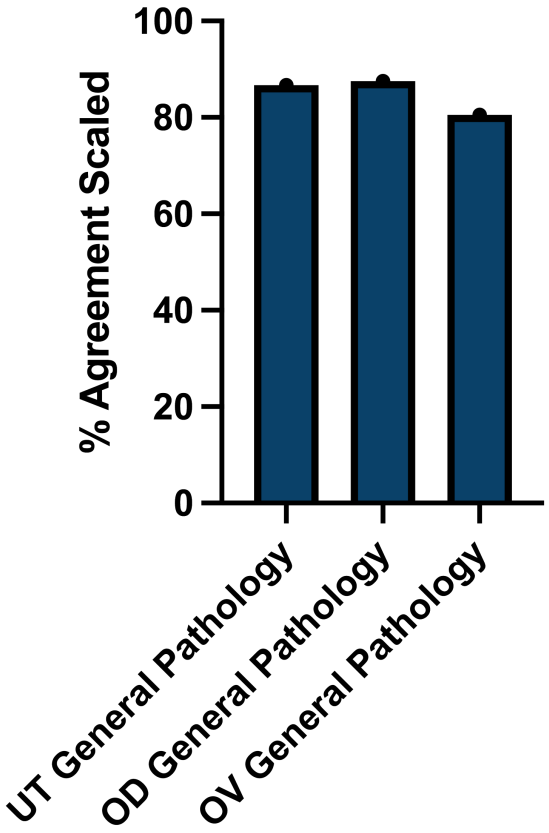

Figure 40. Inter-rater reliability of modified acute pathology scoring system using scaled percent agreement. C57Bl/6 mice were infected transcervically with *C. muridarum.* 3 days post infection, genital tracts were removed and fixed in formalin. Following fixation, tissues were embedded in paraffin, sliced to 4–5 µm, mounted onto slides, and stained with H&E. Tissues were assessed by two pathology scorers in an anonymized manner. Original acute pathology scores were analyzed for agreement between scorers using **Equation 3.** UT, uterine horn. OD, oviduct. OV, ovary.

The scaled percent agreement analysis resulted in less drastically low reliability for each category compared with the ICC analysis. Compared with the scaled percent agreement analysis on the pilot scales, we both reduced the variability of reliability and increased the mean reliability by optimizing the scales. While uterine horns were originally scored with 83.9% reliability (**Fig. 37A**) using this method, they were scored with 86.7% reliability (**Fig. 40**) after adjustment and clarification of the scales. The two scales used to assess oviducts originally had a wide range from 71.4% (oviduct infiltration) to 93% (oviduct edema) and a mean of 82.2% (**Fig. 37A**) between these scales, but were assessed with 87.5% agreement (**Fig. 40**) for the collapsed, combined scale. Finally, ovaries originally assessed with 70.8% agreement for edema and 75% agreement for infiltration (a mean of 72.9% agreement) (**Fig. 37A**) were assessed with 80.6% reliability (**Fig. 40**) for the collapsed and combined scale.

1.4 Testing the Reliability of the Modified Scoring System by Training New Lab Members

Another way to test the reliability of the modified scoring system is to test its teachability. If students improve their accuracy/reliability when compared with a trained pathologist after a training intervention, the system can therefore be considered teachable. This form of reliability means that the scales used are understandable and applicable when scientists are viewing tissues for the first

time. Because the training scientists serve as their own controls when they are assessed before and after training, their learning can be mapped (**Fig. 41**).

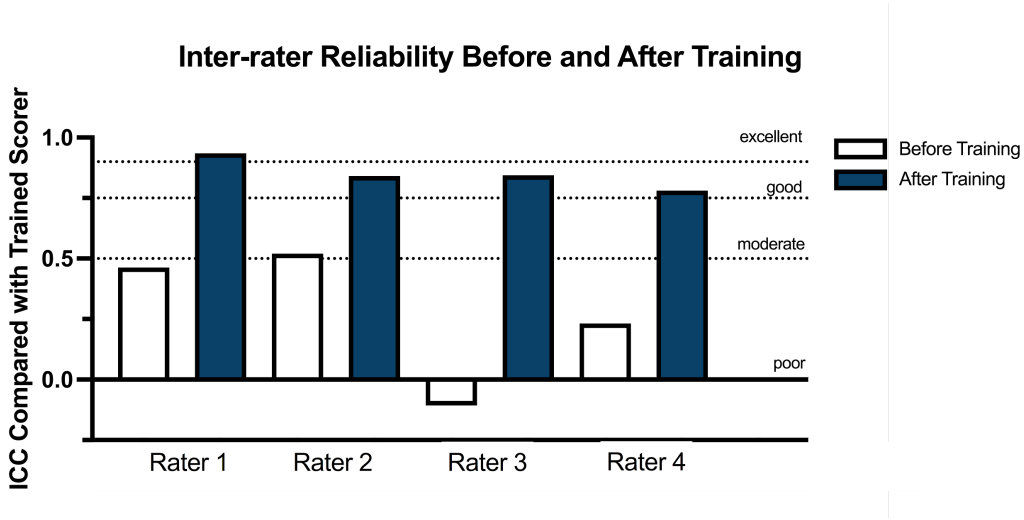

Figure 41. Teachability of modified acute and chronic pathology scoring systems assessed by a training intervention. Four untrained pathologists took a sixty question assessment where they assigned scores to uterine horns, oviducts, and ovaries, without using outside resources or collaboration. For the acute time point, ten questions each were devoted to acute uterine horn, oviduct, and ovary general pathologies. For the chronic timepoint, ten questions each focused on uterine horn dilatation, oviduct hydrosalpinx, and ovary general pathology. The participants then entered a training phase where they learned about mouse anatomy and pathology in groups and individually practiced scoring tissues. Following training, they took the assessment a second time with no resources or collaboration. The Intraclass Correlation Coefficient (ICC) was used to compare training scientists' scores to trained pathologist scores before and after intervention. ICC < 0.5, poor reliability; 0.5 < ICC < 0.75 moderate reliability; 0.75 < ICC < 0.90, good reliability; ICC > 0.90, excellent reliability. ICC, intraclass correlation coefficient.

Each scorer demonstrated strengthened pathology scoring skills after training. ICC analysis comparing their scores to those of a trained scorer revealed a transition from low or moderate reliability to high reliability for each student.

Rater 1 improved their ICC reliability from 0.463 (poor) to 0.95 (excellent), Rater 2 from 0.52 (moderate) to 0.841 (good), Rater 3 from -0.107 (poor) to 0.844 (good), and Rater 3 from 0.232 (poor) to 0.781 (good) (**Fig. 41**).

2. SPECIFIC AIM 1B: To assess immunogenicity and protectiveness of a novel CT166-conjugated VLP vaccine against *Chlamydia* infection.

2.1 QB-CT166 Produces *Chlamydia*-Specific High Titer Sera IgG

A robust sera antibody response to the QB-CT166 VLP vaccine has previously been demonstrated (**Fig. 23**) using CT166 peptide 5 (**Fig. 24**) conjugated to the vaccine. This research involves *C. muridarum* infection, and *C. muridarum* putative cytotoxins Tc-0437-Tc0439 do have sequence homology to peptide 5. We replicate that mice vaccinated in this study also produce antibodies specific to peptide 5 (**Fig. 42**).

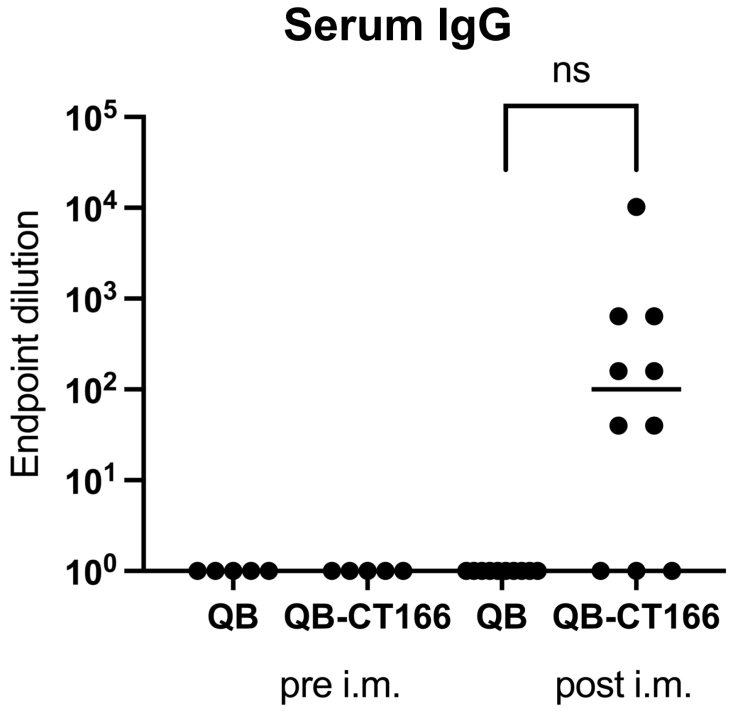

Figure 42. QB-CT166 vaccination generates high endpoint dilution titers of mouse serum antibodies specific to CT166 peptide 5. Sera of C57Bl/6 mice were collected before and after three vaccinations with 50uL of mixed peptide VLPs. Post intramuscular sera collection was performed prior to challenge with *C. muridarum* to measure antibody response before pathogen contact. Antibodies were measured using ELISA. Samples were diluted in a series of 1:40 followed by seven four-fold dilutions. Primary sample antibodies were detected with goat anti-mouse IgG conjugated to horseradish peroxidase (HRP) and the HRP substrate 3,3',5,5'-tetramethylbenzidine (TMB). Positive control (not graphed) used was sera of rabbits vaccinated with the same QB and QB-CT166 VLPs. Secondary antibody used for rabbit antisera was goat anti-rabbit IgG conjugated to HRP. Plates were read at 450nm. Threshold of detection was determined by averaging values from the negative control wells, then multiplying this by 2. Significance was determined using an unpaired, nonparametric Student's T test comparing QB and QB-CT166 mice following vaccination. ns, not significant. i.m., intramuscular.

Serum collected from QB-CT166 mice showed anti-peptide 5 antibody titers ranging from undetectable to 10240 times higher than PBS control samples (**Fig. 42**). Because there were some mice with no detectable antibody, and the mice with detectable antibody to peptide 5 had lower concentrations than expected, we decided to perform ELISA using a different peptide. Additionally, *C. muridarum* Tc0438 has complete sequence homology to *C. trachomatis* CT166 peptide 2, and Tc0437 and Tc0439 have more homology to peptide 2 compared to peptide 5 (**Fig. 24**). It is therefore important to test for antibodies specific to this peptide in order to assess whether they can potentially better protect the host from native *C. muridarum* proteins during infection.

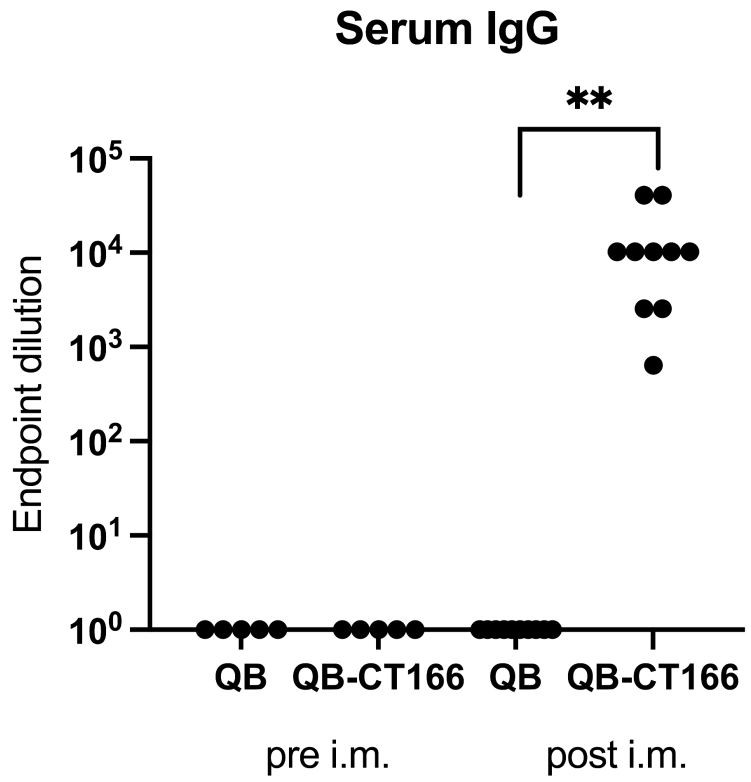

Figure 43. QB-CT166 vaccination generates high endpoint dilution titers of mouse serum antibodies specific to CT166 peptide 2. Sera of C57Bl/6 mice were collected before and after three vaccinations with 50uL of mixed peptide VLPs. Post intramuscular sera collection was performed prior to challenge with *C. muridarum* to measure antibody response before pathogen contact. Antibodies were measured using ELISA. Samples were diluted in a series of 1:40 followed by seven four-fold dilutions. Primary sample antibodies were detected with goat anti-mouse IgG conjugated to horseradish peroxidase (HRP) and the HRP substrate 3,3',5,5'-tetramethylbenzidine (TMB). Positive control (not graphed) used was sera of rabbits vaccinated with the same QB and QB-CT166 VLPs. Secondary antibody used for rabbit antisera was goat anti-rabbit IgG conjugated to HRP. Plates were read at 450nm. Threshold of detection was determined by averaging values from the negative control wells, then multiplying this by 2. Significance was determined using an unpaired, nonparametric Student's T test comparing QB and QB-CT166 mice following vaccination. **, statistically significant ($p = 0.0082$). i.m., intramuscular.

Mice vaccinated with QB-CT166 mixed peptide VLPs had significantly higher endpoint dilution titer sera antibodies specific to peptide 2 compared with QB vaccinated mice, as determined by an unpaired T test ($p = 0.0082$) (**Fig. 43**). Furthermore, one group of QB-CT166 vaccinated mice gained specificity when their sera prior to vaccination were compared to their sera post vaccination. This reproduction of results provides more strong evidence that VLP vaccines produce high titer serum IgG against multiple peptides conjugated to the VLP surface. Though the other CT166 peptides had imperfect sequence homology to Tc0437-Tc0439, these residues had similar chemical properties, which may ensure antibody recognition further. Taken together, we showed there was high titer serum IgG that could potentially neutralize *C. muridarum* via Tc0437-Tc0439. We therefore wanted to test if there were antibodies present local to the genital tract to make this possible during infection.

2.2 QB-CT166 Induces Detectable Vaginal IgG but no Vaginal IgA Production

It has previously been shown that VLP vaccines result in IgG localized to mucosal surfaces, and this is the main mechanism by which HPV VLP vaccines function. It has also been shown that the *Chlamydia* peptide-conjugated VLP vaccine also produces IgG local to the uterine horn using uterine lavage samples (77). However, these samples were taken after *C. trachomatis* infection and genital tract extraction, therefore detected antibodies could be resultant of bacterial exposure rather than vaccination. Whether this vaccine generates

CT166-specific vaginal antibodies in the lower genital tract has not yet been shown. The advantage of collecting mucosal antibodies via vaginal lavage is that it can be performed prior to infection to avoid immune boosting due to *Chlamydia* exposure. Additionally, previous mouse work in peptide-conjugated VLPs has focused primarily on IgG detection. Mucosal IgA has been detected after HPV VLP vaccination (83) and QB peptide VLP vaccination (84), but not specifically tested for after QB-CT166 vaccination.

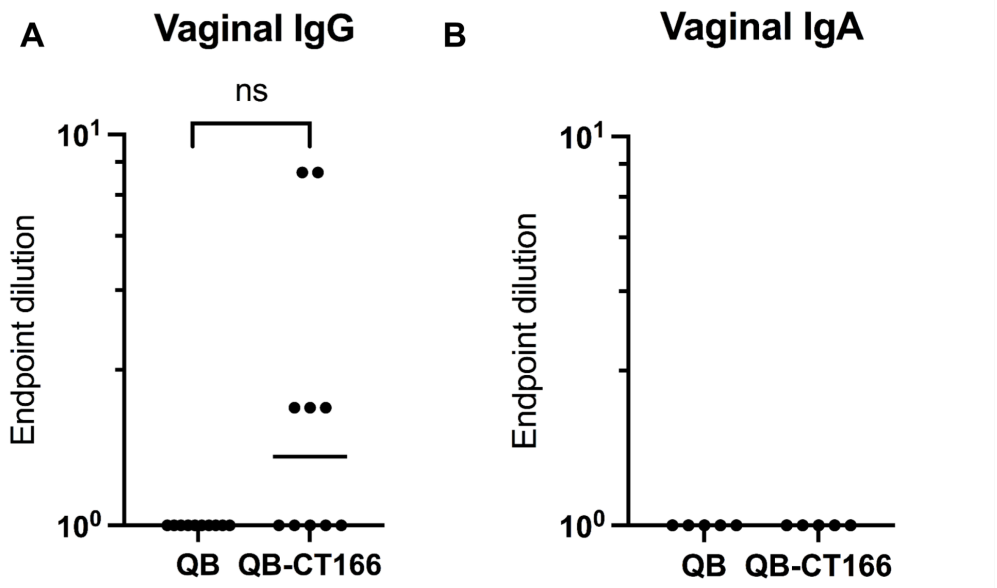

Figure 44. QB-CT166 vaccination generates low titer vaginal IgG but no detectable vaginal IgA specific to CT166 peptide 2. Vaginal lavage samples of C57Bl/6 mice were collected in sterile 1x PBS after three vaccinations with 50uL of mixed peptide VLPs. Collection was performed prior to challenge with *C. muridarum* to measure antibody response before pathogen contact. Antibodies were measured using ELISA. Samples were diluted in a series of 1:2 followed by seven four-fold dilutions. **A:** Primary sample antibodies were detected with goat anti-mouse IgG conjugated to horseradish peroxidase (HRP) and the HRP substrate 3,3',5,5'-tetramethylbenzidine (TMB). **B:** Primary sample antibodies were detected with goat anti-mouse IgA conjugated to HRP and TMB. Positive control (not pictured) used was rabbit sera collected after vaccination with QB and QB-CT166 VLPs. Secondary antibody used for rabbit antisera was goat anti-rabbit IgG conjugated to HRP. Negative control used was milk in 1x PBS blocking buffer. Plates were read at 450nm. Threshold of detection was determined by averaging values from the negative control wells, then multiplying this by 2. Significance was determined using an unpaired, nonparametric Student's T test. ns, not significant.

Quantification of vaginal antibodies via ELISA revealed that QB-CT166 vaccinated mice had variable mucosal CT166-specific IgG levels. These concentrations ranged between undetectable to an endpoint dilution 8 times higher than the PBS control (**Fig. 44A**). These values were approximately 4 logs lower than IgG levels in the serum (**Fig. 42** and **43**). While there was no statistically significant difference between QB and QB-CT166 vaccinated mice, there is a clear distinction in that no QB vaccinated mice had any detectable antibody, while several QB-CT166 had CT166-specific antibodies. This demonstrates specificity, emphasizing the immunogenicity of the vaccine.

We did not detect CT166-specific vaginal IgA in QB-CT166 vaccinated mice (**Fig. 44B**). Because IgA is important in clearing pathogens at mucosal surfaces, this could have implications in vaccine protectiveness. Because we did not detect IgG or IgA in the QB control and previously showed that QB-CT166 vaccinated mice had no serum antibodies prior to immunization (**Fig. 42** and **43**), we did not test pre-immunization vaginal lavage samples.

2.3 QB-CT166 Stimulates Detectable IgG Production in the Upper Genital Tract

To focus on upper genital tract pathology during this study, we infected mice transcervically. We therefore wanted to investigate the antibody response local to the uterine horns in addition to the vagina. Using ELISA, we tested

antibody concentration specific to CT166 peptide 2 for uterine horn homogenates at three and seven days post infection (**Fig. 45**).

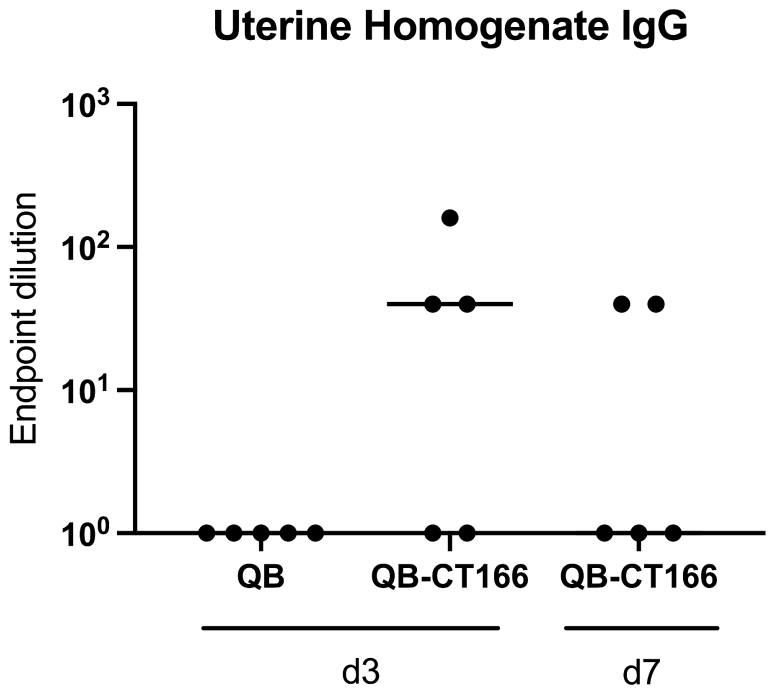

Figure 45. QB-CT166 vaccination generates low titer uterine IgG specific to CT166 peptide 2. C57Bl/6 mice were vaccinated with QB control or QB-CT166 VLP vaccines, then infected transcervically with 10^6 IFU *C. muridarum*. Genital tracts were excised 3 or 7 days post infection and homogenized. Antibodies were measured using ELISA. Samples were diluted in a series of 1:40 followed by six four-fold dilutions. Primary sample antibodies were detected with goat anti-mouse IgG conjugated to horseradish peroxidase (HRP) and the HRP substrate 3,3',5,5'-tetramethylbenzidine (TMB). Positive control (not pictured) used was rabbit sera collected after vaccination with QB and QB-CT166 VLPs. Secondary antibody used for rabbit antisera was goat anti-rabbit IgG conjugated to HRP. Negative control used was milk in 1x PBS blocking buffer. Plates were read at 450nm. Threshold of detection was determined by averaging values from the negative control wells, then multiplying this by 2. An unpaired, nonparametric Student's T test showed no significance between any group. d3, 3 days post infection. d7, 7 days post infection.

We found detectable *Chlamydia*-specific IgG in uterine horn samples from QB-CT166 vaccinated mice at both timepoints. The maximum amount of antibodies three days post infection was 160 times higher than the threshold set by a blocking buffer control. At seven days post infection, this maximum was 40 times higher than the threshold. There was no significant difference in antibody levels for QB-CT166 mice comparing these timepoints. QB vaccinated mice had no detectable uterine IgG in comparison. Despite this, there was no statistically significant difference in antibody concentration between QB and QB-CT166 vaccinated mice at either timepoint (**Fig. 45**).

2.4 QB-CT166 does not Attenuate *C. muridarum* Bacterial Burden in the Female Genital Tract

Previous unpublished work in the Lijek Lab attempted to quantify *Chlamydia* in the genital tract after QB-CT166 vaccination during *C. trachomatis* infection, and found no statistically significant differences (78). However, because *C. trachomatis* does not naturally infect the murine female genital tract, it is valuable to assess bacterial burden during *C. muridarum* infection. Additionally, at three days post infection, the body has not necessarily had ample time to begin clearing and shedding bacteria from the genital tract. It is possible that if there are no statistically significant differences at this timepoint, there may be at a later acute timepoint. This justifies quantifying bacterial burden at seven days post infection in addition to three days post infection. At this time, bacteria are still

present, but the host has had time to remove them, and possible vaccine-mediated efficiency in clearance may be more obvious.

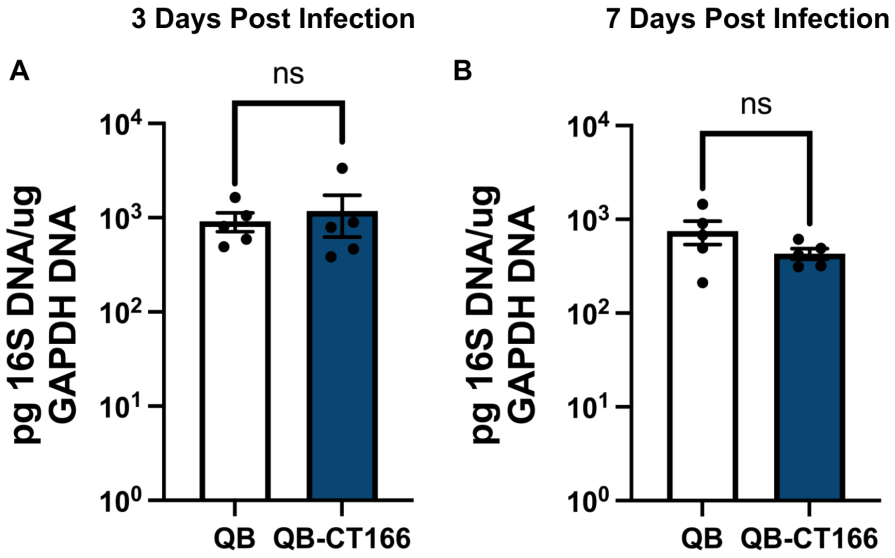

Figure 46. Female genital tract bacterial burden 3 and 7 days post infection. C57Bl/6 mice were vaccinated with QB control or QB-CT166 VLP vaccines, then infected transcervically with 10^6 IFU *C. muridarum*. Genital tracts were excised 3 (**A**) or 7 (**B**) days post infection and homogenized. DNA was extracted from homogenates and quantified via qPCR comparing rodent GAPDH to bacterial 16S gene copies. Error bars show SEM. The sample size of each group is n=5 mice. Significance was determined by an unpaired, nonparametric Student's T test. ns, not significant.

There was no statistically significant difference in bacterial burden between QB control and QB-CT166 vaccinated mice either three or seven days post infection. Three days post infection, the mean ratio of bacterial 16S DNA to mouse GAPDH DNA was 917.8pg/ug and 1175.2pg/ug for QB and QB-CT166 vaccinated mice, respectively (**Fig. 46A**). Seven days post infection, these values were 749.3ng/ug and 431.4ng/ug (**Fig. 46B**). This mirrors previous findings that QB-CT166 does not attenuate pathology via a faster clearance mechanism. While bacterial burden is a useful way to quantify *Chlamydia* infecting the genital tract and determine clearance, it does not paint a full picture of tissue disease, which can be created with pathology assessment.

2.5 QB-CT166 is not Protective Against Acute or Chronic *C. muridarum*-Induced Immunopathology

Chlamydia putative cytotoxins play a role in chronic immunopathology (48) and previous vaccination with QB-CT166 attenuated acute immunopathology during *C. trachomatis* infection (78). It has not been determined before whether QB-CT166 is protective against *C. muridarum* infection at acute and chronic timepoints.

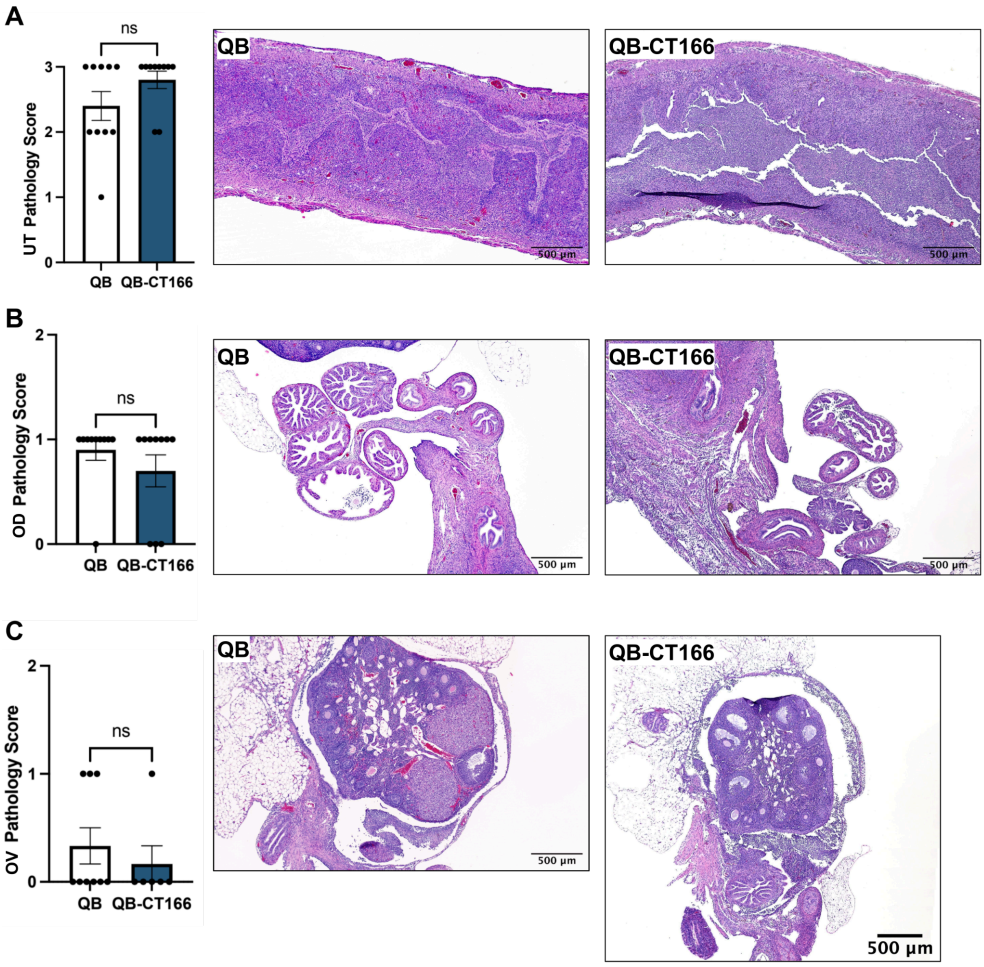

Figure 47. QB-CT166 vaccination does not reduce acute immunopathology 3 days post transcervical *C. muridarum* infection. C57Bl/6 mice were vaccinated with QB control or QB-CT166 mixed peptide VLP vaccines, then infected transcervically with 10^6 IFU *C. muridarum*. Genital tracts were excised 3 days post infection and fixed in formalin. Following fixation, tissues were embedded in paraffin, sectioned to 4-5um, mounted onto slides, and stained with H&E. Each tissue was assessed by two pathology scorers in an anonymized manner. Pathology scorers then came to an anonymized consensus on scores following individual assessment. Representative images are provided next to pathology score data for uterine horns scored a "3" (**A**), oviducts scored a "1" (**B**), and ovaries scored a "1" (**C**). Significance was determined using an unpaired, nonparametric Student's T test. UT, uterine horn. OD, oviduct. OV, ovary.

We found no statistically significant difference in acute immunopathology between QB and QB-CT166 vaccinated mice (**Fig. 47**). Uterine horns, oviducts, and ovaries were assessed using the refined scales developed in the previous aim of this research. Both QB and QB-CT166 vaccinated mice exhibited similar pathological severity as seen through neutrophil infiltration and mucus in the uterine horn lumen (**Fig. 47A**). Oviducts in both groups were equally affected by neutrophils and mucus as well (**Fig. 47B**), and ovaries displayed bursa thickening, cellular infiltration, and mucus regardless of experimental group (**Fig. 47C**).

In the previous Lijek Lab project that showed ameliorated chronic oviduct pathology, there were no significant differences in acute immunopathology (48), similar to what is shown in **Figure 47**. However, the QB-CT166 vaccine was not protective against chronic immunopathology fifty one days post infection (**Fig. 48**).

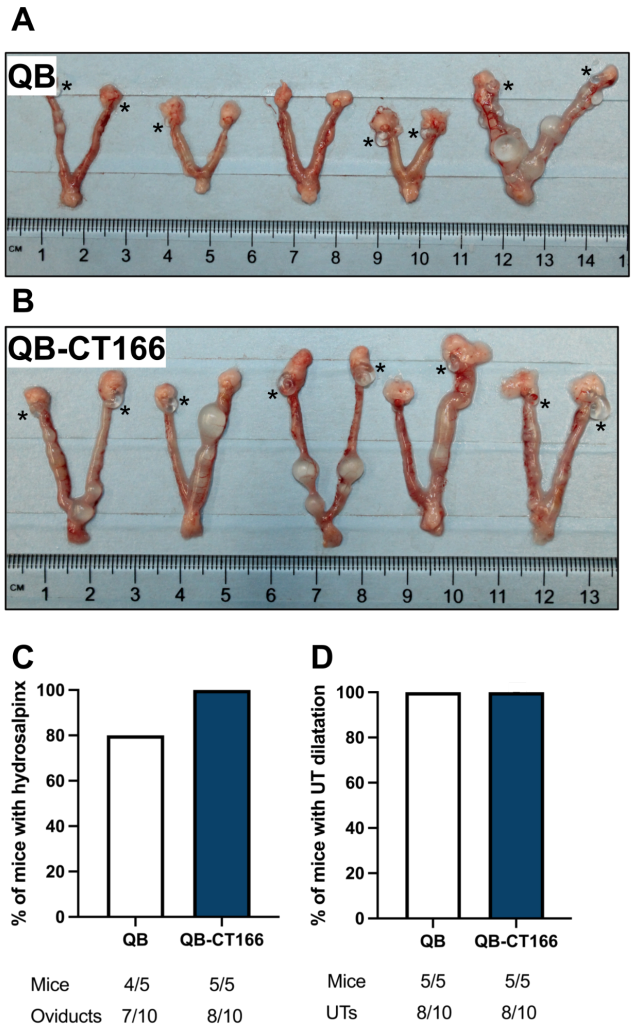

Figure 48. QB-CT166 vaccination does not ameliorate chronic immunopathology 51 days post transcervical *C. muridarum* infection. C57Bl/6 mice were vaccinated with QB control or QB-CT166 mixed peptide VLP vaccines, then infected transcervically with 10^6 IFU *C. muridarum*. Genital tracts were excised 51 days post infection and imaged. **A:** QB control female upper genital tracts. **B:** QB-CT166 female upper genital tracts. Hydrosalpinx is indicated by asterisks (*). **C:** % incidence of mice with hydrosalpinx displayed graphically. Fraction of total oviducts affected (2 per mouse) is also given. **D:** % incidence of mice with uterine horn dilatation graphically. Fraction of total uterine horns affected (2 per mouse) is also given. UTs, uterine horns. Images taken by Lijek Lab member HN ‘27.

Gross pathology showed no difference in prevalence of chronic immunopathology between QB and QB-CT166 vaccinated mice (**Fig. 48**). The incidence of hydrosalpinx in QB vaccinated mice was 80% (**Fig. 48A, 48C**) and 100% in QB-CT166 vaccinated mice (**Fig. 48B, 48C**). In terms of individual sides, 70% of the total oviduct tissues in the QB vaccinated group exhibited hydrosalpinx, compared with 80% of the total oviducts for QB-CT166 mice (**Fig. 48C**). We observed that 100% of the mice in both groups had uterine horn dilatation (**Fig. 48A, 48B, 48D**). Because we were able to determine chronic immunopathology incidence with the naked eye, it was unnecessary to section, stain, and mount the tissues onto slides for further analysis.

DISCUSSION

1. Summary of Specific Aim 1a Results

Specific Aim 1a focused on testing the reliability of a scoring system for *Chlamydia*-induced tissue-specific pathology. We predicted that if double anonymized scoring does not yield perfect agreement among scorers, clearly defining multiple scales for tissue-specific phenotypes and their severities will generate a nuanced and reliable scoring system. Intraclass Correlation Coefficient (ICC) analysis of the pilot scoring system revealed that scales needed to be adjusted and collapsed to make them clearer. We adjusted the pathology scales to make biological sense for the given timepoint post infection and to be clear for pathology scorers to use. In this way, the ICC was useful, but was notably harsh when scorers assigned similar, but not the same, scores to tissues. For this reason, we proposed a modified percent agreement method and applied this analysis to the pilot scores, further justifying the modifications we made.

Both ICC and scaled percent agreement methods were used to determine inter-rater reliability of scorers who used the optimized scales to assess pathology in Specific Aim 1b of this research. Using the ICC, reliability ranged from poor to moderate, while the scaled percent agreement showed slight improvements in reliability. Imperfect reliability may have been due to slide fixation errors.

Reliability was also tested via an intervention study where students with little to no previous pathology scoring experience completed a scoring assessment prior to training and after. The study demonstrated that participants developed

strong pathology scoring skills as a result of training on the optimized scoring system. This indicates that the scoring system is teachable to new thinkers and is usable for future scoring in the lab. Overall our hypothesis was supported because we developed a nuanced, teachable scoring system with resources for training.

1.1 Inter-rater Reliability Should be Transparently Reported but not Rigidly Calculated

The majority of *Chlamydia* studies that analyze pathology do not report any statistical analysis methods that assess inter-rater reliability. This gap is an opportunity to improve the robustness of scoring systems and encourage transparency about reliability. This transparency about how pathology is assessed and how reliable this assessment is can strengthen a common understanding of *Chlamydia*-induced phenotypes in the mouse model and how they depend on infection species, route, and timeline of infection.

As demonstrated in this research, inter-rater reliability calculation methods provide different insights about scoring systems. The scaled percent agreement method employed here was more forgiving and perhaps more biologically relevant than the ICC, which is widely accepted in the broad field of pathology scoring, but not as frequently employed by the *Chlamydia* field. Having multiple interpretations of inter-rater reliability can be viewed as a strength because it adds nuance. If multiple analysis methods indicate low reliability of a scale, it is clear that the scale should be clarified, and more training may need to occur. This nuance also emphasizes that there is never one correct answer when it comes to

scoring a tissue, because the process involves subjective, holistic expertise. In addition to increasing the incidence and specificity of reporting inter-rater reliability in the *Chlamydia* field, it would be beneficial for researchers to employ multiple analysis methods. This is exemplified by two studies designed to improve inter-rater reliability among pathologists (Pavlisko et al. 2025, Abdel-Halim et al. 2022) (85, 86). Both studies employ traditional percent agreement and the Cohen Kappa Coefficient, which adjusts traditional percent agreement by subtracting agreement that may have occurred due to chance. Establishing multiple modes of inter-rater reliability reporting, as we have done here, reflects transparency and scoring system robustness.

1.2 Inter-rater reliability Analysis Yielded New Resources for Robust Pathology Scoring

Statistical analysis is important to transparency, but it was only part of the larger project to develop a robust scoring system in our lab, so future lab members can score with high reliability and expertise. The analysis was productive in many ways. First, it allowed us to collapse our scales so they were less granular and confusing, yet they maintained tissue and timepoint specificity. Second, to clarify these scales, a detailed pathology scoring guide was created for the lab including representative images of scores, annotations, and decision-making flow charts. This guide will be useful for future scoring and training. Third, a new inter-rater reliability analysis method was created in response to the harshness of the ICC. This method adjusted traditional percent agreement reliability by scaling to the

given pathology scale range. The purpose of this was to more heavily consider the biology of pathological severity.

1.3 Limitations of Specific Aim 1a

A limitation of the ICC is that it is not generalizable to any scorers other than those involved in the given dataset (87). In other words, ICC inter-rater reliability determined from one set of scorers does not reflect the reliability of another hypothetical group, had they the opportunity to assess the same slides with the same scoring system. Because of this limitation, we cannot say the ICC-based reliability of our scales applies to any broad, random group of scorers. Despite this, the ICC was still useful for streamlining our pathology scoring system. We used the ICC as an internal measure of inter-rater reliability on datasets from two different groups of scorers. The first group developed the pilot scoring system, and the other tested the modified version of this scoring system. Because neither the scorers nor the scales themselves were the same for the two analyses, our goal was not to test the reliability of one scoring system or group of scorers over time, but to gain a general sense of reliability of each scoring system individually.

1.4. Future Directions for Specific Aim 1a

1.4.1 Assessment of Inter-rater Reliability in the Future of the Lab

To continue our intention of assessing reliability in the context of biology rather than statistics alone, we recommend using the scaled percent agreement analysis method to assess inter-rater reliability in the future. We also propose another stance on reliability analysis, as follows. Based only on the low ICC and moderate percent agreement values presented in this work, it may seem at first that scorers in the lab are poorly reliable. However, these values actually reveal a vital detail about the inter-rater reliability analysis method employed, rather than the scoring itself. Both methods assess the agreement of scorers when they first view tissues. This assesses original, individual opinions of scorers but does not take into account a vital step of the process, which is the consensus meeting between scorers. Science is collaborative, and conversation is imperative to ensure the robustness of consensus scores. The anonymized consensus meeting is a human aspect (**Fig. 25B**) of pathology scoring, because scorers look at tissues together, share their opinions, ask each other questions, and assign a score as a group. The final decision about a score comes not from the first two scorers who rated the tissue, but other scorers present who see it with fresh eyes. In the future, it may be helpful to assess the reliability of the scoring system by comparing original scores to the consensus score. This would assess intra-rater reliability, rather than inter-rater reliability, and would reflect how individual scores compare to a collaboratively determined answer rather than the answer of just one person.

Another variable in the inter-rater reliability analysis of the modified scoring system was scorer confusion due to tissue processing and slide mounting.

If there are slide staining and fixation issues that impact scorer certainty in the future, it may be beneficial to have each rater record their confidence level associated with each score they assign. After this, inter-rater reliability analysis can be performed only on tissues that were scored confidently. This would remove the variable of poorly sliced or stained tissues as it affects reliability.

1.4.2 Future Training on Pathology Scoring Should Follow a Similar Format

Because the intervention study where scientists learned to score pathology demonstrated strong growth in each participant, we recommend that future pathology scoring training follows the same format. A trained scorer will host meetings with new members, showing them various *Chlamydia* infected tissues and explaining anatomy and possible pathologies. The scorer will introduce the scoring guide to the scorers and walk them through several examples of how to score each slide using the guide as a tool. Scorers will practice scoring individually and continue meetings with the trained scorer to ask questions and complete scoring with decreasing amounts of guidance. After this stage of training, new lab members will complete a pathology-scoring workflow where they assess slides under anonymized conditions and hold a consensus meeting to discuss scores. This will provide practice with the collaborative discussion regarding pathology.

2. Summary of Specific Aim 1b Results

Specific Aim 1b sought to assess immunogenicity and protectiveness of a novel CT166-conjugated VLP vaccine against *Chlamydia* infection. We predicted that the vaccine would be highly immunogenic and protective against *C. muridarum* infection. This hypothesis was partially supported. The QB-CT166 VLP vaccine was highly immunogenic, producing a robust systemic antibody response. We show that mice vaccinated with QB-CT166 generate a high endpoint dilution titer IgG response specific to *C. trachomatis* CT166 peptides, which have strong sequence homology to *C. muridarum* Tc0437-Tc0439. We also show that CT166-specific IgG is detectable in the vagina after QB-CT166 vaccination, although there was no detectable IgA. There was detectable IgG in uterine horn homogenates of QB-CT166 vaccinated mice 3 and 7 days post infection, as well. However, these antibodies are not sufficient to protect against *C. muridarum*: we observed no differences in bacterial burden or immunopathology at acute and chronic timepoints comparing QB and QB-CT166 vaccinated mice.

2.1 Possible Explanations for QB-CT166 Lack of Protection Despite Immunogenicity

2.1.1 Antibody-Linked Lack of Protection

One possible explanation for the failure of QB-CT166 VLPs to protect against *C. muridarum* is the low antibody concentration local to the genital tract. The HPV VLP vaccines on the market are the basis for the technology we used in this research. Self-adjuvanting properties of VLPs produce high titer serum IgG

which can travel to the cervical epithelium via active transcytosis or exudation (21, 74). These antibodies can neutralize pathogens and curb infection. The HPV vaccine also produces local IgA at the cervix, and these local IgG and IgA antibodies are long lasting (73, 83).

Compared with other studies that tested VLP vaccines in mice, we report similarly high serum IgG concentrations (between 10^2 and 10^5 logs higher than the control) (77, 88, 89). Our findings also agree with the literature in that we detected IgG at the mucosal surfaces, but at far lower levels than in the serum (77, 84, 88). Also in accordance with the literature, some mice lacked detectable IgG in the vagina. This could be due to their phase of the estrus cycle at the time vaginal lavage was performed: cervix IgG of HPV-vaccinated people in the ovulatory phase of the menstrual cycle is nearly ten fold lower in concentration compared to other phases (90). However, vaginal lavage samples in this research were collected within four days of the mice receiving DMPA. Work by a previous Lijek Lab member shows that within four days of receiving DMPA, all mice in an experimental group were synchronized in diestrus (91). Therefore, hormonal variability was less likely a contributor to differing antibody levels in the vagina.

Unlike the approved HPV vaccines, QB-CT166 did not produce detectable vaginal IgA. One possible explanation for this is that the vaginal lavage samples we collected were heavily diluted in PBS. This, however, would not explain why we detected IgG but not IgA, especially given that IgA is the predominant antibody isotype in the mucosa (63). There are three differences between our

research and the HPV vaccine studies that could cause IgA differences: VLP platform, pathogen, and host. The first possibility is the difference in capsid protein used in the VLP platform. Our vaccine utilized bacteriophage capsid QB, rather than the HPV L1 capsid. These protein multimers are both highly immunogenic, but structural differences may cause differences in immune response. Second, the HPV studies referenced were conducted in humans, rather than mice, and third, studied interactions with HPV, not *Chlamydia*. Unlike humans, mice only have one type of IgA, and class switch recombination to the IgA isotype is dependent on different PAMPs and cytokines (63, 92). These differences may cause lower levels of IgA in mice than in humans.

It is also somewhat surprising that the HPV Gardasil and Cervarix vaccines produce effective local antibodies. Producing a mucosal immune response to a systemically administered vaccine is an ongoing challenge in vaccine development (63, 92–94). This is because the immune response is tailored to the site of infection or vaccination. Because antigen encounter is not occurring in the genital tract upon intramuscular vaccination, the immune response is not specific to that area. T-dependent B cell activation therefore does not involve the proper cytokines that would cause antibody class switch recombination into the IgA isotype, and likewise there would be no B cell migration to the genital tract.

With low IgG levels and no IgA available to neutralize *C. muridarum* in the genital tract, the abundant bacteria could proliferate nearly unhindered and

establish a robust infection with bacterial burden and immunopathology typical of infection without prior vaccination.

2.1.2 Putative Cytotoxins are More Important for *C. trachomatis* Infection than for *C. muridarum* Infection

The lack of QB-CT166 protectiveness can be explained genetically, as well. The Lijek Lab has previously shown that QB-CT166 was protective against acute *C. trachomatis*-induced pathology (78). It is possible that the putative cytotoxin of *C. trachomatis* is more vital for its survival and proliferation than the homologous Tc0437-Tc0439 are for *C. muridarum*. Our collaborators have shared unpublished evidence that Tc0437-Tc0439 are localized to the surface of the *Chlamydia* EB and therefore accessible to antibodies. However, more work needs to be done to confirm this. If the proteins are not vulnerable to antibody neutralization, the B cell response that QB-CT166 is based on would not be advantageous.

Even successful neutralization of these proteins may not affect the ability of *C. muridarum* to invade host cells and ascend the genital tract. Evidence for this difference in importance is seen through the fact that deletion of Tc0437-Tc0439 did not attenuate the cytotoxic cell rounding observed due to large cytotoxins and CT166 in cell culture (48). Additionally, while it is possible to create a viable strain of *C. muridarum* without its putative cytotoxins (48), *C. trachomatis* is unable to survive using the same process to delete CT166 (95). If it

is the case that the vaccine is more effective against *C. trachomatis* infection, it may still be a promising candidate for a human *C. trachomatis* vaccine.

2.2 Limitations of Specific Aim 1b

2.2.1 Vaccination with *C. trachomatis* Antigens Followed by Infection with *C. muridarum*

A possible antibody-linked limitation of this research is that the antigens in the QB-CT166 vaccine were peptides derived from the *C. trachomatis* protein CT166, but we infected mice with *C. muridarum*. If the antibodies generated upon CT166 peptide exposure did not have enough specificity to *C. muridarum* proteins encountered upon infection, this would reduce the neutralization capability of the antibodies. We justified this discrepancy using the high sequence homology between CT166 and Tc0437-Tc0439 of *C. muridarum* (**Fig. 24**). The peptides conjugated to the QB VLP were specifically chosen with the possibility in mind that mice could be infected with either *C. trachomatis* or *C. muridarum*, as any substitutions contain amino acids of similar chemical properties. Therefore, some substitutions may not have impacted the clefts of some antibodies at all.

An adapted ELISA protocol was used to quantify antibody specificity to short peptides in response to QB-CT166 vaccination. One limitation of this protocol was that we had to select one peptide out of the five conjugated to our vaccine to coat the ELISA plate. Therefore, **Figures 43-45** display antibody specificity to peptide 2 but not any of the other peptides. We were purposeful in our selection of CT166 peptide 2 because it has complete sequence homology to

C. muridarum Tc0438. We therefore can conclude that antibodies specific to this peptide could recognize either *C. trachomatis* or *C. muridarum* proteins if an encounter occurred and the peptides were accessible to the antibodies. All peptides were selected using the IEDB because they had high chances of being B cell epitopes, but the exact responses to the other peptides remains unknown. As exemplified by antibody levels specific to CT166 peptide 5 in **Figure 42**, mice may have lower responses depending on the given peptide. This result could be linked to lower peptide 5 immunogenicity, or it could be due to reagent age. Peptide 2 was freshly suspended in water for these experiments, whereas a solution of peptide 5 was thawed from previous Lijek Lab experiments. In the future, we could conduct ELISA using peptides 1, 4, or 7 to determine their relative immunogenicity.

2.2.2 Tissue Selection and Collection Method for ELISA

Performing ELISA on different tissue samples allowed us to quantify both systemic and local antibodies. We analyzed the following samples: sera, vaginal lavage fluid, and uterine homogenates collected three and seven days post infection. While sera antibody concentrations were high, antibody levels in vaginal lavages and uterine homogenates were low. There are potential procedural explanations for these values in addition to the biological possibilities explained above.

In vaginal lavage samples, we observed low levels of IgG. A non-biological explanation for these dilute levels could have been the large volume of PBS (200uL) used to collect the lavage. One study by Jamu et al. (2025) performed vaginal lavage to collect vaginal antibodies in mice, but used a smaller volume (30uL) to collect a more concentrated sample, and did so three times over the course of a week (84). This frequency is advantageous because it reduces the hormonal variability affecting IgG levels by pooling samples from multiple days in the mouse's cycle. This protocol could be employed in the future to improve ELISA using vaginal lavage samples. Despite this potential difference, low mucosal levels of antibodies align with the literature, as explained above.

In contrast, uterine horn homogenates displayed low antibody concentrations (ranging from undetectable to 160 times higher than the control) compared to previous Lijek Lab work on the QB-CT584 VLP, where homogenates had similar antibody concentrations to sera (77). In this case, a methodological explanation is more likely. Uterine horns are vascularized. It is consequently unavoidable to create a uterine horn homogenate sample without traces of sera antibodies. Differences between past homogenate ELISAs and those presented here are likely due to the amount of vascularization on the uterine horns. More thorough fat removal during dissection will remove more vasculature, thus reducing the amount of serum antibody in the sample.

Another method we could use in the future to quantify mucosal antibody in the uterine horn is uterine lavage. This technique involves washing uterine

horns posthumously with PBS in a similar way to vaginal lavage. The difference between the two is that uterine lavage antibody levels may be inflated due to immune boosting of *Chlamydia* exposure, because the technique can only be performed after infection and tissue excision. Despite this caveat, this method allows for mucosal antibody quantification only, rather than potential quantification of serum antibodies present due to vasculature in uterine horn homogenate samples.

2.2.3 Selection of Transcervical *C. muridarum* Infection in a Mouse Model

Using female mice as our model system provides a highly representative picture of what occurs in humans during VLP vaccination and *Chlamydia* infection. However, this model is not a perfect representation of human disease. It is possible that our results differ from what would occur with humans in two ways. First, the exposure of the host to the vaccine results in a different immune response in mice compared to humans, especially given the complete lack of genetic diversity in C56Bl/6 mice. This sameness is unrealistic compared to human diversity and therefore does not allow for the nuanced dependence of the immune response on genetics (43). Contrastingly, genetic identicalness allowed us to control variables during experimental design. Importantly, VLP vaccines are known to be highly immunogenic in humans, which demonstrates that the model is still a powerful and representative tool.

Second, in using *C. muridarum* instead of *C. trachomatis*, we did not assess interactions between the host and the human-infecting strain, which is

another way in which our methods differ from natural human infection. *C. trachomatis* infection is more representative of natural infection, because it causes mild acute immunopathology and results only occasionally in chronic immunopathology. Additionally, by bypassing the cervix during transcervical infection, we gave the bacteria an advantage they would not have upon natural, intravaginal infection (22). The reason for our selection of the *C. muridarum* transcervical infection model was to enable consistently observable chronic immunopathology, which allowed us to test the protectiveness of our vaccine against uterine horn dilation and oviduct hydrosalpinx. Furthermore, using *C. muridarum* is advantageous because mice are its natural host.

Because of the limitations of our model, we cannot conclude that the vaccine is not protective against *C. trachomatis* in humans. Our lab has demonstrated its protectiveness against *C. trachomatis* in mice (78), and as described above, lack of protectiveness may be due to lesser genetic importance of putative cytotoxins *C. muridarum* compared to *C. trachomatis*. Further experimentation, described below, is necessary to draw more conclusions about its protectiveness against both strains.

2.2.4 Use of qPCR to Quantify Bacterial Burden

Additionally, our use of qPCR to determine bacterial burden is limited. While qPCR is highly sensitive at amplifying even low amounts of DNA to quantify gene copies, it does not necessarily result in quantification of live

Chlamydia EBs, because even dead *Chlamydia* contain 16S genes which can be amplified. For this reason, inclusion forming unit (IFU) analysis is another possible technique that can quantify the bacteria. Bacteria preserved at -80℃ in SPG are allowed to infect cell monolayers, and the inclusions created are counted (96). This demonstrates how many live and infecting *Chlamydia* are present in a sample. At both 3 and 7 days post infection, homogenates were frozen at -80℃ in SPG to preserve live *Chlamydia* and therefore could be analyzed in this way in the future. However, because the vaccine was not protective against immunopathology, it is not likely that there will be differences in viability of bacteria. It is also possible to perform bacterial burden analysis at a slightly later timepoint, such as 10 or 15 days post infection, to determine if there are differences in bacterial clearance. However, it is unlikely that there will be differences, as there are no chronic pathology differences between groups 51 days post infection.

2.3 Future Directions of Specific Aim 1b

2.3.1 Determining Whether CT166-Specific Antibodies are Capable of Protection Against *C. muridarum*

The antibody response generated by QB-CT166 was not sufficient to protect against *C. muridarum*. Whether this is due to the antibodies themselves (either their low amounts locally or specificity to CT166 rather than Tc0437-Tc0439) can be determined through a pre-opsonization experiment. In

this investigation, both *C. trachomatis* and *C. muridarum* will be preincubated with pooled, heat-inactivated sera collected from QB and QB-CT166 vaccinated mice from the current study. High titer IgG in the QB-CT166 sample is given the chance to opsonize the bacteria prior to infection, allowing the mouse to receive a passive vaccination. The sera will be heat-inactivated to prevent complement-mediated destruction of *Chlamydia* EBs as a confounding variable. Mice will be infected transcervically with preincubated sera and bacteria and genital tracts will be analyzed for differences in clearance via bacterial burden 3 days post infection. If mice infected with QB-CT166 sera and *Chlamydia* show reduced bacterial burden compared to mice infected with QB sera and *Chlamydia*, we can conclude that the antibodies generated by active vaccination are protective but not concentrated enough locally. A previous study in our lab by Webster et al. (2022) found that there was a reduction in bacterial burden using sera created from the novel QB-CT584 peptide vaccine, incubated with *C. trachomatis* (77). If there is a reduction in bacterial burden in pre-opsonized *C. trachomatis* but not pre-opsonized *C. muridarum*, this may be due to differences in antibody specificity and incomplete protein homology of CT166 and Tc0437-Tc0439. An alternative explanation would be that Tc0437-Tc0439 is not necessary for *C. muridarum* to establish robust infection, or that the tertiary structure of the peptides in a fully folded protein is not recognizable to antibodies that are specific to linear peptide sequences present on the QB-CT166 VLP.

Another potential outcome is that the vaccine is not protective against either strain. This would indicate that it should no longer be a candidate for further study. This information would also provide insight to a larger question in the field, which is whether a B cell response is sufficient to protect against *Chlamydia* infection. A limitation of our vaccine strategy is that it relies only on a B cell response, but it is possible that a T cell response is required in *Chlamydia* clearance (9, 47). If this is true, we would have strong evidence that vaccine research in our field should focus primarily on inducing at least a T cell response.

2.3.2 Improvements of QB-CT166 to Generate Highly Concentrated Local Antibody

Should the vaccine-generated antibodies prove to be protective during pre-opsonization, there are improvements that can be made to vaccine administration to induce higher levels of local IgG and IgA. Jamus et al. (2025) administered a QB VLP peptide vaccine via varying vaccination schedules: either three intramuscular injections or an intramuscular prime followed by two intranasal aerosol boosts. The latter vaccination schedule involving the mucosal site of the lungs produced comparable levels of sera IgG to the intramuscular injections alone, but in contrast produced much longer lasting levels of mucosal IgA measured through vaginal lavage (84). Another study by Nardellihaefliger et. al (2005) tested HPV VLP vaccines in humans and compared intramuscular and aerosol vaccination intranasally and through the mouth. The outcome was that the vaccine inhaled through the mouth was as immunogenic as the intramuscularly

administered vaccine, with comparable levels of systemic IgG and sera IgG and IgA at the cervix. The only vaccines that produced secretory IgA were the mucosally administered vaccines (97). Mucosally administered vaccines are promising due to their comfortability and accessibility (84, 97). Should pre-opsonization demonstrate potential of QB-CT166 generated antibodies to protect against *Chlamydia* infection, a mucosal route of administration could optimize the vaccine.

There are other ways to optimize vaccines to induce a mucosal immune response. The first, developed by Shin and Iwasaki (2012) to protect against Herpes Simplex Virus (HSV), uses "prime and pull" technology, where an intramuscular "prime" injection is followed by a topical chemokine "pull" boost applied in the vagina to induce immune cell migration to the genital tract (98). This method induced high amounts of pathogen-specific CD4 and CD8 T cells at the vagina compared with systemic immunization alone. Tregoning et al. (2013) investigated whether a B cell response could be amplified at the genital tract using the same strategy. This is relevant to the current research in terms of improving the QB-CT166 vaccine. Per this research, applying a topical chemokine was not successful, but applying the adjuvant monophosphoryl lipid A (MPLA), an LPS derivative, induced pathogen-specific IgA following intranasal vaccination of mice (99). Another study by Prior et al. (2023) identified a particular adjuvant that could be administered systemically, rather than topically, to pull antibodies to the genital tract. Double mutant heat-labile toxin (dmLT) caused production of

mucosal, class-switched IgA when added to an intradermal vaccination in mice (100). These strategies are useful options for improving our vaccine, should pre-opsonization show us that our antibodies are protective.

2.3.3 Further Investigations of *Chlamydia* Immunopathology Mechanism

This vaccinology research is part of a larger investigation into how *Chlamydia* evades the immune system and causes dangerous chronic immunopathology observed in humans. In this project we took an immunological approach in an attempt to neutralize the putative cytotoxins Tc0437-Tc0439 of *C. muridarum* with antibodies. In the past, we have taken a genetic approach, infecting mice with the novel *C. muridarum* strain Δtox, from which the putative cytotoxin genes of interest were deleted. Mice infected with this strain demonstrated reduced hydrosalpinx incidence. This work can extend further to investigate the mechanism by which this occurred. Our lab recently developed a tissue-sectioning technique, where oviduct and ovary tissue can be separated from uterine horns prior to homogenization. This technique opens many doors for testing new scientific questions. Using tissue-sectioned homogenates, we can use qPCR to analyze differences in tissue-specific bacterial burden over time. This would inform us about *Chlamydia* ascension in particular tissues. Additionally, we can examine tissue-specific host gene expression using RT-qPCR. A future project could involve infecting mice with Δtox *C. muridarum* and comparing ascension over time, as well as host inflammatory cytokine expression, to control

C. muridarum infection. Differences could reveal the mechanism by which chronic immunopathology was attenuated in Δtox infected mice, thus giving us more insight into *Chlamydia*-induced tissue disease.

3. Conclusions

This research has provided important insights into female upper genital tract disease caused by *Chlamydia*. The first aim of this work sought to develop a reliable and descriptive pathology scoring system for *Chlamydia* infection. In carrying this out, we refined our pilot pathology scoring scales to become more understandable and biologically representative of expected pathologies for acute and chronic infection. We demonstrated the teachability of this scoring system in an intervention study where students improved their pathology scoring abilities. This helped us identify a training workflow for future lab members' learning. Additionally, we eased the process of scoring and learning to score by creating a detailed scoring guide accessible to all lab members. Finally, we identified multiple ways to assess inter-rater reliability in a nuanced way to address the lack of reporting in the literature.

The second specific aim explored the potential of the virus-like particle QB-CT166 as a *Chlamydia* vaccine candidate. We show that QB-CT166 is highly immunogenic: it produces high titer *Chlamydia*-specific serum antibodies and low levels of local antibodies. However, these antibodies are not sufficient to protect against *C. muridarum* infection. This emphasizes the importance of a local immune response, as well as the genetic importance of putative cytotoxins for

different *Chlamydia* strains. This research can be contextualized in a massive body of work done to develop a *Chlamydia* vaccine, which is collaborative and cumulative. Non-protective vaccines shed light on what does and does not work and move the field forward. Because *C. trachomatis* causes life-altering, dangerous conditions such as hydrosalpinx, pelvic inflammatory disease, ectopic pregnancy, and tubal factor infertility in people with uteri, it is essential that a prophylactic vaccine be developed. Together as scientists, our end goal is to develop a safe, effective, and accessible *Chlamydia* vaccine, which this research will support.

LITERATURE CITED

1. Grygiel-Górniak, B., and Folga, B. A. (2023) Chlamydia trachomatis—An Emerging Old Entity? *Microorganisms*. **11**, 1283
2. World Health Organization (2024) Chlamydia
3. Cheng, Y., Zheng, G., Song, Z., Zhang, G., Rao, X., and Zeng, T. (2024) Trends in chlamydia prevalence in the United States, 2005–2016. *Sci. Rep.* **14**, 11825
4. CDC (2025) Sexually Transmitted Infections Surveillance, 2024 (Provisional)
5. Huai, P., Li, F., Chu, T., Liu, D., Liu, J., and Zhang, F. (2020) Prevalence of genital Chlamydia trachomatis infection in the general population: a meta-analysis. *BMC Infect. Dis.* **20**, 589
6. Tilson, E. C., Sanchez, V., Ford, C. L., Smurzynski, M., Leone, P. A., Fox, K. K., Irwin, K., and Miller, W. C. (2004) Barriers to asymptomatic screening and other STD services for adolescents and young adults: focus group discussions. *BMC Public Health*. **4**, 21
7. Witkin, S. S., Minis, E., Athanasiou, A., Leizer, J., and Linhares, I. M. (2017) Chlamydia trachomatis: the Persistent Pathogen. *Clin. Vaccine Immunol. CVI*. **24**, e00203-17
8. Elendu, C., Amaechi, D. C., Elendu, I. D., Elendu, T. C., Amaechi, E. C., Usoro, E. U., Chima-Ogbuiyi, N. L., Arrey Agbor, D. B., Onwuegbule, C. J., Afolayan, E. F., and Balogun, B. B. (2024) Global perspectives on the burden of sexually transmitted diseases: A narrative review. *Medicine (Baltimore)*. **103**, e38199
9. Murray, S. M., and McKay, P. F. (2021) Chlamydia trachomatis: Cell biology, immunology and vaccination. *Vaccine*. **39**, 2965–2975
10. Brunham, R. C., and Rey-Ladino, J. (2005) Immunology of Chlamydia infection: implications for a Chlamydia trachomatis vaccine. *Nat. Rev. Immunol.* **5**, 149–161
11. Haggerty, C. (2003) Lower quality of life among women with chronic pelvic pain after pelvic inflammatory disease*1. *Obstet. Gynecol.* **102**, 934–939
12. CDC (2024) Screening Recommendations and Considerations Referenced in Treatment Guidelines and Original Sources
13. Bierer, B. E., Meloney, L. G., Ahmed, H. R., and White, S. A. (2022) Advancing the inclusion of underrepresented women in clinical research. *Cell Rep. Med.* **3**, 100553
14. Daitch, V., Turjeman, A., Poran, I., Tau, N., Ayalon-Dangur, I., Nashashibi, J., Yahav, D., Paul, M., and Leibovici, L. (2022) Underrepresentation of women in randomized controlled trials: a systematic review and meta-analysis. *Trials*. **23**, 1038
15. Regensteiner, J. G., McNeil, M., Faubion, S. S., Bairey-Merz, C. N., Gulati, M., Joffe, H., Redberg, R. F., Rosen, S. E., Reusch, J. Eb., and Klein, W.

(2025) Barriers and solutions in women's health research and clinical care: a call to action. *Lancet Reg. Health - Am.* **44**, 101037

16. Schautteet, K., De Clercq, E., and Vanrompay, D. (2011) *Chlamydia trachomatis* Vaccine Research through the Years. *Infect. Dis. Obstet. Gynecol.* **2011**, 1–9
17. Broder, K. C., Matrosova, V. Y., Tkavc, R., Gaidamakova, E. K., Ho, L. T. V. T., Macintyre, A. N., Soc, A., Diallo, A., Darnell, S. C., Bash, S., Daly, M. J., Jerse, A. E., and Liechti, G. W. (2024) Irradiated whole cell Chlamydia vaccine confers significant protection in a murine genital tract challenge model. *Npj Vaccines*. **9**, 207
18. Murthy, A. K., Chambers, J. P., Meier, P. A., Zhong, G., and Arulanandam, B. P. (2007) Intranasal Vaccination with a Secreted Chlamydial Protein Enhances Resolution of Genital *Chlamydia muridarum* Infection, Protects against Oviduct Pathology, and Is Highly Dependent upon Endogenous Gamma Interferon Production. *Infect. Immun.* **75**, 666–676
19. Poston, T. B. (2024) Advances in vaccine development for *Chlamydia trachomatis*. *Pathog. Dis.* **82**, ftae017
20. Paavonen, J., Jenkins, D., Bosch, F. X., Naud, P., Salmerón, J., Wheeler, C. M., Chow, S.-N., Apter, D. L., Kitchener, H. C., Castellsague, X., De Carvalho, N. S., Skinner, S. R., Harper, D. M., Hedrick, J. A., Jaisamrarn, U., Limson, G. A., Dionne, M., Quint, W., Spiessens, B., Peeters, P., Struyf, F., Wieting, S. L., Lehtinen, M. O., and Dubin, G. (2007) Efficacy of a prophylactic adjuvanted bivalent L1 virus-like-particle vaccine against infection with human papillomavirus types 16 and 18 in young women: an interim analysis of a phase III double-blind, randomised controlled trial. *The Lancet*. **369**, 2161–2170
21. Frietze, K. M., Lijek, R., and Chackerian, B. (2018) Applying lessons from human papillomavirus vaccines to the development of vaccines against *Chlamydia trachomatis*. *Expert Rev. Vaccines*. **17**, 959–966
22. De Clercq, E., Kalmar, I., and Vanrompay, D. (2013) Animal Models for Studying Female Genital Tract Infection with Chlamydia trachomatis. *Infect. Immun.* **81**, 3060–3067
23. Robinson, M., James, J., Thomas, G., West, N., Jones, L., Lee, J., Oien, K., Freeman, A., Craig, C., Sloan, P., Elliot, P., Cheang, M., Rodriguez-Justo, M., Verrill, C., and UK National Cancer Research Institute (NCRI) Cellular-Molecular Pathology (CM-Path) clinical trials working group (2019) Quality assurance guidance for scoring and reporting for pathologists and laboratories undertaking clinical trial work. *J. Pathol. Clin. Res.* **5**, 91–99
24. McHugh, M. L. (2012) Interrater reliability: the kappa statistic. *Biochem. Medica*. **22**, 276–282
25. Everett, K. D. E., Bush, R. M., and Andersen, A. A. (1999) Emended description of the order Chlamydiales, proposal of Parachlamydiaceae fam. nov. and Simkaniaceae fam. nov., each containing one monotypic genus,

revised taxonomy of the family Chlamydiaceae, including a new genus and five new species, and standards for the identification of organisms. *Int. J. Syst. Evol. Microbiol.* **49**, 415–440
26. Chen, H., Wen, Y., and Li, Z. (2019) Clear Victory for Chlamydia: The Subversion of Host Innate Immunity. *Front. Microbiol.* **10**, 1412
27. Elwell, C., Mirrashidi, K., and Engel, J. (2016) Chlamydia cell biology and pathogenesis. *Nat. Rev. Microbiol.* **14**, 385–400
28. Bugalhão, J. N., and Mota, L. J. (2019) The multiple functions of the numerous Chlamydia trachomatis secreted proteins: the tip of the iceberg. *Microb. Cell*. **6**, 414–449
29. Lee, J. K., Enciso, G. A., Boassa, D., Chander, C. N., Lou, T. H., Pairawan, S. S., Guo, M. C., Wan, F. Y. M., Ellisman, M. H., Sütterlin, C., and Tan, M. (2018) Replication-dependent size reduction precedes differentiation in Chlamydia trachomatis. *Nat. Commun.* **9**, 45
30. Grieshaber, S. S., Grieshaber, N. A., Miller, N., and Hackstadt, T. (2006) *Chlamydia trachomatis* Causes Centrosomal Defects Resulting in Chromosomal Segregation Abnormalities. *Traffic*. **7**, 940–949
31. Panzetta, M. E., Valdivia, R. H., and Saka, H. A. (2018) Chlamydia Persistence: A Survival Strategy to Evade Antimicrobial Effects in-vitro and in-vivo. *Front. Microbiol.* **9**, 3101
32. Chumduri, C., and Turco, M. Y. (2021) Organoids of the female reproductive tract. *J. Mol. Med.* **99**, 531–553
33. Cora, M. C., Kooistra, L., and Travlos, G. (2015) Vaginal Cytology of the Laboratory Rat and Mouse: Review and Criteria for the Staging of the Estrous Cycle Using Stained Vaginal Smears. *Toxicol. Pathol.* **43**, 776–793
34. Quispe Calla, N. E., Vicetti Miguel, R. D., Boyaka, P. N., Hall-Stoodley, L., Kaur, B., Trout, W., Pavelko, S. D., and Cherpes, T. L. (2016) Medroxyprogesterone acetate and levonorgestrel increase genital mucosal permeability and enhance susceptibility to genital herpes simplex virus type 2 infection. *Mucosal Immunol.* **9**, 1571–1583
35. Wessels, J. M., Lajoie, J., Cooper, M. I. J. H., Omollo, K., Felker, A. M., Vitali, D., Dupont, H. A., Nguyen, P. V., Mueller, K., Vahedi, F., Kimani, J., Oyugi, J., Cheruiyot, J., Mungai, J. N., Deshiere, A., Tremblay, M. J., Mazzulli, T., Stearns, J. C., Ashkar, A. A., Fowke, K. R., Surette, M. G., and Kaushic, C. (2019) Medroxyprogesterone acetate alters the vaginal microbiota and microenvironment in women and increases susceptibility to HIV-1 in humanized mice. *Dis. Model. Mech.* **12**, dmm039669
36. Hu, J., Brendle, S. A., Li, J. J., Walter, V., Cladel, N. M., Cooper, T., Shearer, D. A., Balogh, K. K., and Christensen, N. D. (2022) Depo Medroxyprogesterone (DMPA) Promotes Papillomavirus Infections but Does Not Accelerate Disease Progression in the Anogenital Tract of a Mouse Model. *Viruses*. **14**, 980
37. Teepe, A. G., Allen, L. B., Wordinger, R. J., and Harris, E. F. (1990) Effect of the estrous cycle on susceptibility of female mice to intravaginal

inoculation of herpes simplex virus type 2 (HSV-2). *Antiviral Res.* **14**, 227–235
38. Islam, E. A., Shaik-Dasthagirisaheb, Y., Kaushic, C., Wetzler, L. M., and Gray-Owen, S. D. (2016) The reproductive cycle is a pathogenic determinant during gonococcal pelvic inflammatory disease in mice. *Mucosal Immunol.* **9**, 1051–1064
39. Kaushic, C., Ashkar, A. A., Reid, L. A., and Rosenthal, K. L. (2003) Progesterone Increases Susceptibility and Decreases Immune Responses to Genital Herpes Infection. *J. Virol.* **77**, 4558–4565
40. Pal, S., Hui, W., Peterson, E. M., and De La Maza, L. M. (1998) Factors influencing the induction of infertility in a mouse model of Chlamydia trachomatis ascending genital tract infection. *J. Med. Microbiol.* **47**, 599–605
41. Tian, Q., Zhang, T., Shu, C., Han, Z., Huang, Y., Wan, J., Wang, L., and Sun, X. (2024) Diverse animal models for Chlamydia infections: unraveling pathogenesis through the genital and gastrointestinal tracts. *Front. Microbiol.* **15**, 1386343
42. Tuffrey, M., and Taylor-Robinson, D. (1981) Progesterone as a key factor in the development of a mouse model for genital-tract infection with *Chlamydia trachomatis*. *FEMS Microbiol. Lett.* **12**, 111–115
43. Kim, J., Ślęczkowska, M., Nobre, B., and Wieringa, P. (2025) Study Models for Chlamydia trachomatis Infection of the Female Reproductive Tract. *Microorganisms*. **13**, 553
44. The IACUC, The Institutional Animal Care and Use Committee
45. Callan, T., Woodcock, S., and Huston, W. M. (2021) Ascension of Chlamydia is moderated by uterine peristalsis and the neutrophil response to infection. *PLOS Comput. Biol.* **17**, e1009365
46. Lee, H. Y., Schripsema, J. H., Sigar, I. M., Murray, C. M., Lacy, S. R., and Ramsey, K. H. (2010) A link between neutrophils and chronic disease manifestations of *Chlamydia muridarum* urogenital infection of mice. *FEMS Immunol. Med. Microbiol.* **59**, 108–116
47. Lijek, R. S., Helble, J. D., Olive, A. J., Seiger, K. W., and Starnbach, M. N. (2018) Pathology after *Chlamydia trachomatis* infection is driven by nonprotective immune cells that are distinct from protective populations. *Proc. Natl. Acad. Sci.* **115**, 2216–2221
48. Berclaz, L. H., Eicher, G., Wieselquist, G., Frimpong, A., Mallare, A., Lijek, R. S., and Fields, K. A. (2025) Complete deletion of the *Chlamydia muridarum* putative cytotoxin locus reveals contributions during invasion in tissue culture and oviduct pathology during murine genital tract infection. *Infect. Immun.* **93**, e00419-25
49. Chen, J., Zhang, H., Zhou, Z., Yang, Z., Ding, Y., Zhou, Z., Zhong, E., Arulanandam, B., Baseman, J., and Zhong, G. (2014) Chlamydial Induction of Hydrosalpinx in 11 Strains of Mice Reveals Multiple Host Mechanisms for Preventing Upper Genital Tract Pathology. *PLoS ONE*. **9**, e95076

50. Koo, T. K., and Li, M. Y. (2016) A Guideline of Selecting and Reporting Intraclass Correlation Coefficients for Reliability Research. *J. Chiropr. Med.* **15**, 155–163
51. Melgoza, I. P., Chenna, S. S., Tessier, S., Zhang, Y., Tang, S. Y., Ohnishi, T., Novais, E. J., Kerr, G. J., Mohanty, S., Tam, V., Chan, W. C. W., Zhou, C., Zhang, Y., Leung, V. Y., Brice, A. K., Séguin, C. A., Chan, D., Vo, N., Risbud, M. V., and Dahia, C. L. (2021) Development of a standardized histopathology scoring system using machine learning algorithms for intervertebral disc degeneration in the mouse model—An ORS spine section initiative. *JOR SPINE*. **4**, e1164
52. Liang, W., Menke, A. L., Driessen, A., Koek, G. H., Lindeman, J. H., Stoop, R., Havekes, L. M., Kleemann, R., and van den Hoek, A. M. (2014) Establishment of a general NAFLD scoring system for rodent models and comparison to human liver pathology. *PloS One*. **9**, e115922
53. Koelink, P. J., Wildenberg, M. E., Stitt, L. W., Feagan, B. G., Koldijk, M., Van ‘T Wout, A. B., Atreya, R., Vieth, M., Brandse, J. F., Duijst, S., Te Velde, A. A., D’Haens, G. R. A. M., Levesque, B. G., and Van Den Brink, G. R. (2018) Development of Reliable, Valid and Responsive Scoring Systems for Endoscopy and Histology in Animal Models for Inflammatory Bowel Disease. *J. Crohns Colitis*. **12**, 794–803
54. Belland, R. J., Scidmore, M. A., Crane, D. D., Hogan, D. M., Whitmire, W., McClarty, G., and Caldwell, H. D. (2001) *Chlamydia trachomatis* cytotoxicity associated with complete and partial cytotoxin genes. *Proc. Natl. Acad. Sci.* **98**, 13984–13989
55. Orrell, K. E., and Melnyk, R. A. (2021) Large Clostridial Toxins: Mechanisms and Roles in Disease. *Microbiol. Mol. Biol. Rev.* **85**, e00064-21
56. Malito, E., D’Urzo, N., Bottomley, M. J., Biancucci, M., Scarselli, M., Maione, D., and Martinelli, M. (2012) Crystal structure of the GT domain of Clostridium difficile toxin A (TcdA) in complex with UDP and Manganese: 4dmw. 10.2210/pdb4dmw/pdb
57. Just, I., and Gerhard, R. (2005) Large clostridial cytotoxins. in *Reviews of Physiology, Biochemistry and Pharmacology*, pp. 23–47, Reviews of Physiology, Biochemistry and Pharmacology, Springer Berlin Heidelberg, Berlin, Heidelberg, **152**, 23–47
58. Thalmann, J., Janik, K., May, M., Sommer, K., Ebeling, J., Hofmann, F., Genth, H., and Klos, A. (2010) Actin Re-Organization Induced by Chlamydia trachomatis Serovar D - Evidence for a Critical Role of the Effector Protein CT166 Targeting Rac. *PLoS ONE*. **5**, e9887
59. Bothe, M., Dutow, P., Pich, A., Genth, H., and Klos, A. (2015) DXD Motif-Dependent and -Independent Effects of the Chlamydia trachomatis Cytotoxin CT166. *Toxins*. **7**, 621–637
60. Lacroix, G., Gouyer, V., Gottrand, F., and Desseyn, J.-L. (2020) The Cervicovaginal Mucus Barrier. *Int. J. Mol. Sci.* **21**, 8266

61. Oh, K.-J., Lee, H.-S., Ahn, K., and Park, K. (2016) Estrogen Modulates Expression of Tight Junction Proteins in Rat Vagina. *BioMed Res. Int.* **2016**, 4394702
62. Judith A. Owen, Jenni Punt, Sharon A. Stranford (2009) *Kuby Immunology*, 7th Ed., W. H. Freeman and Company
63. Boyaka, P. N. (2017) Inducing Mucosal IgA: A Challenge for Vaccine Adjuvants and Delivery Systems. *J. Immunol.* **199**, 9–16
64. Xiang, W., Yu, N., Lei, A., Li, X., Tan, S., Huang, L., and Zhou, Z. (2021) Insights Into Host Cell Cytokines in Chlamydia Infection. *Front. Immunol.* **12**, 639834
65. Jenny, M., Schroecksnadel, S., Gostner, J. M., Ueberall, F., and Fuchs, D. (2013) Cacao for the Prevention of Cardiovascular Diseases. in *Bioactive Food as Dietary Interventions for Cardiovascular Disease*, pp. 271–281, Elsevier, 10.1016/B978-0-12-396485-4.00015-3
66. Nelson, D. E., Virok, D. P., Wood, H., Roshick, C., Johnson, R. M., Whitmire, W. M., Crane, D. D., Steele-Mortimer, O., Kari, L., McClarty, G., and Caldwell, H. D. (2005) Chlamydial IFN-γ immune evasion is linked to host infection tropism. *Proc. Natl. Acad. Sci.* **102**, 10658–10663
67. Chen, X., Yang, W., Hu, Y., Zhou, Y., and Zhou, Z. (2025) Role of IFN-γ from Different Immune Cells in Chlamydia Infection. *Microorganisms*. **13**, 2374
68. Morrison, S. G., and Morrison, R. P. (2001) Resolution of secondary Chlamydia trachomatis genital tract infection in immune mice with depletion of both CD4+ and CD8+ T cells. *Infect. Immun.* **69**, 2643–2649
69. Johnson, R. M., Yu, H., Strank, N. O., Karunakaran, K., Zhu, Y., and Brunham, R. C. (2018) B Cell Presentation of Chlamydia Antigen Selects Out Protective CD4γ13 T Cells: Implications for Genital Tract Tissue-Resident Memory Lymphocyte Clusters. *Infect. Immun.* **86**, e00614-17
70. De La Maza, L. M., Zhong, G., and Brunham, R. C. (2017) Update on Chlamydia trachomatis Vaccinology. *Clin. Vaccine Immunol.* 10.1128/CVI.00543-16
71. Follmann, F., Olsen, A. W., Jensen, K. T., Hansen, P. R., Andersen, P., and Theisen, M. (2008) Antigenic Profiling of a *Chlamydia trachomatis* Gene‐Expression Library. *J. Infect. Dis.* **197**, 897–905
72. Awate, S., Babiuk, L. A., and Mutwiri, G. (2013) Mechanisms of action of adjuvants. *Front. Immunol.* **4**, 114
73. Scherpenisse, M., Mollers, M., Schepp, R. M., Meijer, C. J. L. M., de Melker, H. E., Berbers, G. A. M., and van der Klis, F. R. M. (2013) Detection of systemic and mucosal HPV-specific IgG and IgA antibodies in adolescent girls one and two years after HPV vaccination. *Hum. Vaccines Immunother.* **9**, 314–321

74. Schiller, J. T., Castellsagué, X., and Garland, S. M. (2012) A review of clinical trials of human papillomavirus prophylactic vaccines. *Vaccine*. **30 Suppl 5**, F123-138
75. Nunes, A., Nogueira, P. J., Borrego, M. J., and Gomes, J. P. (2010) Adaptive Evolution of the Chlamydia trachomatis Dominant Antigen Reveals Distinct Evolutionary Scenarios for B- and T-cell Epitopes: Worldwide Survey. *PLoS ONE*. **5**, e13171
76. Crane, D. D., Carlson, J. H., Fischer, E. R., Bavoil, P., Hsia, R., Tan, C., Kuo, C., and Caldwell, H. D. (2006) *Chlamydia trachomatis* polymorphic membrane protein D is a species-common pan-neutralizing antigen. *Proc. Natl. Acad. Sci.* **103**, 1894–1899
77. Webster, E., Seiger, K. W., Core, S. B., Collar, A. L., Knapp-Broas, H., Graham, J., Shrestha, M., Afzaal, S., Geisler, W. M., Wheeler, C. M., Chackerian, B., Frietze, K. M., and Lijek, R. S. (2022) Immunogenicity and Protective Capacity of a Virus-like Particle Vaccine against Chlamydia trachomatis Type 3 Secretion System Tip Protein, CT584. *Vaccines*. **10**, 111
78. Everett P Webster, Lijek Lab Member 2016-2020. (2020) Unpublished Results
79. Lucie H. Berclaz (2023) Chlamydia trachomatis open reading frames CT166 and CT584 act as virulence factors during uterine infection in mice
80. Kyra W. Seiger (2019) *Two Approaches to Addressing Chlamydia Trachomatis Virulence: Evaluating C. Trachomatis Vaccines and Virulence Factor Expression*. Ph.D. thesis, Mount Holyoke College
81. LeBreton, J. M., and Senter, J. L. (2008) Answers to 20 Questions About Interrater Reliability and Interrater Agreement. *Organ. Res. Methods*. **11**, 815–852
82. Matthew Graham, Anthony Milanowski, and Jackson Miller (2012) Measuring and Promoting Inter-Rater Agreement of Teacher and Principal Performance Ratings. *Cent. Educ. Compens. Reform*
83. Ferreira Costa, A. P., Gonçalves, A. K., Machado, P. R. L., Souza, L. B. F. C. de, Sarmento, A., Cobucci, R. N. O., Giraldo, P. C., and Witkin, S. S. (2018) Immune Response to Human Papillomavirus One Year after Prophylactic Vaccination with AS04-Adjuvanted HPV-16/18 Vaccine: HPV-Specific IgG and IgA Antibodies in the Circulation and the Cervix. *Asian Pac. J. Cancer Prev. APJCP*. **19**, 2313–2317
84. Jamus, A. N., Wilton, Z. E. R., Armijo, S. D., Flanagan, J., Romano, I. G., Core, S. B., and Frietze, K. M. (2025) Nasal and Ocular Immunization with Bacteriophage Virus-like Particle Vaccines Elicits Distinct Systemic and Mucosal Antibody Profiles. *Vaccines*. **13**, 829
85. Pavlisko, E. N., Neely, M. L., Wikenheiser-Brokamp, K. A., Fishbein, G. A., Litzky, L., Farver, C. F., Pal, P., He, M., Illei, P. B., Deshpande, C., Robien, M. A., Kirchner, J., Frankel, C. W., Lang, J. E., Belperio, J. A., Palmer, S. M., and Sweet, S. C. (2025) Diagnostic alignment to optimize inter-rater

reliability among lung transplant pathologists. *J. Heart Lung Transplant.* **44**, 173–181
86. Abdel-Halim, C. N., Rohde, M., Larsen, S. R., Green, T. M., Ulhøi, B. P., Woller, N. C., Gerke, O., Høilund-Carlsen, P. F., Sørensen, J. A., and Godballe, C. (2022) Inter- and Intrarater Reliability and Agreement Among Danish Head and Neck Pathologists Assessing Extranodal Extension in Lymph Node Metastases from Oropharyngeal Squamous Cell Carcinomas. *Head Neck Pathol.* **16**, 1082–1090
87. Alavi, M., Biros, E., and Cleary, M. (2022) A primer of inter‐rater reliability in clinical measurement studies: Pros and pitfalls. *J. Clin. Nurs.* 10.1111/jocn.16514
88. Caldeira, J. do C., Medford, A., Kines, R. C., Lino, C. A., Schiller, J. T., Chackerian, B., and Peabody, D. S. (2010) Immunogenic display of diverse peptides, including a broadly cross-type neutralizing human papillomavirus L2 epitope, on virus-like particles of the RNA bacteriophage PP7. *Vaccine*. **28**, 4384–4393
89. Tumban, E., Peabody, J., Tyler, M., Peabody, D. S., and Chackerian, B. (2012) VLPs displaying a single L2 epitope induce broadly cross-neutralizing antibodies against human papillomavirus. *PloS One*. **7**, e49751
90. Nardelli-Haefliger, D., Wirthner, D., Schiller, J. T., Lowy, D. R., Hildesheim, A., Ponci, F., and De Grandi, P. (2003) Specific Antibody Levels at the Cervix During the Menstrual Cycle of Women Vaccinated With Human Papillomavirus 16 Virus-Like Particles. *JNCI J. Natl. Cancer Inst.* **95**, 1128–1137
91. Shannon Breen (2024) Effect of Depo Provera dosage schedules on mouse estrous cycles and relevance for Chlamydia infection
92. Cerutti, A. (2008) The regulation of IgA class switching. *Nat. Rev. Immunol.* **8**, 421–434
93. Boyaka, P. N., Marinaro, M., Vancott, J. L., Takahashi, I., Fujihashi, K., Yamamoto, M., Van Ginkel, F. W., Jackson, R. J., Kiyono, H., and McGhee, J. R. (1999) Strategies for mucosal vaccine development. *Am. J. Trop. Med. Hyg.* **60**, 35–45
94. Patel, H., Yewale, C., Rathi, M. N., and Misra, A. (2014) Mucosal Immunization: A Review of Strategies and Challenges. *Crit. Rev. Ther. Drug Carrier Syst.* **31**, 273–303
95. Fields Lab Unpublished Data
96. Keck, J., Chambers, J. P., Forsthuber, T., Gupta, R., and Arulanandam, B. P. (2019) A modified method for rapid quantification of Chlamydia muridarum using Fluorospot. *MethodsX*. **6**, 1925–1932
97. Nardellihaefliger, D., Lurati, F., Wirthner, D., Spertini, F., Schiller, J., Lowy, D., Ponci, F., and Grandi, P. (2005) Immune responses induced by lower airway mucosal immunisation with a human papillomavirus type 16 virus-like particle vaccine. *Vaccine*. **23**, 3634–3641

98. Shin, H., and Iwasaki, A. (2012) A vaccine strategy that protects against genital herpes by establishing local memory T cells. *Nature*. **491**, 463–467
99. Tregoning, J. S., Buffa, V., Oszmiana, A., Klein, K., Walters, A. A., and Shattock, R. J. (2013) A "prime-pull" vaccine strategy has a modest effect on local and systemic antibody responses to HIV gp140 in mice. *PloS One*. **8**, e80559
100. Prior, J. T., Limbert, V. M., Horowitz, R. M., D'Souza, S. J., Bachnak, L., Godwin, M. S., Bauer, D. L., Harrell, J. E., Morici, L. A., Taylor, J. J., and McLachlan, J. B. (2023) Establishment of isotype-switched, antigen-specific B cells in multiple mucosal tissues using non-mucosal immunization. *Npj Vaccines*. **8**, 80

APPENDIX A: METHODOLOGY

1. Pathology Scoring

A researcher (RL) who did not participate in scoring concealed the experimental label on each slide and assigned it a random number to eliminate researcher bias. Each number was randomly assigned to two pathology scorers. The initial assessment of slide pathology was performed individually.

Following individual assessments, scorers came together for a consensus meeting, which was also conducted under anonymized conditions. If there was initial agreement between two scorers, the agreed upon score was assigned to the tissue. If there was disagreement, the slide was viewed by all scorers who discussed the tissue in detail. The scorer(s) not originally assigned the slide determined the consensus score based on their expertise and the discussion. If there was continued uncertainty, RL provided expertise on what the score should be.

If possible, for each category of pathology, each individual tissue type was assigned two total scores per mouse, one for each side of the genital tract. Therefore for each phenotype, there were two uterine horn scores (left and right) and two ovary scores (left and right). Oviducts were assigned one score per side as well, even if multiple cross sections were visible. Assigning scores was not always possible due to occasional missing tissues or poor cross sections. For the former, tissues were assigned an “M,” and for the latter, tissues were assigned “no score.” For various experiments, two different cross sections were provided per

mouse on two separate slides. In these cases, the slide labeler picked the slide with the more clear cross section to assign to individual scorers. Once the anonymized consensus was reached, arbitrary number assignments were removed and scores were matched with experimental condition.

APPENDIX B: SUPPLEMENTARY FIGURES AND TABLES

Table 6. Products used listed with manufacturer and product number.

Reagent/Product	Manufacturer	Product Number
30G Needle	Becton Dickinson	305106
Non-heparinized Capillary Tubes	Thermo Fisher Scientific	22260943
Sterile 1x PBS	Thermo Fisher Scientific	10010023
Immulon 2HB Plates	Thermo Fisher Scientific	3455
Streptavidin	Thermo Fisher Scientific	434302
SMPH	Thermo Fisher Scientific	22363
CT166 Peptides	GenScript	N/A (Custom sequence)
HRP-conjugated goat anti-rabbit IgG	Bio Rad	1706515
HRP-conjugated goat anti-mouse IgG	Thermo Fisher Scientific	31444
HRP-conjugated goat anti-mouse IgA	Thermo Fisher Scientific	626720
TMB	Sigma-Aldrich	613544
Concentrated HCl	Thermo Fisher Scientific	AA43335AP
Depomedroxyprogesterone acetate (DMPA)	Prasco	NDC 6699337083
Non-Surgical Embryo Transfer Device (NSET)	ParaTechs	60010
1:10 buffered formalin	Applied Biosystems	305-510
DNeasy blood and tissue purification kit	Qiagen	69504

200 Proof Ethanol	Pharmco	100135
Taq 2x Buffer	Applied Biosystems	44-445-56
GAPDH Forward & Reverse Primers, GAPDH Probe	Applied Biosystems	43-083-13
16S Forward & Reverse Primers, 16S Probe	Integrated DNA Technologies	N/A (Custom sequence)

A: Cq = -3.61log[GAPDH DNA] + 33.8 $\log([\text{GAPDH DNA}]) = \frac{Cq-33.8}{-3.61}$ $[\text{GAPDH DNA}] = 10^{\frac{Cq-33.8}{-3.61}}$	**B:** Cq = -3.78log[16S DNA] + 25.1 $\log([\text{16S DNA}]) = \frac{Cq-25.1}{-3.78}$ $[\text{16S DNA}] = 10^{\frac{Cq-25.1}{-3.78}}$

Equation 4. Standard Curve of Cq versus [gDNA] A: solved for [GAPDH gDNA] (pg/uL) and **B:** solved for[16S gDNA] (pg/uL). The Cq value substituted in each equation was the mean of triplicate values. Data and equations gathered and solved by Lijek Lab member KS, 2018 (80).

Table 7. Pilot acute pathology scoring system. Uterine horns were assessed for general pathology (**A**), where "pathology" was considered mucus and cellular infiltration. Oviducts were assessed for cellular infiltration (**B**) and edema (**C**) based on severity. Ovaries were assessed for cellular infiltration (**D**) and edema (**E**) based on severity.

A: Uterine horn general pathology	
0	No pathology
1	Mild/rare pathology; less than 1/3 of tissue affected
2	Moderate/multifocal pathology; between 1/3 and 2/3 of tissue affected
3	Severe/coalescing pathology; greater than 2/3 of tissue affected
B: Oviduct cellular infiltration	

0	No pathology
1	Mild/moderate pathology, affects some of tissue
2	Severe pathology, significantly affects all tissue
C: Oviduct edema	
0	No pathology
1	Mild/moderate pathology, affects some of tissue
2	Severe pathology, significantly affects all tissue
D: Ovary cellular infiltration	
0	No pathology
1	Mild/moderate pathology, affects some of tissue
2	Severe pathology, significantly affects all tissue
E: Ovary edema	
0	No pathology
1	Mild/moderate pathology, affects some of tissue
2	Severe pathology, significantly affects all tissue

Table 8. Pilot chronic pathology scoring system. Uterine horns were assessed for general pathology (**A**), where "pathology" was considered mucus and cellular infiltration, as well as dilatation (**B**). Oviducts were assessed for cellular infiltration (**C**) based on severity and hydrosalpinx (**D**). Ovaries were assessed for cellular infiltration (**D**) and edema (**E**) based on severity.

A: Uterine horn general pathology	
0	No pathology
1	Mild/rare pathology; less than 1/3 of tissue affected
2	Moderate/multifocal pathology; between 1/3 and 2/3 of tissue affected
3	Severe/coalescing pathology; greater than 2/3 of tissue affected
B: Uterine horn dilatation	

0	No significant dilatation
1	Mild dilation of a single cross section
2	One to three dilated cross sections
3	More than three dilated cross sections
4	Confluent-pronounced dilation
C: Oviduct cellular infiltration	
0	No pathology
1	Mild/moderate pathology, affects some of tissue
2	Severe pathology, significantly affects all tissue
D: Oviduct hydrosalpinx	
0	No hydrosalpinx
1	Hydrosalpinx detectable visually but requiring microscopic confirmation
2	Hydrosalpinx clearly visible with naked eyes but the size is smaller than the ovary on the same side
3	Equal to the ovary on the same side
4	Hydrosalpinx larger than the ovary on the same side
E: Ovary cellular infiltration	
0	No pathology
1	Mild/moderate pathology, affects some of tissue
2	Severe pathology, significantly affects all tissue
F: Ovary edema	
0	No pathology
1	Mild/moderate pathology, affects some of tissue
2	Severe pathology, significantly affects all tissue

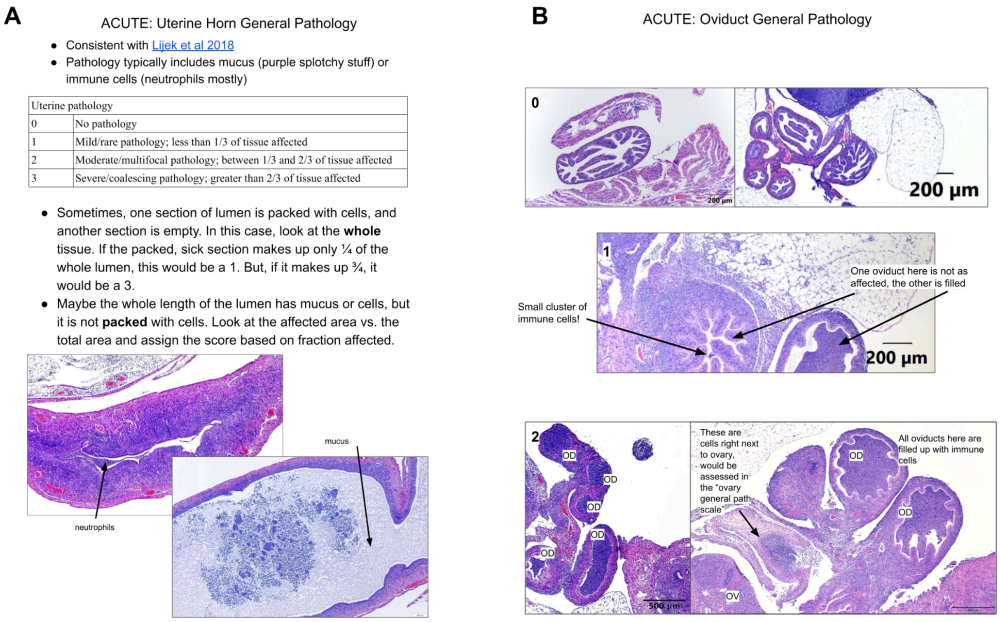

Figure 49. Excerpt from annotated pathology scoring guide. A: Every scale was explained with an introductory page with written descriptions of score in table form, explanations of what constitutes pathology, and important notes about assessing that phenotype. This example is of uterine horn general pathology at the acute timepoint. **B:** Introductory pages were followed by a page with representative images of each score, accompanied by annotations for what the viewer should notice about the tissue. The example used here is for acute oviduct pathology.

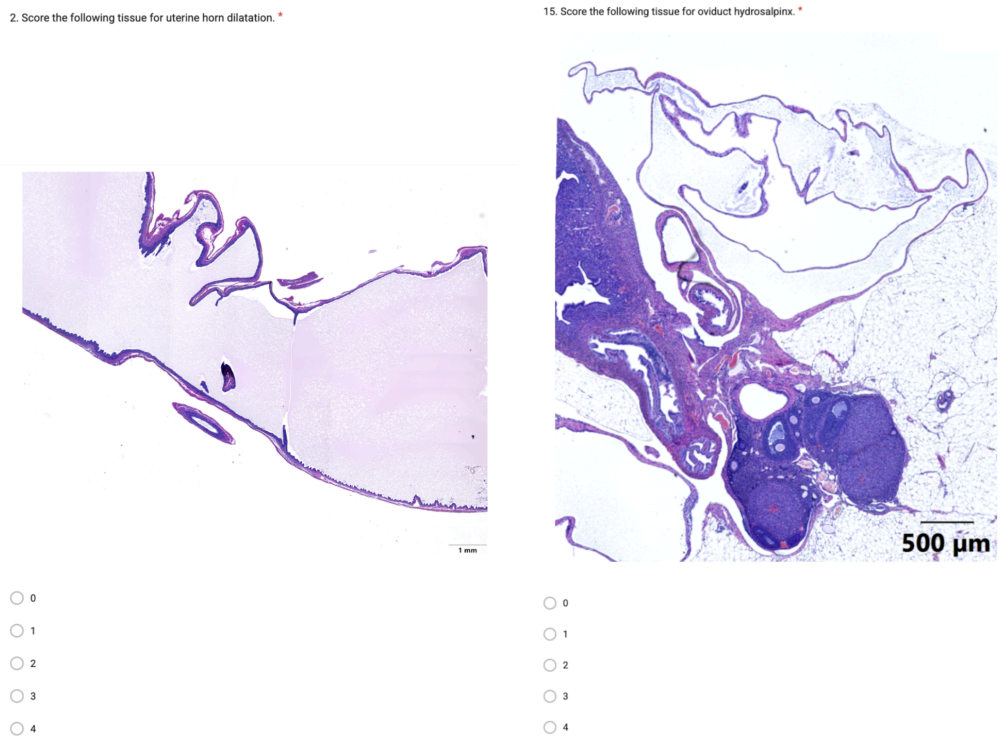

Figure 50. Sample question from intervention assessment used in pathology scoring training.